UNDERSTANDING OPEN QUANTUM SYSTEMS WITH COUPLED HARMONIC OSCILLATORS

Vignesh Venkataraman

Department of Physics

Imperial College London

Thesis submitted in partial fulfilment of the
requirements for the degree of
Doctor of Philosophy in Physics
of
Imperial College London

April 2015

Abstract

When a quantum system interacts with many other quantum mechanical objects, the behaviour of the system is strongly affected; this is referred to as an open quantum system (OQS). Since the inception of quantum theory the development of OQSs has been synonymous with realistic descriptions of quantum mechanical models. With recent activity in the advancement of quantum technologies, there has been vested interest in manipulating OQSs. Therefore understanding and controlling environmental effects, by structuring environments, has become an important field. The method of choice for tackling OQSs is the master equation approach, which requires approximations and doesn't allow direct assessment of the environment. This thesis tackles the issues of OQSs with an unorthodox method; we employ a series of coupled quantum harmonic oscillators to simulate an OQS. This permits the use of the covariance matrix technique which allows us to avoid approximations and analyse the environment modes. We investigate the Markov approximation and Rotating-Wave approximation (RWA), which are commonly used in the field. By considering four OQS models, we study an entanglement-based non-Markovian behaviour (NMB) quantifier (ENMBQ). The relevance of detuning, coupling strength and bath structures in determining the amount of NMB is noted. A brief study of the factors that affect a fidelity-based NMB quantifier is also conducted. We also analyse the effect on the ENMBQ if the terms excluded by the RWA are included in the models. Finally, an examination of the applicability of the RWA in the presence of strong coupling is undertaken in a three oscillator model. The fidelity-based analysis utilised could allow one to ascertain when and if the RWA can be applied to a model of interest, including OQSs. The knowledge within, and the methodology used throughout this thesis, could arm researchers with insights to control the flow of quantum information in their systems.

Declaration of Originality

I hereby declare that this thesis, and the work reported herein, was composed by and originated entirely from myself. Information utilised from the published and unpublished work of others has been acknowledged in the text with references.

Copyright declaration

The copyright of this thesis rests with the author and is made available under a Creative Commons Attribution Non-Commercial No Derivatives licence. Researchers are free to copy, distribute or transmit the thesis on the condition that they attribute it, that they do not use it for commercial purposes and that they do not alter, transform or build upon it. For any reuse or redistribution, researchers must make clear to others the licence terms of this work.

In dedication to

Sudha chitti, who let me draw all over her lab book

Gopal thatha, who would have been the only person to read this word for word

Sethu thatha, who showed me the joy of service to others

Acknowledgements

Please bear with the length of these acknowledgments because there are many people I would like to thank; family, friends and fellow academics. I genuinely believe that I would not have got through this PhD without them.

First and foremost, I would like to thank my parents for giving me the freedom to study the subject that I have loved since I was seven. From the time I saw the stars inside that inflatable dome, they have supported my fascination and intent to explore and understand the world around me. They have worked incredibly hard to ensure that I have had every available opportunity throughout my life and for that there isn't yet the word to describe my gratitude. I would not have been in a position to study a PhD at Imperial if they had not pushed me during my education and the patience they have shown me is astounding. I attribute all my academic achievements to them.

To my little brother Vivaek, what can I say, you have the ability, more than anyone else ever will on this planet, to make me laugh. Having you in my life is an immeasurable joy and has kept me in high spirits during my PhD, Masters and undergraduate. You always have and always will bring me back to the real world and I cannot thank you enough for that. I know you do not believe half the stuff I work on but I hope that one day I can convince you that it is actually real!

I would like to thank my supervisor Myungshik for all the support and guidance he has given me throughout my PhD. Most importantly, I am very glad I had a nice person as my academic father! Discovering yet another unbelievable aspect of your life never ceases to surprise me; such as test-driving cars, being an assistant chef at a Michelin star restaurant, having a black-belt in Taekwondo, to name but a few. I will surely miss your seemingly random anecdotes at the most seemingly random times, but I have many memories which I shall always cherish (particularly the great mouse hunt of 2013). I truly hope that one day I can come for some pasta at 'Minnimo's Italian Restaurant', which hopefully has a maple tree in the foyer.

To the two main post-docs in my life: Doug and Tommaso, without you my knowledge in this field would probably approach zero. Doug, although I will *never* be your minion, I am extremely grateful that you always had the time and patience to answer my, mostly simple/trivial, questions; which I am sure, at one point was me, essentially, not understanding that one plus one is two. I also want to thank you for keeping an eye out for me from time to time. Tommaso, I cannot tell you how happy I am that I had the opportunity to work alongside someone who has

a true love and passion for the subject. You approach everything you do with pure intentions and for that I am thankful and I will definitely miss your 'stupid' (but not so stupid) questions!

Didier and Ruben, a paragraph is not nearly enough. Thank you for all the support, advice and laughs, basically everything. Didi - Mr. Perfect, I have enjoyed every single tea break, all the lunches, the un-beaten run of squash games, the football, building an instrument, the Lake District road trip and so many other things. Having you there every step of the way has been tremendously important to me and it's sad that we won't be hanging out everyday. Ruby - the baby, I have many fond memories; our sporcle addiction, your energiser bunny running in football, the handball stories, the laser stories, the Rube - Goldberg machine, the twenty girlfriends theory, the hiking bandana and so many many more. I also have to thank you for starting my addiction to TableTop and board games! I am incredibly happy that you have been around and once again, it's sad that we won't be hanging out that often. The three of us have had so much fun together right from day one; whether we were in a lecture, climbing mountains, playing board games, in the pub, or just having lunch. Spending time with the two of you has been the best part of my PhD. I sincerely hope that in the future we all hang out together as much as humanly possible!

Aunty Fern; says it all in the name, thanks for always pushing me. Your support and advice throughout the degree has meant a lot to me. Also, I want to apologise for all the organised fun I made you endure. Aizar - Mr. 4G, I will never understand the hours you are at the office. Yameng, or should I say Adam, I will never forget your comment on our Lake District road trip. Graham, it has been a pleasure to share a football pitch with you and I hope one day you score a header at Selhurst with Big Dave Wineland putting in the cross. Ohm, I know it is only a matter of time before you are either made CEO of Subway or become a superhero from the amount of static you generate. Gatis, the spy, there's no point saying anymore because it's just going to be redacted. Iain, I promise I will eventually come down to the lab to lock a laser! There are too many great memories from the Masters, Glasgow, Quebec, the team building challenge and so many other things that it is impossible to list them all here. So I will just say that it has been amazing to be in Cohort 2 with all of you and you have definitely made my PhD so much more enjoyable than it should have been.

To the biggest SJ super fan in the whole entire world/research group - Kate, I thank for so many things. Putting up with my moaning has to be at the top of that list. I have earnestly and wholly enjoyed our time together as fellow MSK students, especially the fandom mocking,

M-cat doodling, the Seoul trip, the endless sarcasm and constant uh-hmms. I will really miss sharing an office with you. I really hope that you find a job you love, become friends with your favourite SJ members and most importantly, get seven hours of sleep every night!

To the chaotic cohort; Matteo and Kamil (The Dream Team), Claudio (Mr. 'I pulled a hamstring'), Izzy (Ms. Smiling and Dancing) and Antony (there aren't even enough words), you have given me copious amounts of laughter and for that I applaud you.

To my desk buddies, Kyle and Chaunqi, it has been a pleasure to sit next to you. I will not be able to forget Kyle's imaginary grenade throws and Chaunqi's mid-afternoon naps. I sincerely apologise for my constant, not-so-constant presence and the many distractions I have undeniably caused. Speaking of which, I would like to mention Howard who shares my interest in distractions, our interactions have brought me much amusement and kept me in a buoyant mood.

I also thank all the post-docs who have helped me with various things during my PhD, namely Ahsan, David, Mark and Sean, you guys have been, as Sean would say, ace. A truly special thanks goes out to my fellow Jose Mourinho loving friend Marco. You have helped me tremendously throughout my doctorate. I thoroughly enjoyed your presence in the office and have missed all the football banter since you left. I still owe you a trip to Stamford Bridge to see the great man doing his thing!

To my cricket companion Gary; it has been a pleasure to play alongside and bowl to you. I am sure one day you will be able to hit me out of the park! It was incredibly nice of you to take me to all those net sessions, trying to teach us trading, explaining some maths and the odd spattering of life lessons, thank you for all of it!

Terry, where do I start, there is never a dull moment with you around. Despite some of the ridiculousness my ears had to endure, I am proud to have been taught by you and be in the same research group as you; even though I was just another calculation monkey! It was nice to see such a smart guy have such a good heart. Danny you are, without a shadow of a doubt, the nicest academic I have ever had the pleasure to meet. I have fond memories of all our dealings within the CQD and I am looking forward to seeing you back in the lab soon.

Miranda and Lisa, Hallo! They say you can't really say how things would have been, can't compare with the road not taken. However, in this case, I can say for certain that without you two I would not have had half as much fun as I did during my PhD. Miranda, my Chirstmas - buddy, thank you for all the amazing work you have done for me and all the other students. I

never had any non-academic issues and I know that it was all down to your hard work. I hope the rest of CQD appreciate you as much as I do. It has been a great comfort knowing I had such a good friend to see everyday of my degree. You have helped me in more ways than you know. Lisa, my F-cubed, my last year in the PhD has been rainbow coloured because of you. It is near on impossible to be in a bad mood with you around, what with all the hugs, sweets and fat unicorns. I am unbelievably happy that you came to the Whiteley suite, I just wish it was with the CQD! The two of you have looked out for me more than anyone else at Imperial and for that I will never be able to thank you enough. Knowing you both has been one of the best parts of my PhD. The three of us have had too many fun times to be listed here but I'll try and give it a go; tea times, Christmas times, woman-naming times, cupcake-induced hysteria times, apple-jacking times, a-pink times, craft club times, I'm okay times and nudder udder times. I will really miss seeing you both everyday and the only thing I would have changed is the accent nails.

Terry, Danny and Myungshik; thank you for giving me the chance to be part of the CDT-CQD family, it has been an incredible experience and I will never regret taking up the offer. From the Masters to the PhD, the Christmas parties, team building challenges, film nights, ice skating, RSD course, I have enjoyed every minute of it (mostly!) I express my gratitude to Lillian, who helped me get an interview for the CQD and for her help during the first year of the PhD. I would also like to take the opportunity to now thank all those involved with the CQD who I haven't thanked already, including the lecturers and the students from the other cohorts.

To every person, past and present, in the Quantum Information group, whom I have had the privilege of sharing an office with on Level 12, I am honoured to have spent over three years of my life with you. From the breakfast meetings, 'Team Myungshik' meetings, pub trips, chess games, Mario Kart, Magic, to the random discussions about physics, sports, puzzles, academia, jobs, lunch efficiency, etc... it has been an absolute blast. I am quite sure that I will never find a more fun-loving, chilled out place of work! I also extended my thanks to everyone else at QOLS, especially Judith, Marcia and Sanja for all they do for the group.

Nic, Simon and Adam, I cannot thank you enough for introducing me into the world of outreach. You gave me the chance to share my passion with the public and it is one of things I am most proud of doing during my PhD. I will be indebted to you more than you know.

I also want to thank the students from the RCA-IED course, especially Olly, Gina and Meng.

It was so much fun to work with you on our collaborative art project. I will remember the work we did together fondly and hope we can team up again in the future!

I would like to thank the CCM and Physics football crews for some great and some not-so-great games of five-a-side! Special thanks to Rich and John for organising the games, which one hundred percent helped me keep my sanity (at least off the pitch).

Li-Fay, you are a great friend and have been since the first year of university. The amount of support you have given me throughout these years is incredible and it would have been so much harder without you. I literally cannot thank you enough Leafy.

Meenal, you really are like my little sister, you're always looking out for me and always make the extra effort. I can't tell you how much I appreciate it. Maybe I would have done something crazy by now if you didn't keep telling me not to! Rupal, I miss our lunches from my first year and I know you will cringe if I say anything else, so just for you I will make sure your favourite word makes it into my acknowledgments - beautiful.

To the rest of the SL crew, including Bhavina, Naman, Komal, Rishni, Liz, Shubs and Ed. It was an amazing experience being in Yonibana with all of you and I am so glad we still hang out together. Special mention to Shubs and Ed for their terrible, terrible jokes and fake physics theory titles, they were certainly not pun-tastic.

I want to thank Priya for caring as much as she does, it really means a lot to me. Maybe one of these days I may actually do what you tell me to. I hope that you one day somehow edge a six, which I know will make you happy. Which brings me to the Imperial Cricket Club, where I have had some great times through many a season, I want to thank all those I have had the pleasure to share the field with.

To Raj and the rest of DYC, there is only one word I can and need to say - 'true'.

2644, the absolute joy of my life, there are not enough superlatives to describe how lucky I am to be part of this family. To say that you all make me happy would be a severe understatement. I am sure that I would not have the strength and energy to finish this PhD without you. The unequivocal support you have shown me is something most people can only dream of. Preethums, Divoo, Viv, Ash and Shivs, the times I spend with you are the best of my life, and those moments have kept me going throughout this period. I cannot wait for our numerous future gatherings. Chittu, Anu and Jai, the Parliament View era meant the world to me. Seeing you guys everyday during my Masters and first year of my doctorate made the days so much better. Chandar mama, Manjula mami and Vardu, thank you for all that you do for me. I also

really want to thank Uma chitti, who has done so much for me when I was growing up, to me you will always be new. Finally to Sudha chitti and Sethu thatha, you two are more responsible for the person I am today then you possibly could have imagined.

I want to thank all my Madras family, especially Kups, Pattu chittappa and Sai chittappa, for the faith that you have shown in my ability to do this PhD. Over the last three (kotekans) and a half years it has taken me to finish, I know I have had your support and that means a lot to me. Gopal thatha, out of all the people I have ever known, I think you would have been the happiest and proudest person knowing I gained a PhD. I hope you are somehow able to flick through my thesis.

Some random thanks to the legends who brought me much joy during my time in the CQD, namely, Lampard, Drogba et. al. for winning the UEFA Champions League for Chelsea Football Club and Tendulkar, Dhoni et. al. for winning the Cricket World Cup for India. Also to Peter from the sandwich bar for being so friendly. I want to thank Divya B. for all of her support, all the people in my startup world, Kate C. and Vivi for all their help during the Masters.

This thesis would have been a series of nonsensical ramblings if it were not for the following people who kindly offered to proofread my thesis; Lisa, Antony, Didier, Ahsan, Marco, Kate, Pete, Ruben, Fern and my mother. I express to you my eternal gratitude.

I would like to thank in advance Dr. Derek Lee and Dr. Alessio Serafini for agreeing to read this thesis and be my examiners. I very much appreciate the time and effort you have volunteered.

I have to acknowledge all the pre-university academic institutions who provided me with a great platform; Aurobindo, Alexandra Junior School and Langley Grammar School. A special mention has to go to Mr. Coleman, my first teacher in England who did his utmost to help me settle in. To my Physics teachers, especially Mr. Hallows, who nurtured my interest in the subject. Also to my fellow undergrads from Imperial, you made the course enjoyable.

Finally, I would like to thank Imperial College London for sheltering me for over eight years. I knew I wanted to study Physics since the age of seven, and I am so incredibly grateful I had the opportunity to do so. When I think that I will no longer be solving formulas on a wall or learning more about the subject that I love, it fills me with a great sadness; but I sincerely hope that I will return to it one day. It is with a smile on my face that I submit this thesis knowing that I was able to contribute a grain of knowledge to the world, and as the Imperial motto says 'Knowledge is the adornment and protection of the Empire'!

Contents

List of Figures **9**

Nomenclature **10**

Introduction **12**

1 The master equation and approximations **18**
1.1 General Form . . . 18
1.2 Born approximation . . . 19
1.3 Markov approximation . . . 20
1.4 Secular approximation . . . 21
1.5 Concluding remarks . . . 23

2 Gaussian states **25**
2.1 Symplectic Form . . . 26
2.2 Covariance matrix . . . 27
2.3 Symplectic eigenvalues . . . 28
2.3.1 Partial trace approach . . . 29
2.3.2 Explicit approach . . . 29
2.4 Evolving Gaussian states . . . 30
2.4.1 Position and momentum representation . . . 30
2.4.2 Ladder representation . . . 31
2.5 Initial states . . . 32
2.5.1 Single mode vacuum state . . . 33
2.5.2 Single mode thermal state . . . 33
2.5.2.1 Average thermal photon number state . . . 34
2.5.2.2 Thermal state with temperature T . . . 35
2.5.3 Squeezed state . . . 35
2.5.3.1 Single mode squeezed vacuum . . . 36
2.5.3.2 Single mode squeezed thermal state . . . 36
2.5.3.3 Two mode squeezed vacuum state . . . 37
2.6 Calculating quantities from Gaussian states . . . 38
2.6.1 Entanglement . . . 38
2.6.1.1 Entanglement for Gaussian states . . . 39

2.6.1.2 Logarithmic negativity . . . 40
2.6.2 Fidelity . . . 41
2.6.2.1 Single-mode fidelity . . . 42
2.6.2.2 Two-mode fidelity . . . 43
2.7 Concluding remarks . . . 43

3 Entanglement-based non-Markovian behaviour quantifier 44
3.1 Definition and quantification . . . 45
3.1.1 Definition . . . 45
3.1.2 Entanglement-based non-Markovian behaviour quantifier . . . 47
3.2 Analysing coupled oscillators . . . 48
3.2.1 Single bath oscillator . . . 48
3.2.1.1 Entanglement dynamics of a single oscillator . . . 49
3.2.1.2 Analytical expression of entanglement for the large detuning case 50
3.2.1.3 ENMBQ and the single oscillator . . . 54
3.2.2 Analytics for two 'bath' oscillators . . . 56
3.2.2.1 Resonant modes . . . 56
3.2.2.2 A resonant mode and an off-resonant mode . . . 58
3.2.3 Many bath oscillators . . . 63
3.2.3.1 Spectral densities . . . 64
3.2.3.2 Simulation details . . . 67
3.2.3.3 ENMBQ for ohmic baths . . . 67
3.2.3.4 Model 1 with an ohmic bath . . . 68
3.2.3.5 Model 1 with a super ohmic bath . . . 71
3.2.3.6 Model 2 . . . 72
3.2.3.7 Model 3 . . . 74
3.3 Concluding remarks . . . 78

4 Fidelity-based non-Markovian behaviour quantifier 79
4.1 Definition and quantification . . . 80
4.2 Analysis . . . 81
4.2.1 Energy dynamics of two coupled oscillators . . . 81
4.2.2 Fidelity and energy dynamics of an open system . . . 83
4.3 Concluding remarks . . . 85

5 Role of counter rotating terms on the entanglement-based non-Markovian behaviour quantifier 86
5.1 Counter rotating terms . . . 87
5.2 Adapted models . . . 88
5.2.1 Model 4 - Model 1 with counter rotating terms . . . 89
5.2.1.1 Ohmic bath . . . 89
5.2.1.2 Super ohmic bath . . . 91
5.2.2 Model 5 - Model 2 with counter rotating terms . . . 93

5.2.3 Model 6 - Model 3 with counter rotating terms . . . 95
5.3 Concluding remarks . . . 99

6 Finding the limits of the Rotating-Wave approximation 101
6.1 Three oscillator model . . . 102
6.2 Effects of the strong coupling limit . . . 103
6.3 Fidelities and Uhlmann's theorem . . . 110
6.4 Rotating-Wave approximation coupling bound . . . 114
6.5 Finding the instability point of a 'blue'-detuned Hamiltonian . . . 116
6.6 Concluding remarks . . . 118

Conclusions 120

References 124

Appendices 130

Appendix A Derivations of initial states in the covariance matrix formalism 131
A.1 Vacuum state . . . 131
A.2 Thermal state . . . 132
A.3 Average thermal photon number state . . . 133
A.4 Squeezed state . . . 135
A.4.1 Single mode squeezed vacuum state . . . 135
A.4.2 Two mode squeezed vacuum state . . . 137

Appendix B Master equations in a covariance matrix formalism 141
B.1 A markovian master equation . . . 141
B.2 A non-Markovian master equation . . . 142

Appendix C Other Works 144
C.1 Heat and entanglement . . . 144
C.2 Entanglement broadcasting . . . 146

Appendix D Outreach 147
D.1 Science busking . . . 147
D.2 Physics happens in a dark place exhibition . . . 148
D.2.1 Resonance Revenant . . . 149
D.2.2 Systems and Baths . . . 149
D.2.3 Quantum Love . . . 149

List of Figures

3.1 Diagram of single 'bath' mode model 48
3.2 Entanglement dynamics for the single 'bath' mode model 50
3.3 Validity of the entanglement expression for large detuning 54
3.4 Invalidity of the entanglement expression for small detuning 54
3.5 ENMBQ for the single 'bath' oscillator model 55
3.6 Diagram of the two 'bath' mode model 56
3.7 Entanglement of the two resonant 'bath' mode model 57
3.8 Entanglement of a model with multiple resonant 'bath' modes 58
3.9 Effective model for the large detuning case 60
3.10 Validity of the effective large detuning model - $g > h$ 60
3.11 Validity of the effective large detuning model - $g < h$ 61
3.12 Validity of the effective large detuning model - $g = h$ 61
3.13 Effective model for the small detuning case 62
3.14 Validity of the effective small detuning model - $g > h$ 63
3.15 Validity of the effective small detuning model - $g < h$ 63
3.16 Validity of the effective small detuning model - $g = h$ 64
3.17 Diagram of Model 1 64
3.18 Ohmic spectral density 66
3.19 Super ohmic spectral density 66
3.20 Scaling effect of the squeezing parameter 67
3.21 ENMBQ for Models 1-3 with an ohmic bath 68
3.22 Entanglement dynamics for Model 1 with an ohmic bath 69
3.23 Occupancy for Model 1 with an ohmic bath 70
3.24 ENMBQ for Model 1 with a super ohmic bath 71
3.25 Entanglement dynamics for Model 1 with a super ohmic bath 72
3.26 Occupancy for Model 1 with a super ohmic bath 73
3.27 Diagram of Model 2 73
3.28 Entanglement dynamics for Model 2 74
3.29 Occupancy for Model 2 75
3.30 Diagram of Model 3 76
3.31 Entanglement dynamics for Model 3 76
3.32 Occupancy of the bath modes for Model 3 77

4.1 Diagram of the single 'bath' mode model 81

4.2 Energy dynamics of single 'bath' mode model 82
4.3 Diagram of the open system model 83
4.4 Fidelity dynamics between a pair of squeezed thermal states 83
4.5 Energy dynamics for a pair of squeezed thermal states 84

5.1 Non-Markovianity of Models 1 and 4 with an ohmic bath 89
5.2 Entanglement dynamics for Model 4 with an ohmic bath 90
5.3 Occupancy of bath modes for Model 4 with an ohmic bath 90
5.4 Non-Markovianity of Models 1 and 4 with a super ohmic bath 91
5.5 Entanglement dynamics for Model 4 with a super ohmic bath 92
5.6 Occupancy of bath modes for Model 4 with a super ohmic bath 92
5.7 Non-Markovianity of Models 2 and 5 93
5.8 Non-Markovianity of Models 2 and 5 for small alpha 94
5.9 Entanglement dynamics for Model 5 94
5.10 Occupancy of the bath modes for Model 5 95
5.11 Non-Markovianity of Models 3 and 6 96
5.12 Non-Markovianity of Models 3 and 6 for small alpha 96
5.13 Entanglement dynamics for Model 6 97
5.14 Occupancy of the bath modes for Model 6 97
5.15 Entanglement dynamics for Model 6 for small alpha 98
5.16 Occupancy of the bath modes for Model 6 for small alpha 98

6.1 Three oscillator model 102
6.2 Scaling of coupling terms in M1 110
6.3 Scaling of coupling terms in M2 110
6.4 Fidelity between M1 and M2 for $\epsilon = 0.1$ - bare modes 111
6.5 Fidelity between M1 and M2 for $\epsilon = 0.01$ - bare modes 111
6.6 Fidelity between M1 and M2 for $\epsilon = 0.1$ - normal modes 113
6.7 Fidelity between M1 and M2 for $\epsilon = 0.01$ - normal modes 113
6.8 Maximum fidelity bound for the three oscillator model 114
6.9 Maximum fidelity bound for varying α and $\bar{m}$ 115
6.10 Fidelity bound for a blue detuned Hamiltonain 118

C.1 Model to investigate heat flow 144
C.2 Model to investigate entanglement broadcasting 146

D.1 Tibetan singing bowl 148
D.2 Resonance Revenant 150
D.3 Systems and Baths 151
D.4 Quantum Love 152

Nomenclature

CM	Covariance matrix
CR	Counter rotating
CV	Continous variable
ENMBQ	Entanglement-based non-Markovian behaviour quantifier
EO	Entanglement oscillation
FNMBQ	Fidelity-based non-Markovian behaviour quantifier
GS	Gaussian state
NM	Non-Markovian
NMB	Non-Markovian behaviour
OQS	Open quantum system
RWA	Rotating-Wave approximation

Introduction

In 1900 Max Planck hypothesised the existence of *quanta*, energy elements that discretised the energy spectrum of a physical system [1] and thus, in this moment, quantum theory was born. Extensive work was undertaken in the early part of the twentieth century to establish the foundations of this newly found field by (now) world famous physicists such as Planck, Bohr, Heisenberg, de Broglie, Compton, Einstein, Schrödinger, Born, von Neumann, Dirac, Fermi, Pauli, Hilbert and Bose to name but a few. The culmination of this preliminary work was undoubtedly the Fifth Solvay International Conference in October 1927 which hosted twenty-nine of the most notable physicists at the time, seventeen of whom held or would hold Nobel prizes. The nature of the '*Electrons et photons*' event was to decide the future of quantum physics and ultimately it was Bohr's view of the quantum world that has been engrained into the study of this field.

One-hundred and fifteen years since its inception, quantum mechanics still lies at the forefront of our curiosity in unlocking the secrets of the universe, and in recent years there has been vested interest in the development of quantum technologies. Indeed there has not only been significant investment by governments and universities but also large technology companies who see quantum mechanics as the next major step for technology and computing. This has piqued public interest in the subject and physicists usually attempt to communicate the complicated strangeness of quantum mechanics through the, now infamous, thought experiment '*Schrödinger's cat*'. At the climax of this story, an audience who are unfamiliar with the workings of quantum theory would, quite rightly, question why we do not witness half-dead cats strutting the streets of the world. The answer to this is in fact the exact reason why quantum technologies are difficult to build. When a quantum system interacts with many other quantum mechanical objects, it severely affects its behaviour and in most cases destroys its '*quantum-ness*' entirely. This is known as an *open quantum system* (OQS).

A closed physical system by definition, whether classical or quantum, can be described in its

entirety by an equation of motion. This is clearly an ideal scenario, as one can make predictions on the state of the system at any point in time. The result of a measurement on the system will depend on whether we are discussing a classical or quantum object, but in both cases it tells us the most we could ever hope to learn about the model. When the system of interest is coupled to a secondary quantum system, it will necessarily affect its behaviour. Combined, they are still considered to be a closed system unless this second quantum system is considerably larger than the first. In the latter case the secondary object is known as an environment, bath or reservoir, and the first an OQS. One could argue that this is still just part of one large closed system which technically is true, but practically it results in an intractable amount of information that makes it difficult to have a complete microscopic description. Consequently one has to resort to a simpler, effectively probabilistic description of the open system's dynamics.

Historically, this statistical approach was first seen in one of Einstein's 1905 papers, specifically the theory of Brownian movement [2]. In fact from the outset of quantum theory, OQSs have been synonymous with realistic quantum-mechanical models where it was utilised to describe dissipation and damping effects. As one can imagine, this has led to significant developments on the subject for a broad range of fields; quantum optics, quantum measurement theory, quantum information, quantum cosmology, condensed matter systems, biophysics and even some aspects of chemical physics. The discussion of these advancements is far too vast for the scope of this introduction but can be found in many books and reviews [3–11]. It is worth mentioning however that for our particular field of interest, quantum optics, OQSs became relevant at the dawn of coherent light, i.e a laser. Like all other sources of light, a laser is an open system which requires quantum theory to account for dissipative effects [12, 13]. These damping and dissipative effects, caused by the interaction with an environment, act to destroy the quantum coherences of the OQS. This is known as *decoherence*, and remains a problem for all quantum technologies to date.

As mentioned earlier, there is at present tremendous investment in quantum technologies which could one day produce the current holy grail of the quantum world; the world's first universal quantum computer. Unlike a classical computer based on bits of information, a quantum computer would operate with quantum bits (qubits) which can exist in a superposition of zero and one. Consequently this leads to a significant speed-up in the run-time of a substantial set of algorithms. In the modern age, where computers are engrained into all aspects of daily life, it truly would be a monumental discovery that will go down as a critical juncture of human

history.

As one can imagine, there are many research groups all around the world that are chasing this golden goose of physics with a variety of possible experimental realisations. These range from ion traps, cold atoms and molecules, nuclear magnetic resonance and superconducting qubits to quantum dots, optical lattices, linear optics, Bose-Einstein condensates and nitrogen-vancany centres. Despite all these attempts, it remains a significant experimental challenge to isolate the quantum systems of interest from their environment. Therefore, decoherent effects come into play, which effectively nullify the advantages quantum mechanics allows for. Thus, many realistic quantum-mechanical models are formulated in the framework of OQSs.

Current research into OQSs is not restricted to the understanding of decoherence for the interests of quantum computing. For instance, there is noteworthy work in the description of quantum effects on macroscopic systems. Specific examples include dephasing and decoherence in photosynthesis, memory effects in bio and solid state physics and the detrimental ramifications in the construction of macroscopic superposition states in the field of optomechanics.

Essentially, the modus operandi for OQSs research is to gain a better understanding of the effects that play a significant role in the dynamics of macroscopic processes and quantum technologies. Any knowledge garnered about OQSs could then be potentially used to manipulate, maintain and control the flow of quantum information, the importance of which has been clearly highlighted above. Thus it is the aim of this thesis to further the field in a similar vein, and gain a better understanding of OQSs, explicitly for the scenario of a series of coupled harmonic oscillators.

As stated previously, OQSs yield an unmanageable amount of information and there are several theoretical methods that deal with this issue in various ways. The most common technique to describe an OQS is the master equation approach, where environmental modes are traced out to leave an equation of motion for the density matrix of the system. The master equation was developed by Pauli in 1928 to describe a many-state quantum system using transition probabilities gained from perturbation theory [14]. This method was slow to gain popularity but subsequent advancements from people such as Wigner and Weisskopf [15], Nakajima [16], Zwanzig [17], van Hove [18], Emch [19] and Agarwal [20] has seen the approach propelled to the top of the OQS food chain with countless papers published on the subject. The basics of this method are outlined in Chapter 1, where we also cover a series of approximations which are usually applied to make the problem more tractable. Specifically these are the Born, Markov and

secular approximations which, more or less, ignore changes in the environment state, memory effects and fast oscillating terms respectively. Although this technique has proved successful in many scenarios it does have restrictions, namely the presence of approximations and the inability to analyse the environment.

Throughout this thesis we avoid approximations by utilising the theory of Gaussian states (GSs) which is covered in Chapter 2. Many states in quantum information theory, such as the vacuum state in quantum electrodynamics and the majority of experimentally accessible states, are in fact GSs. It is therefore not of great hindrance that we restrict ourselves to an exclusive investigation of GSs. The crucial advantage gained is the ability to use the covariance matrix (CM) approach. The CM methodology allows us to investigate a large, finite set of coupled harmonic oscillators to effectively simulate an OQS. The caveat being that only Hamiltonians of bi-linear form are used, in order to maintain the state of the model as a GS. However it has no provisos which require the Born, Markov or secular approximations and it consents to a direct analysis of the environment.

For many OQSs a master equation approach employing the Markov approximation cannot reliably describe the dynamical behaviour of a model. This is the case, for example, in a number of solid state or biological systems. The Markov approximation implies that the evolution of the system is only dependent on its current state, i.e. the future dynamics do not depend on its previous trajectory. This is not valid for some models, where the effect of non-Markovian behaviour (NMB) cannot be neglected. In recent times, a line of research has been aimed at quantifying the amount of NMB in a given model.

Chapter 3 describes the definition of non-Markovianity we adopt in order to quantify the NMB in the models we investigate, and concentrates on an entanglement-based NMB quantifier which we term the ENMBQ. The analysis starts with the entanglement dynamics of systems which consider interactions between two and three modes, giving an intuition as to the factors that could affect an OQS. Four OQS models are considered. The first two are the paradigmatic scenario of a quantum harmonic oscillator coupled to an environment of bosonic bath modes with beam-splitter like interactions for two different spectral densities. The other two models add a single strongly coupled oscillator to the model in an extra bath mode and 'buffer' configurations. The motivation here is to comprehend how NMB is altered by changing the structures of the environment. Chapter 4 delves into a brief investigation of another quantifier of NMB based on fidelity. Coined the FNMBQ it aims to draw parallels with the ENMBQ in order to find an

underlying cause for NMB. The overall aim is to recognise the effect various bath modes have on the quantifiers. Not only is this exercise useful for our knowledge of NMB, but it could be utilised to manipulate how and when quantum information can be fed back to the system.

As mentioned, the models that were studied used beam-splitter like interactions, which have applied what is known as the Rotating-Wave approximation (RWA). The RWA removes the fast oscillating terms from the Hamiltonian, which are known as the counter rotating (CR) terms. In fact there are many models which cannot make the RWA, particularly ones that involve strong couplings, thus requiring CR terms to be included in the Hamiltonian that describes them. In Chapter 5 we scrutinise the four models in Chapter 3 with CR terms now included and observe the effect this has on the NMB predicted by the ENMBQ.

Coupled harmonic oscillators have been used to describe a multitude of physical experiments and phenomena. Whether it is the study of optomechanical systems or electromechanical devices, understanding even a few oscillators provides an interesting insight into the models describing these physical events. A significant portion of this work has focused on oscillators which display strong coupling between them, i.e. CR terms become important in describing the dynamics. When one usually considers an OQS, the system-bath couplings apply a RWA since a weak coupling to the environment is assumed. However, there has been some work showing that, when considering a strongly coupled system, a weak coupling approximation to the environment may not accurately describe the model. Chapter 6 shows our attempt to understand when the application of the RWA is appropriate: with the simplest possible scenario, a three oscillator model; with a strongly coupled pair of oscillators; and a single weakly coupled oscillator. Moreover we describe a fidelity-based methodology that could be applied to any model, including OQSs, to understand whether an RWA coupling could be applied for the parameter regime used by the investigator.

Simply, this thesis uses an uncommon methodology for OQSs, i.e. covariance matrices, which allows us to gain a better understanding of the approximations, particularly the Markov approximation and the RWA, that surround the theory behind it. Along with our ability to analyse the environment directly, the understanding or intuition we have developed could prove invaluable in the development of quantum technologies.

There are four appendices included within this thesis; Appendix A includes detailed calculations of initial states in the CM formalism. Appendix B displays how two particular master equations can be described in a CM formalism. Appendix C outlines works based on heat and

entanglement broadcasting that can be undertaken in relation to coupled oscillators, and finally Appendix D chronicles the outreach activities that have been undertaken during this PhD that are directly related to this particular field of study.

Please note that, throughout this thesis, natural units are applied, i.e. $\hbar = c = k_B = 1$, for simplicity.

Chapter 1

The master equation and approximations

The dynamics of an OQS can be described by two principle methods based on the two pictures of quantum mechanics. The quantum Langevin equation, first proposed by Senitzky to explain dissipation in a quantum harmonic oscillator model [12], is based on the Heisenberg equation which depicts the model by the evolution of the operators that describe the OQS and the environment. The more common approach is to represent the OQS by an equation of motion for its density matrix, i.e. working in the Schrödinger or interaction picture. This equation of motion is called the (quantum) master equation and was first used by Pauli [14] to describe a many-state quantum system. This chapter covers a brief derivation of the master equation, primarily to introduce the approximations which are commonly used within that derivation.

1.1 General Form

We follow the derivation of the master equation outlined in '*The theory of open quantum systems*' by Breuer and Petruccione [9]. The Hamiltonian for a OQS has three components; the Hamiltonian for the system (S), the Hamiltonian for the environment (E) and finally the Hamiltonian for the system - environment interaction (SE)

$$H = H_S + H_E + H_{SE}. \tag{1.1}$$

The dynamics of the density matrix of a system with the above Hamiltonian is given by the von Neumann equation

$$\frac{d\rho(t)}{dt} = -i\left[H_{SE}(t), \rho(t)\right]. \tag{1.2}$$

Note that we are now in the interaction picture and accordingly only include H_{SE}. In its integral form the equation can be written as

$$\rho(t) = \rho(0) - i\int_0^t ds\left[H_{SE}(s), \rho(s)\right]. \tag{1.3}$$

Substituting Eq. (1.3) into Eq. (1.2) and tracing out the environment we find an equation to describe the dynamics of the system

$$\frac{d\rho_S(t)}{dt} = -i\,\mathrm{Tr}_E\left[H_{SE}(t), \rho(0)\right] - \int_0^t ds\,\mathrm{Tr}_E\left[H_{SE}(t), \left[H_{SE}(s), \rho(s)\right]\right]. \tag{1.4}$$

Assuming no initial correlation between system and environment, and that the environment operators are trace zero, we are left with the following equation

$$\frac{d\rho_S(t)}{dt} = -\int_0^t ds\,\mathrm{Tr}_E\left[H_{SE}(t), \left[H_{SE}(s), \rho(s)\right]\right]. \tag{1.5}$$

A series of approximations are applied to the equation above to make the computation more tractable. We now proceed to outline a few of these approximations.

1.2 Born approximation

The most common simplification made is the Born approximation, sometimes referred to as the weak-coupling approximation. Eq. (1.5) shows that the system dynamics is dependent on $\rho(s)$, the density matrix of the entire model. In order to simplify the expression we remove this dependence by making the Born approximation.

The system-environment coupling necessarily causes correlations to be created between them, by assuming that this coupling is weak we restrict ourselves to the first order in H_{SE} effectively reducing it to an uncorrelated state. Additionally the environment is assumed to be very large to ensure that it is unaffected by the coupling. The justification is that the environment is in thermal equilibrium and the excitations caused by the system is not resolved within the characteristic time scale of the system. These assumptions allow us to express the total

density matrix at time s as

$$\rho(s) \approx \rho_S(s) \otimes \rho_E. \tag{1.6}$$

Eq. (1.5) can thus be written as

$$\frac{d\rho_S(t)}{dt} = -\int_0^t ds\, \mathrm{Tr}_E \left[H_{SE}(t), \left[H_{SE}(s), \rho_S(s) \otimes \rho_E\right]\right]. \tag{1.7}$$

1.3 Markov approximation

To simplify the expression further one makes the Markov approximation which states that the evolution of the state is only dependent on its current state, i.e. it has no memory of its previous states. (The precise definition of Markovianity is discussed in greater detail in Chapter 3.) This approximation is valid when the environment correlation functions (shown later in Eq. (1.19)) are short-lived, and therefore the system state at time s can be replaced by that at present time t without significant loss of accuracy. Thus $\rho_S(s)$ is replaced by the present state of the system $\rho_S(t)$ in Eq. (1.7) giving us the Redfield equation

$$\frac{d\rho_S(t)}{dt} = -\int_0^t ds\, \mathrm{Tr}_E \left[H_{SE}(t), \left[H_{SE}(s), \rho_S(t) \otimes \rho_E\right]\right]. \tag{1.8}$$

The Redfield equation still depends on the initial state of the system which implies that the system dynamics cannot always be described by a quantum dynamical semigroup. This is important because the generators of a quantum dynamical semigroup preserves complete positivity (CP) (see Ref. [9]) and thus maintains the physical interpretation of the density matrix. The full Markov approximation also includes the assumption that the relaxation time of the open system τ_R, over which the system changes noticeably, is much longer when compared to τ_E, the characteristic time scale of the environment. This amounts to replacing s with $t - s$ in the Redfield equation and letting the upper limit of the integral go to infinity since the assumption allows the integrand to disappear sufficiently fast for $s \gg \tau_E$

$$\frac{d\rho_S(t)}{dt} = -\int_0^\infty ds\, \mathrm{Tr}_E \left[H_{SE}(t), \left[H_{SE}(t-s), \rho_S(t) \otimes \rho_E\right]\right]. \tag{1.9}$$

This expression is known as the Born-Markov master equation.

1.4 Secular approximation

The Born-Markov approximation does not always guarantee that Eq. (1.9) defines the generator of a quantum dynamical semigroup [21]. This is achieved by enforcing the secular approximation which averages over the fast oscillating terms in the master equation. To identify the fast oscillating terms we decompose H_{SE} into operators of the system and the environment

$$H_{SE} = \sum_{\alpha} A_{\alpha} \otimes B_{\alpha} \tag{1.10}$$

where A_{α} and B_{α} are Hermitian matrices that act on the system and environment respectively. The A_{α} operator is split into eigenoperators of H_S by discretising the energy spectrum of the system into eigenvalues ϵ

$$A_{\alpha}(\omega) \equiv \sum_{\epsilon' - \epsilon = \omega} \Pi(\epsilon) A_{\alpha} \Pi\left(\epsilon'\right) \tag{1.11}$$

where $\Pi(\epsilon)$ are projectors onto the eigenspace of ϵ. The summation is made over all the eigenvalues, which have a fixed separation of ω, implying that $A_{\alpha}(\omega)$ follows the commutation relations

$$\begin{aligned} \left[H_S, A_{\alpha}(\omega)\right] &= -\omega A_{\alpha}(\omega) \\ \left[H_S, A_{\alpha}^{\dagger}(\omega)\right] &= \omega A_{\alpha}^{\dagger}(\omega). \end{aligned} \tag{1.12}$$

The relations show $A_{\alpha}(\omega)$ and $A_{\alpha}^{\dagger}(\omega)$ are eigenoperators of H_S with eigenvalues $-\omega$ and ω respectively. Summing over all these eigenoperators we get

$$\sum_{\omega} A_{\alpha}(\omega) = \sum_{\omega} A_{\alpha}^{\dagger}(\omega) = A_{\alpha} \tag{1.13}$$

due to the completeness relation [22]. This allows us to write Eq. (1.10) as

$$H_{SE} = \sum_{\alpha,\omega} A_{\alpha}(\omega) \otimes B_{\alpha}. \tag{1.14}$$

In the interaction picture the Hamiltonian is of the form

$$H_{SE}(t) = \sum_{\alpha,\omega} e^{iH_S t} A_{\alpha}(\omega) e^{-iH_S t} \otimes e^{iH_E t} B_{\alpha} e^{-iH_E t}. \tag{1.15}$$

Eq. (1.12) allows the following substitution

$$e^{iH_S t} A_\alpha(\omega)\, e^{-iH_S t} = e^{-i\omega t} A_\alpha(\omega) \tag{1.16}$$

and by defining $e^{iH_E t} B_\alpha e^{-iH_E t} = B_\alpha(t)$, the interaction Hamiltonian in the interaction picture becomes

$$H_{SE}(t) = \sum_{\alpha,\omega} e^{-i\omega t} A_\alpha(\omega) \otimes B_\alpha(t)\,. \tag{1.17}$$

Substituting this into the Born-Markov master equation (Eq. (1.9)) we obtain after some algebra

$$\begin{aligned} \frac{d\rho_S(t)}{dt} = &\sum_{\omega,\omega'} \sum_{\alpha,\beta} e^{i(\omega'-\omega)t} \Gamma_{\alpha\beta}(\omega) \left(A_\beta(\omega)\, \rho_S(t)\, A_\alpha^\dagger(\omega') - A_\alpha^\dagger(\omega')\, A_\beta(\omega)\, \rho_S(t) \right) \\ &+ h.c.. \end{aligned} \tag{1.18}$$

Here $h.c.$ refers to the hermitian conjugate of the expression and the one-sided Fourier transforms of the reservoir correlation functions, $\Gamma_{\alpha\beta}(\omega)$, are defined as

$$\begin{aligned} \Gamma_{\alpha\beta}(\omega) &\equiv \int_0^\infty ds e^{i\omega s}\, \mathrm{Tr}_B \left[B_\alpha^\dagger(t)\, B_\beta(t-s)\, \rho_B \right] \\ &\equiv \int_0^\infty ds e^{i\omega s} \langle B_\alpha^\dagger(t)\, B_\beta(t-s) \rangle \end{aligned} \tag{1.19}$$

where $\langle B_\alpha^\dagger(t)\, B_\beta(t-s)\rangle$ are the environment correlation functions. Note the Markov approximation assumes that it is these correlation functions that decay sufficiently fast over τ_E which is much smaller than τ_R, i.e. the correlations in the environment do not last long enough to feed back into the system.

The secular approximation considers τ_S, the characteristic time scale of the system, given by $|\omega' - \omega|^{-1}$, $\omega' \neq \omega$. If $\tau_S \ll \tau_R$ one can ignore the terms which are proportional to $\exp[i(\omega' - \omega)t]$ for $\omega' \neq \omega$. This is because they oscillate rapidly when compared to the relaxation time of the OQS, τ_R, over which ρ_S varies significantly. Therefore, we can express Eq. (1.18) as

$$\frac{d\rho_S(t)}{dt} = \sum_{\omega} \sum_{\alpha,\beta} \Gamma_{\alpha\beta}(\omega) \left(A_\beta(\omega)\, \rho_S(t)\, A_\alpha^\dagger(\omega) - A_\alpha^\dagger(\omega)\, A_\beta(\omega)\, \rho_S(t) \right) + h.c.. \tag{1.20}$$

Parameterising this, the above equation can be rewritten into a simple general form of the

master equation

$$\frac{d\rho_S(t)}{dt} = \mathcal{L}(\rho_S) = -i[H_{LS}, \rho_S(t)] + \mathcal{D}(\rho_S(t)) \tag{1.21}$$

where

$$H_{LS} = \sum_{\omega} \sum_{\alpha,\beta} S_{\alpha\beta}(\omega) A_\alpha^\dagger(\omega) A_\beta(\omega) \tag{1.22}$$

and is often called the Lamb-shifted Hamiltonian (since it leads to a reorganisation of the unperturbed energy levels due to the system-environment coupling and is analogous to a Lamb-type shift). $S_{\alpha\beta}(\omega)$ is given by

$$S_{\alpha\beta}(\omega) = \frac{1}{2i}\left(\Gamma_{\alpha\beta}(\omega) - \Gamma_{\beta\alpha}^*(\omega)\right). \tag{1.23}$$

In Eq. (1.21) we also have $\mathcal{D}(\rho_S(t))$ which is known as a dissipater and has the form

$$\mathcal{D}(\rho_S(t)) = \sum_{\omega} \sum_{\alpha,\beta} \gamma_{\alpha\beta}(\omega) \left(A_\beta(\omega) \rho_S A_\alpha^\dagger(\omega) - \frac{1}{2}\{A_\alpha^\dagger(\omega) A_\beta(\omega), \rho_S\} \right) \tag{1.24}$$

where

$$\gamma_{\alpha\beta}(\omega) = \Gamma_{\alpha\beta}(\omega) + \Gamma_{\beta\alpha}^*(\omega). \tag{1.25}$$

By diagonalising the $\gamma(\omega)$ matrices, Eq. (1.21) is said to be of Lindblad form. The importance of which being that when a master equation is in this form it is a generator of a quantum dynamical semigroup ($\mathcal{L}$). This ensures that the density matrix for the system, ρ_S, remains positive semi-definite.

1.5 Concluding remarks

In this chapter we have shown a brief derivation and applications of the approximations that lead to a Lindblad-form master equation, the most commonly used equation of motion to describe an OQS. Despite its extensive use there remains significant investigation into models where these approximations may not be valid. The validity of the Born approximation has been questioned by considering the weak coupling limit for both the time dependent [23–26] and stationary [26, 27] cases.

For many models the Markov approximation is not valid, particularly scenarios where the short time dynamics play a crucial role, examples include solid-state and biological systems

[28–32]. The first two approaches to a non-Markovian equation of motion were the Nakajima-Zwanzig approach using projection operators [16, 17] and the time-convolutionless projection operator approach [33, 34]. Since then there has been significant advances in this particular field including some exact solutions for particular systems. A few examples of these works can be found in various papers and books shown in Ref. [5, 9, 35–42]. A significant part of this thesis is dedicated to understanding when this approximation is no longer valid, including the definition, quantification of non-Markovian behaviour (NMB) and the parameters that affect it (see Chapters 3-5).

With recent advances in quantum technologies stronger interactions are being observed and subsequently there has been interest in the application of the Rotating-Wave approximation [43–48]. Once again this approximation is investigated in greater detail later in this thesis in Chapters 5 and 6.

The next chapter describes the theory and methodology which allows us to effectively simulate an OQS without requiring approximations to make the problem tractable. Moreover this technique also allows for an investigation of the environment.

Chapter 2

Gaussian states

The aim of quantum technologies is to process quantum information, and there exist two general schemes to achieve this goal. One can encode the information in a discrete, finite-dimensional system, termed the 'digital' approach, or in the degrees of freedom of a continuous spectrum, the 'analog' approach [49–51].

Quantum bits or *qubits* are the most common implementation of the finite-dimensional approach, where the information is represented in a 2-D system, e.g. the polarisation of a photon, nuclear spins or ground-excited states of ions.

In *continuous variables* (CVs) models the information is encoded in the continuous spectrum of infinite-dimensional operators, which obey the canonical commutation relations. The paradigmatic scenario is the quantum harmonic oscillator which can be described by CVs, specifically the position and momentum. The motivation for utilising CV systems is the ease of implementation; for example in quantum optics, one uses the continuous quadrature amplitudes of the quantised electromagnetic field. The quadratures can be measured using homodyne detection and optical modes displaced in phase space through feedforward techniques. The drawback of CV entanglement-based quantum protocols is that they are imperfect, whereas a discrete system would be, in principle, perfect. In general, for quantum optical realisations the trade-off is between the efficiency of the implementation and the quality of the prepared states. Other examples of CV quantum systems include vibrational modes of solids (phonons), atomic ensembles, Josephson junctions and Bose-Einstein condensates.

The fact that a CV system describes the propagation of the electromagnetic field, highlights its relevance for quantum communication and quantum-limited techniques for sensing, detection and imaging. In addition, quantum operations such as cloning, teleportation and entanglement

purification are all possible in CV systems [49–52]. A particularly useful subset of CVs are Gaussian states (GSs).

Although the most common way to express quantum dynamics is to utilise states in a particular Hilbert space and unitary operations which act on said states, it is not the only way to characterise the system. In 1932 Wigner developed a method to describe a quantum system in phase space using the 'characteristic function' [53]. If this function is Gaussian in nature then the state is referred to as a GS [54]. They are an important field of interest, the basic reason for which stems from the fact that the vacuum state in quantum electrodynamics is a GS. It also appears in various other setups such as optomechanics, trapped ions, atomic ensembles and quantum optics [49]. With current technology the most accessible states experimentally are GSs, and the evolutions of these states are governed by Hamiltonians which are at most bi-linear. The advantage of bi-linear evolutions is that they maintain the Gaussian nature of the state in phase space. In addition to the fact that tracing out a mode(s) from a multipartite GS preserves the Gaussian nature makes this a valuable mathematical tool in describing the dynamics of CV systems.

This chapter briefly covers some of the basic background theory behind GSs which are utilised in this thesis. More detailed and complete descriptions of GSs can be found in many books and reviews, such as those in Refs. [40, 49–52, 55]. The formalism outlined in this chapter will allow us to describe the quantum state of our models at any given time. This is achieved through what is known as the covariance matrix (CM) approach. All the models contained in this thesis are characterised by bi-linear Hamiltonians and initial GSs. These properties allow us to make use of the Gaussian formalism for our purposes.

2.1 Symplectic Form

An N-mode CV system contains infinite degrees of freedom, making it intractable, but if expressed in *symplectic* form it can be described in a 2N-dimensional vector space. Here N denotes the number of bosonic modes for a given system (which in this thesis will be the number of quantum harmonic oscillators). By arranging the position and momentum operators of the modes into a basis of the form

$$R^T = (\hat{x}_1, \hat{x}_2, ..., \hat{x}_n, \hat{p}_1, \hat{p}_2, ..., \hat{p}_n) \tag{2.1}$$

and imposing the canonical commutation relations, we obtain

$$[R_a, R_b] = i\sigma_{ab} \tag{2.2}$$

where σ is known as the symplectic matrix

$$\sigma = \begin{pmatrix} 0 & \mathbb{1}_n \\ -\mathbb{1}_n & 0 \end{pmatrix} \tag{2.3}$$

and $\mathbb{1}_n$ is an identity matrix of dimension n. This symplectic form is important because any canonical transformations of the vector R can be described by a 2N-dimensional symplectic matrix, S, which preserves the kinematic relations brought upon by the canonical commutation relations. Mathematically, $R'_a = S_{ab}R_b$ provided that $S\sigma S^T = \sigma$. These symplectic transformations are therefore a set of linear transformations on a 2N-dimensional vector space which preserves the non-degenerate, skew-symmetric, bi-linear form, i.e. symplectic form.

2.2 Covariance matrix

As mentioned previously, a state can be represented in phase space and the dynamics can be described by considering functions on the aforementioned phase space. The phase space distribution best suited for GSs is the Wigner function [53, 54].

A phase space representation is constructed by assigning a weight function $w(\alpha)$ to each density matrix ρ, where α represents a point in phase space. The expectation value of an operator, $\hat{O}$, is found by expressing the operator as a function, $f(\alpha)$, and calculating an integral over the complex plane

$$\mathrm{Tr}\left[\rho\hat{O}\right] = \int w(\alpha) f(\alpha) d^2\alpha. \tag{2.4}$$

The quantum characteristic function $\chi_\rho(\xi)$ uses the Weyl operator W_ξ.

$$\begin{aligned} \chi_\rho(\xi) &= \mathrm{Tr}\left[\rho W_\xi\right] \\ W_\xi &= e^{i\xi^T\sigma R} \qquad\qquad \xi \in \mathbb{R}^{2n} \end{aligned} \tag{2.5}$$

The state of a system can be found from the characteristic function through the Fourier-Weyl

transform

$$\rho = \frac{1}{(2\pi)^{2n}} \int d^{2n}\xi \chi_\rho(-\xi) W_\xi. \tag{2.6}$$

GSs are then defined as the states for which the characteristic function is a Gaussian function in phase space [54]

$$\chi_\rho(\xi) = \chi_\rho(0) e^{-\frac{1}{4}(\sigma\xi)^T \gamma(\sigma\xi) - d^T(\sigma\xi)}. \tag{2.7}$$

As shown above, the Gaussian function can be completely specified by d and γ, its first and second moments respectively. The first moments give the expectation values of the canonical coordinates $d_j = \mathrm{Tr}[R_j\rho]$ and the second moments are given by the *covariance matrix* (CM), γ, shown below

$$\gamma_{jk} = 2Re\,\mathrm{Tr}[\rho(R_j - \langle R_j\rangle_\rho)(R_k - \langle R_k\rangle_\rho)]. \tag{2.8}$$

This expression is often simplified by reducing the first moments to zero by making local translations in phase space. Thus the state can be described in its entirety using the following form of the CM

$$\gamma_{jk} = 2Re\,\mathrm{Tr}[\rho R_j R_k] = 2Re\langle R_j R_k\rangle \tag{2.9}$$

which is used throughout this thesis. The CM is a $2N \times 2N$ real and symmetric matrix, but it must also satisfy the uncertainty principle to adhere to quantum theory [56]. Using the commutations relations given above, it is possible to show the following condition

$$\gamma + i\sigma \geq 0 \tag{2.10}$$

which implies the positive definiteness of the CM, i.e. $\gamma > 0$. Eq. (2.10) is sometimes referred to as the *physicality condition* because any physical state has to obey it, i.e. it satisfies Heisenberg's uncertainty principle. Additionally, for GSs it is a necessary and sufficient condition to ensure the positivity of the density matrix, ρ [57].

2.3 Symplectic eigenvalues

An important property of the CM is the applicability of Williamson's theorem [58]. It states that every positive definite real matrix of even dimension can be expressed in diagonal form by a symplectic transformation. Given that a CM, γ, represents an N-mode state, there exists a

symplectic matrix S such that

$$\gamma = S\gamma^{(d)}S^T \tag{2.11}$$

where the diagonal matrix $\gamma^{(d)}$ is known as the Williamson form of γ, and is given by

$$\gamma^{(d)} := \bigoplus_{k=1}^{N} \lambda_k \mathbb{1}_N. \tag{2.12}$$

The positive quantities λ_k are called the symplectic eigenvalues of the CM. The importance of the symplectic spectrum is that it provides simple, effective methods to express the fundamental properties of the corresponding quantum state. For example, the physicality condition given in Eq. (2.10) can now be expressed in terms of the symplectic eigenvalues

$$\lambda_k \geq 1 \tag{2.13}$$

given that the CM is positive definite. For our purposes we utilise the symplectic eigenvalues to calculate the logarithmic negativity (Section 2.6.1) but it can also be used to find other quantities such as the von Neumann entropy [51, 59]. We now briefly outline two possible approaches to obtain the symplectic eigenvalues of a CM.

2.3.1 Partial trace approach

To find the symplectic eigenvalues one can use the partial transpose of the CM, γ^{T_S}, where the superscript T_S is the partial transpose operation (see Section 2.6.1.1). To find the symplectic eigenvalues of γ^{T_S}, as shown in Ref. [60], one need only find the positive eigenvalues of the following matrix, Y,

$$Y = i\sigma\gamma^{T_S} \tag{2.14}$$

where σ is the symplectic matrix.

2.3.2 Explicit approach

As shown in Refs. [52, 61] the symplectic eigenvalues can also be calculated explicitly from the components of the CM. Since we only consider the two-mode entanglement in this thesis, we have

$$\lambda_{k\pm} = \sqrt{\frac{I_T \mp \sqrt{I_T^2 - 4I_4}}{2}} \tag{2.15}$$

where

$$I_T = I_1 + I_2 - 2I_3 \tag{2.16}$$

with

$$\begin{aligned} I_1 &= \gamma_{11}\gamma_{33} - \gamma_{13}\gamma_{31} \\ I_2 &= \gamma_{22}\gamma_{44} - \gamma_{24}\gamma_{42} \\ I_3 &= \gamma_{12}\gamma_{34} - \gamma_{14}\gamma_{32} \\ I_4 &= Det\ \gamma. \end{aligned} \tag{2.17}$$

Note that this is true for the case where the CM is in the position-momentum basis and has the ordering shown in Eq. (2.1) for a two mode system.

2.4 Evolving Gaussian states

Utilising GSs gives two distinct advantages. Firstly, Hamiltonians which are quadratic in canonical position and momentum operators (such as for a quantum harmonic oscillator) preserve the Gaussian nature when they act on a GS. Secondly, when the partial trace of a GS is taken it will remain a GS [40]. This is an important property when working with OQS where partial trace operations are often needed. There are two possible symplectic basis one can choose to represent the GS, the position-momentum and ladder representations.

2.4.1 Position and momentum representation

A possible choice for the symplectic basis, R, is the position and momentum representation, as given by Eq. (2.1). This allows us to express a Hamiltonian in the following form

$$H = \frac{1}{2} R^T K R = \frac{1}{2} \sum_{r,s}^{2n} R_r K_{rs} R_s. \tag{2.18}$$

K is a time-independent Hermitian matrix containing the energy information of the Hamiltonian. To evolve the state under the action of the Hamiltonian we consider the Heisenberg equation for the R vector

$$\dot{R}_j(t) = i\left[H, R_j\right]. \tag{2.19}$$

Substituting in the Hamiltonian (Eq. (2.18)) and using the commutation relations (Eq. (2.2)) we find that

$$\dot{R}_j(t) = \frac{1}{2}\sum_{r,s}^{2n} \sigma_{jr} K_{rs} R_s - \sigma_{js}^T K_{sr}^T R_r. \tag{2.20}$$

Noting that in general $K^T = K$ and $\sigma^T = -\sigma$, allows us to write Eq. (2.20) as

$$\dot{R}_j(t) = \frac{1}{2}\left(\sum_{r,s}^{2n} \sigma_{jr} K_{rs} R_s + \sigma_{js} K_{sr} R_r\right) = \sum_{r,s}^{2n} \sigma_{jr} K_{rs} R_s. \tag{2.21}$$

This equation has the following solution

$$R(t) = e^{\sigma K t} R(0) = \mathcal{M} R(0). \tag{2.22}$$

As mentioned earlier under the action of a bi-linear Hamiltonian a GS will remain a GS. Therefore, we need only be concerned with the CM and its subsequent evolution to describe the dynamics of the system. The time evolution of the CM is obtained by using Eqs. (2.22) and (2.9)

$$\gamma_{jk}(t) = 2Re \sum_{l,m}^{2n} \mathcal{M}_{jl}\mathcal{M}_{km}\langle R_l(0) R_m(0)\rangle = \sum_{l,m}^{2n} \mathcal{M}_{jl}\mathcal{M}_{km}\gamma_{lm}(0). \tag{2.23}$$

Expressed in matrix form, the equation is given by

$$\gamma(t) = \mathcal{M}\gamma(0)\mathcal{M}^T = e^{\sigma K t}\gamma(0)\, e^{-K\sigma t} \tag{2.24}$$

which we can simulate by discretising the time, t.

2.4.2 Ladder representation

In this thesis the Hamiltonians are expressed in terms of creation, $a_j^\dagger$, and annihilation, a_j, operators (i.e. ladder operators) defined as the following

$$a_j^\dagger = \frac{1}{\sqrt{2}}(\hat{x}_j - i\hat{p}_j) \qquad a_j = \frac{1}{\sqrt{2}}(\hat{x}_j + i\hat{p}_j). \tag{2.25}$$

In the position-momentum representation, the vector R collects both operators, similarly the ladder operators are combined in a vector $A^{(c)}$

$$A^{(c)T} = \left(a_1, a_2, ..., a_n, a_1^\dagger, a_2^\dagger, ..., a_n^\dagger\right). \tag{2.26}$$

We have adopted the convention used in Ref. [40] where the (c) superscript denotes vectors and matrices defined using ladder operators. With this new basis there is a complementary commutation relation

$$\left[A_j^{(c)}, A_k^{(c)}\right] = \sigma_{jk} \tag{2.27}$$

where once again σ is the symplectic matrix. The transformation matrix, Ω, that takes the x and p representations to the ladder basis is given by

$$\Omega = \frac{1}{\sqrt{2}} \begin{pmatrix} \mathbb{1}_n & i\mathbb{1}_n \\ \mathbb{1}_n & -i\mathbb{1}_n \end{pmatrix} \tag{2.28}$$

such that $A^{(c)} = \Omega R$ and so that it obeys $i\Omega\sigma\Omega^T = \sigma$. Concordantly the K matrix is also transformed

$$K = \Omega^T K^{(c)} \Omega \tag{2.29}$$

which changes the Hamiltonian to the following form

$$H = \frac{1}{2} A^{(c)T} K^{(c)} A^{(c)}. \tag{2.30}$$

For our works we find the K matrix by using the transformation in Eq. (2.29) on the $K^{(c)}$ matrix obtained from a Hamiltonian in the ladder basis. The evolution of the model is obtained through the use of the equation of motion for the CM (Eq. (2.24)).

2.5 Initial states

This section outlines the form of the CM for various initial states used throughout this thesis. For the single mode states we choose the R vector of the form

$$R^T = (\hat{x}, \hat{p}) \tag{2.31}$$

and for the two mode case we choose

$$R^T = (\hat{x}_1, \hat{x}_2, \hat{p}_1, \hat{p}_2)\,. \tag{2.32}$$

The explicit calculation of all initial states can be found in Appendix A.

2.5.1 Single mode vacuum state

We start by inputing the vacuum state into Eq. (2.9)

$$\gamma_{j,k} = 2Re\,\mathrm{Tr}\left[|0\rangle\langle 0|R_j R_k\right] \tag{2.33}$$

and then express the position and momentum operators in the ladder basis (shown below) to find the elements of the CM.

$$\hat{x} = \frac{1}{\sqrt{2}}\left(a^\dagger + a\right) \qquad \hat{p} = \frac{i}{\sqrt{2}}\left(a^\dagger - a\right) \tag{2.34}$$

The single mode vacuum state can therefore be calculated as shown below.

$$\gamma_{11} = 2Re\langle 0|\frac{1}{\sqrt{2}}\left(a^\dagger + a\right)\frac{1}{\sqrt{2}}\left(a^\dagger + a\right)|0\rangle = 1 \tag{2.35}$$

$\gamma_{12} = \gamma_{21} = 0$ because all terms are purely imaginary.

$$\gamma_{22} = 2Re\langle 0|\frac{i}{\sqrt{2}}\left(a^\dagger - a\right)\frac{i}{\sqrt{2}}\left(a^\dagger - a\right)|0\rangle = 1 \tag{2.36}$$

Which gives a CM of the form

$$\gamma_{vac} = \begin{pmatrix} 1 & 0 \\ 0 & 1 \end{pmatrix} \tag{2.37}$$

i.e. the identity matrix.

2.5.2 Single mode thermal state

The majority of the following derivation of the thermal state is shown in Ref. [62]. When describing the state of the system it is common that one does not have enough information to completely specify it and so is expressed as a mixed state, i.e. we have minimum information about this state. Thermal states are therefore used frequently within this thesis as we consider environments which cannot usually be fully specified but can be taken to be in thermal equilibrium. We consider the thermal state for a single mode and the density matrix is given by

$$\rho = \frac{\exp\left(-\omega\hat{n}\beta\right)}{\mathrm{Tr}\left[\exp\left(-\omega\hat{n}\beta\right)\right]} \tag{2.38}$$

where $\hat{n}$, ω and $\beta = 1/T$ are the number operator, mode frequency and one over the temperature T respectively. Considering that the density matrix is only dependant on $\hat{n}$ it will be of diagonal form in the number basis. Therefore it is possible to express the density matrix of a thermal state as the following

$$\rho = \sum_{n=0}^{\infty} P(n) |n\rangle\langle n| \tag{2.39}$$

where we have a Bose-Einstein probability distribution $P(n)$ of the form

$$P(n) = \exp(-n\omega\beta)(1 - \exp(-\omega\beta)). \tag{2.40}$$

Using this form of the density matrix we can calculate the mean/average photon number, $\bar{n}$, (Eq. 2.41) by taking the expectation value of $\hat{n}$ as shown in Appendix A.

$$\bar{n} = \frac{1}{(\exp(\omega\beta) - 1)} \tag{2.41}$$

2.5.2.1 Average thermal photon number state

An initial thermal state of an oscillator can be expressed in terms of the average photon number $\bar{n}$ [62]

$$\rho = \sum_n \frac{1}{1+\bar{n}} \left(\frac{\bar{n}}{1+\bar{n}}\right)^n |n\rangle\langle n|. \tag{2.42}$$

Expressing this in the CM formalism, we have

$$\gamma_{j,k} = 2Re \sum_n \frac{1}{1+\bar{n}} \left(\frac{\bar{n}}{1+\bar{n}}\right)^n \mathrm{Tr}\left[|n\rangle\langle n| R_j R_k\right]. \tag{2.43}$$

Explicitly this gives

$$\gamma_{11} = \sum_n \frac{1}{1+\bar{n}} \left(\frac{\bar{n}}{1+\bar{n}}\right)^n + \sum_n \frac{1}{1+\bar{n}} \left(\frac{\bar{n}}{1+\bar{n}}\right)^n 2n. \tag{2.44}$$

The first term is just a probability distribution on n and so the sum will be equal to one. The second term is therefore just an average since it is the summation of the probability of n, times n, resulting in a value of $\bar{n}$, the average photon number. Thus the first element of the CM is given by

$$\gamma_{11} = 2\bar{n} + 1. \tag{2.45}$$

The off-diagonal terms, $\gamma_{12} = \gamma_{21}$, are zero because all terms are purely imaginary. The final element is also given as

$$\gamma_{22} = 2\bar{n} + 1 \tag{2.46}$$

which gives a CM of the form

$$\gamma = \begin{pmatrix} 2\bar{n}+1 & 0 \\ 0 & 2\bar{n}+1 \end{pmatrix}. \tag{2.47}$$

Note that if we set $\bar{n} = 0$ we recover the vacuum state (see Section 2.5.1).

2.5.2.2 Thermal state with temperature T

For our purposes with OQS where we employ a large number of oscillators in a thermal state, it is often more convenient to express it in terms of a temperature T. Therefore the thermal energy is split into a Bose-Einstein distribution rather than specifying the average thermal photon number for each individual mode. Thus, using the explicit form of $\bar{n}$ shown in Eq. (2.41), we get the following form of the CM

$$\gamma = \begin{pmatrix} \frac{2}{\exp(\omega_i/T)-1} + 1 & 0 \\ 0 & \frac{2}{\exp(\omega_i/T)-1} + 1 \end{pmatrix} \tag{2.48}$$

where ω_i is the frequency of the specific bath mode at temperature T.

2.5.3 Squeezed state

A squeezed state is a general class of minimum-uncertainty states that have less noise in one quadrature than the other (a coherent state would have equal noise in both quadratures) [63]. For CV systems, squeezed states have proved to be a useful avenue for quantum information processing due to the fact the quadratures exhibit sub-shot-noise quantum correlations giving an opportunity for entanglement. There have been many realisations of squeezed states. In quantum optics, for example, it has been achieved with an optical parametric oscillator, where the squeezing of the pump field was first measured in 1997 [64]. It has been shown a two-mode squeezed state displays entanglement [65] and it is primarily for this reason that squeezed states are investigated in this thesis. This sub-section displays single and two mode squeezed states in the CM formalism with detailed derivations shown in Appendix A.

2.5.3.1 Single mode squeezed vacuum

The single mode squeezing operator is defined as

$$\hat{S}(z) = \exp\left(\frac{1}{2}\left(za^{\dagger 2} - z^* a^2\right)\right) \tag{2.49}$$

where

$$z = re^{i\theta} \tag{2.50}$$

and r and θ are the squeezing parameter and the phase respectively [49]. Considering a squeezed vacuum state $\hat{S}|0\rangle$ the CM is given by

$$\gamma_{j,k} = 2Re\langle 0|\hat{S}^\dagger R_j R_k \hat{S}|0\rangle. \tag{2.51}$$

To calculate the elements of the CM we utilise the Hadamard Lemma,

$$e^X Y e^{-X} = Y + [X,Y] + \frac{1}{2!}[X,[X,Y]] + \frac{1}{3!}[X,[X,[X,Y]]] + ... \tag{2.52}$$

As shown in Appendix A, the first element is given by

$$\gamma_{11} = 2Re\langle 0|\hat{S}^\dagger \hat{x}\hat{x}\hat{S}|0\rangle = \cosh(2r) + \cos(\theta)\sinh(2r). \tag{2.53}$$

Similarly, we can calculate the other elements of the CM for a single mode squeezed state, shown below

$$\gamma = \begin{pmatrix} \cosh(2r) + \cos(\theta)\sinh(2r) & \sin(\theta)\sinh(2r) \\ \sin(\theta)\sinh(2r) & \cosh(2r) - \cos(\theta)\sinh(2r) \end{pmatrix}. \tag{2.54}$$

2.5.3.2 Single mode squeezed thermal state

Combining the calculations employed in Sections 2.5.2 and 2.5.3.1 the CM of a single mode squeezed thermal state can be shown to be of the following form

$$\gamma = \begin{pmatrix} \Upsilon_1 & -(2\bar{n}+1)\sin(\theta)\sinh(2r) \\ -(2\bar{n}+1)\sin(\theta)\sinh(2r) & \Upsilon_2 \end{pmatrix} \tag{2.55}$$

where

$$\begin{aligned}\Upsilon_1 &= (2\bar{n}+1)\left(\cosh(2r)+\cos(\theta)\sinh(2r)\right)\\ \Upsilon_2 &= (2\bar{n}+1)\left(\cosh(2r)-\cos(\theta)\sinh(2r)\right)\end{aligned} \tag{2.56}$$

and

$$\bar{n} = \frac{1}{e^{\frac{\omega}{T}}-1}. \tag{2.57}$$

For all uses of this state within this thesis we consider only states with zero phase, i.e. $\theta = 0$. Therefore the state is given as

$$\gamma_0 = \begin{pmatrix} \Upsilon_1' & 0 \\ 0 & \Upsilon_2' \end{pmatrix} \tag{2.58}$$

where

$$\begin{aligned}\Upsilon_1' &= (2\bar{n}+1)\left(\cosh(2r)+\sinh(2r)\right)\\ \Upsilon_2' &= (2\bar{n}+1)\left(\cosh(2r)-\sinh(2r)\right).\end{aligned} \tag{2.59}$$

2.5.3.3 Two mode squeezed vacuum state

The two mode squeezing operator is defined as

$$\hat{U}_{ab}(z) = \exp\left(\frac{1}{2}\left(za^\dagger b^\dagger - z^* ab\right)\right) \tag{2.60}$$

where

$$z = \zeta e^{i\phi} \tag{2.61}$$

and $a^\dagger(a)$ and $b^\dagger(b)$ are the creation (annihilation) ladder operators for modes one and two respectively. For the purposes of this thesis we just consider a two mode squeezed vacuum state $\hat{U}_{ab}|0_1 0_2\rangle$, the CM of which is given by

$$\gamma_{j,k} = 2Re\langle 00|\hat{U}_{ab}^\dagger R_j R_k \hat{U}_{ab}|00\rangle \tag{2.62}$$

with

$$R^T = (\hat{x}_1, \hat{x}_2, \hat{p}_1, \hat{p}_2). \tag{2.63}$$

Note we have dropped the indices for the modes for simplicity. To calculate the elements of the CM we again utilise the Hadamard Lemma. Thus the first element is given by

$$\gamma_{11} = 2Re\langle 00|\hat{U}_{ab}^\dagger \hat{x}_1 \hat{x}_1 \hat{U}_{ab}|00\rangle = \cosh(\zeta). \tag{2.64}$$

Calculating the other elements in a similar fashion, the CM for a two mode squeezed vacuum state is given by

$$\gamma = \begin{pmatrix} \mathfrak{m} & \mathfrak{I} & 0 & \mathfrak{z} \\ \mathfrak{I} & \mathfrak{m} & \mathfrak{z} & 0 \\ 0 & \mathfrak{z} & \mathfrak{m} & -\mathfrak{I} \\ \mathfrak{z} & 0 & -\mathfrak{I} & \mathfrak{m} \end{pmatrix} \tag{2.65}$$

where

$$\begin{aligned} \mathfrak{m} &= \cosh(\zeta) \\ \mathfrak{I} &= \cos(\phi)\sinh(\zeta) \\ \mathfrak{z} &= \sin(\phi)\sinh(\zeta). \end{aligned} \tag{2.66}$$

For the purposes of our work in this thesis, the expression can be further simplified as we only consider states with zero phase, $\phi = 0$, giving the matrix

$$\gamma = \begin{pmatrix} \cosh(\zeta) & \sinh(\zeta) & 0 & 0 \\ \sinh(\zeta) & \cosh(\zeta) & 0 & 0 \\ 0 & 0 & \cosh(\zeta) & -\sinh(\zeta) \\ 0 & 0 & -\sinh(\zeta) & \cosh(\zeta) \end{pmatrix}. \tag{2.67}$$

2.6 Calculating quantities from Gaussian states

In this thesis the quantities we are interested in analysing are entanglement and fidelity, and these can be calculated from the CM using the methods outlined in this section.

2.6.1 Entanglement

The concept of quantum entanglement was first introduced by Einstein et. al. in the infamous Einstein-Podolsky-Rosen (EPR) paper of 1935 to show the incompleteness of quantum theory [66]. In response to this thought experiment, Schrödinger would coin the term entanglement (*Verschränkung*) to describe the effect later that year. Einstein would eventually refer to it as '*spukhafte Fernwirkung*' or 'spooky action at a distance' [67]. In 1964, Bell outlined the flaw of the EPR paradox by showing that no physical theory of local hidden variables could ever reproduce all of the predictions of quantum mechanics [68]. This therefore makes entanglement a truly quantum effect, since spatially separated entangled particles can show non-local effects, a deep departure from classical physics.

The definition of entanglement is slightly different for bipartite pure and mixed states. A pure state $|\Psi_{AB}\rangle$ is said to be entangled if it cannot be factorised, i.e. if it cannot be written as

$$|\Psi\rangle = |\Psi_1\rangle \otimes |\Psi_2\rangle. \tag{2.68}$$

For a mixed state, ρ_{AB}, this concept is extended to a separability condition. Consider two bosonic systems A and B with N and M modes respectively and a global Hilbert space $\mathcal{H}$ composed of the Hilbert spaces of the two sub-systems, $\mathcal{H} = \mathcal{H}_\mathcal{A} \otimes \mathcal{H}_\mathcal{B}$. A quantum state, ρ_{AB}, is separable if it can be written as a convex combination of product states

$$\rho = \sum_i p_i \rho_i^A \otimes \rho_i^B \tag{2.69}$$

where $p_i \geq 0$, $\sum_i p_i = 1$ and ρ_A, ρ_B belong to $\mathcal{H}_\mathcal{A}$, $\mathcal{H}_\mathcal{B}$ respectively. A state is considered entangled iff it is not separable.

In general it is difficult to decide whether a given density operator is separable; in fact it has been shown to be NP-hard [69]. However, in 1996, Peres [70] and Horodecki et. al. [71] suggested a convenient method for testing separability, the partial transposition.

For separable states, a transposition of either of the sub-system density matrices results in a legitimate density matrix, i.e. a non-negative density operator with unit trace

$$\rho^{'} = \sum_i p_i \rho_i^A \otimes \left(\rho_i^B\right)^T \tag{2.70}$$

since $\left(\rho_i^B\right)^T = \left(\rho_i^B\right)^*$ is also a proper density matrix. This implies the positivity of the partial transpose operation, $\rho^{'} \geq 0$. Therefore, this positive partial transpose (PPT) criterion, also known as the Peres-Horodecki condition, says that ρ is only separable if a partial transposition of the matrix has non-negative eigenvalues. In general, this is only a necessary condition for a separable state [71], but there exists some classes of states for which it is both necessary and sufficient.

2.6.1.1 Entanglement for Gaussian states

The Peres-Horodecki criterion was translated into the CV realm by Simon [65]. Since a density operator is Hermitian, a transposition corresponds to a complex conjugation of the matrix, which results in the time reversal of the Schrödinger equation. Simon noticed that for CV

systems, a time reversal would mean a sign change for the momentum variables. Thus the partial transpose of a CM is simply a sign change on the sub-system momenta it acts on. Therefore, for a bipartite GS, the partial transpose of the corresponding CM can be written as

$$\gamma^{'} = P\gamma P \tag{2.71}$$

where in the position-momentum basis P is given by

$$P = \begin{pmatrix} 1 & 0 & 0 & 0 \\ 0 & 1 & 0 & 0 \\ 0 & 0 & 1 & 0 \\ 0 & 0 & 0 & -1 \end{pmatrix} \tag{2.72}$$

if the transpose is performed on the second mode. Note that $\gamma^{'}$ is positive definite and so, if the state is separable, it must satisfy the physicality condition (Eq. (2.10)). This can be checked by confirming $\gamma^{'(d)} \geq \mathbb{1}$, where $\gamma^{'(d)}$ is the Williamson form of the partially transposed CM; or equivalently if the minimum symplectic eigenvalue (λ_{k_-}) of $\gamma^{'}$ obeys the condition $\lambda_{k_-} \geq 1$.

The violation of this condition has been proven necessary and sufficient for inseparability (and therefore entanglement) for particular classes of $N \times M$ GSs. The simplest case, where $N = M = 1$, was shown by Simon [65]. It has also been demonstrated for $1 \times M$ GSs by Werner and Wolf [57] and for $N \times M$ bi-symmetric GSs by Serafini et. al. [72]. The straightforward example in which the condition is no longer necessary for inseparability is a 2×2 bound entangled GS [57].

2.6.1.2 Logarithmic negativity

The entanglement measure of choice in this thesis is logarithmic negativity. The main reason for which is that it is easy to compute when compared to other mixed-state entanglement measures such the entanglement cost [73] or distillable entanglement [73]. This is especially true for GSs [60]. The negativity was first proposed to be a measure of entanglement by Lee et. al. [74] and then extended by Vidal and Werner for CVs [60]. The measure is given by

$$E_{\mathcal{N}}(\rho) \equiv \log_2 \|\rho^{T_S}\|_1 \tag{2.73}$$

where the superscript T_S refers to a partial transpose on a system S and $\|M\|_1 = \mathrm{Tr}\left[|M|\right]$ is the trace norm operation. This is an entanglement measure on the basis of separability. As shown in the previous section, a matrix ρ is only separable if a partial transposition of the matrix has non-negative eigenvalues. Logarithmic negativity quantifies this in the sense that it measures the degree to which ρ^{T_S} is not positive, hence the name. Qualitatively it can be seen that the more 'negative' ρ^{T_S} is, the further ρ is from separability and thus more entangled.

For our purposes, another important property of logarithmic negativity is that it is an entanglement monotone [75]. This is crucial because it means that the entanglement does not increase under Local Operations and Classical Communications (LOCC) and is essential for our use of the measure in Chapters 3 and 5.

As mentioned earlier, it is easy to compute logarithmic negativity for GSs because it can be calculated using the symplectic eigenvalues of the CM that represents that GS. If we consider a case where there are two modes A and S (as used throughout the thesis) the entanglement between them is given by

$$E_{\mathcal{N}}(\rho_{AS}) = -\sum_{j=1}^{2} \log_2(min(1, |\lambda_k|)) \tag{2.74}$$

where ρ_{AS} is the two mode density matrix and λ_k are the symplectic eigenvalues [49, 52].

2.6.2 Fidelity

In classical communication theory, the 'fidelity' of a transmission was defined to be the difference between the input and output signals. As explained in Refs. [76, 77], due to Shannon's noiseless coding theorem [78] and channel capacity theory [79] it is known that any transmission of an arbitrarily long bit string will generally be imperfect. Therefore the fidelity essentially measures the degree to which the classical transmission is imperfect. In the quantum scenario, the fidelity is a measure of distance between any two density operators and basically describes how different two states are from each other. In the case of a quantum channel it is the difference between the input and output state. The concept of a distance measure between any two mixed states was first proposed by Uhlmann in 1976 [80] and was clarified by Jozsa in 1994 [76] who coined the term 'fidelity'. Uhlmann, and later Jozsa, argued that the similarity of two mixed states could be calculated from the transition probability of the purifications of those states in an extended Hilbert space. Uhlmann showed this for the general case of C*-algebras but was simplified by

Jozsa for the case of finite dimensional Hilbert spaces where the fidelity has a clearer meaning. Therefore the fidelity is defined as

$$F(\rho_1, \rho_2) = max|\langle\phi_1|\phi_2\rangle|^2 \tag{2.75}$$

where $\phi_1(\phi_2)$ is a pure state and the purification of any state ρ_1 (ρ_2) in an extended Hilbert space. Purification refers to the fact that a mixed state can be expressed as the reduced density matrix of a pure state in a higher-dimensional Hilbert space [22]. The fidelity is most commonly expressed by the formula (essentially given in Uhlmann's paper [80]) below

$$F(\rho_1, \rho_2) = Tr\left[\sqrt{\sqrt{\rho_1}\rho_2\sqrt{\rho_1}}\right]. \tag{2.76}$$

It is worth noting that the fidelity is not a metric in the space of density matrices [76] but if a metric is needed, one can use the fidelity to easily calculate the Bures distance [81].

This measure is used for our analysis of states for investigations of non-Markovianity (Chapter 4) and counter rotating terms (Chapter 6). Fidelity is used as opposed to other distance measures (such as trace distance [22]) because for single-mode and two-mode GSs there exists an analytical expression for the fidelity, which can be calculated from their respective covariances matrices. The expression for single-mode GSs was calculated in 1998 [82–84] and for some special two-mode GSs [85–89] but Marian and Marian [90] have shown analytical forms for all single and two-mode GSs.

2.6.2.1 Single-mode fidelity

The expression for the single mode GS is shown in Refs. [90, 91] and is given below

$$F(\rho_1, \rho_2) = \frac{1}{\sqrt{\Delta + \Lambda} - \sqrt{\Lambda}} \tag{2.77}$$

where

$$\begin{aligned} \Delta &= det\left(\frac{\gamma_1}{2} + \frac{\gamma_2}{2}\right) \\ \Lambda &= 4det\left(\frac{\gamma_1}{2} + \frac{i}{2}\sigma\right) det\left(\frac{\gamma_2}{2} + \frac{i}{2}\sigma\right). \end{aligned} \tag{2.78}$$

In the above expressions γ is the corresponding CM of the state and σ is the symplectic matrix.

2.6.2.2 Two-mode fidelity

The analytical expression for a two mode GS is given in Ref. [90] and is shown below

$$F\left(\rho_1,\rho_2\right)=\frac{1}{\sqrt{\Gamma}+\sqrt{\Lambda}-\sqrt{\left(\sqrt{\Gamma}+\sqrt{\Lambda}\right)^2-\Delta}} \tag{2.79}$$

where

$$\begin{aligned}\Delta &= det\left(\frac{\gamma_1}{2}+\frac{\gamma_2}{2}\right)\\ \Gamma &= 16det\left(\left(\frac{\sigma\gamma_1}{2}\right)\left(\frac{\sigma\gamma_2}{2}\right)-\frac{\mathbb{1}}{4}\right)\\ \Lambda &= 16det\left(\frac{\gamma_1}{2}+\frac{i}{2}\sigma\right)det\left(\frac{\gamma_2}{2}+\frac{i}{2}\sigma\right).\end{aligned} \tag{2.80}$$

In the above expressions γ is the corresponding CM of the state and σ is the symplectic matrix.

2.7 Concluding remarks

This chapter has briefly covered the general background theory behind GSs and their representation in the CM formalism. All the models we investigate in this thesis will use this approach and calculate quantities from GSs as shown. The next chapter investigates non-Markovianity by considering the entanglement of a two mode squeezed state.

Chapter 3

Entanglement-based non-Markovian behaviour quantifier

The introduction to this thesis highlighted the importance of OQSs with regards to replicating realistic models of physical systems and Chapter 1 displayed the most common approach to tackle OQSs, the master equation formalism. As mentioned in that chapter, a series of approximations are made to make the problem tractable, one of which is the Markov approximation (Section 1.3). Simply, this implies that the evolution of the system is only dependent on its current state, i.e. the future dynamics does not depend on its previous trajectory. In a significant range of models the effect of non-Markovian behaviour (NMB) of the environment on the OQS cannot be neglected and the Markov approximation is not valid to make. The evidence for the importance of non-Markovianity on the dynamics of various systems is too vast to be covered here but can be found in books, papers and reviews [9, 36, 92, 93].

The intriguing consequences of NMB in an OQS has generated significant attention to the field. Indeed we have seen many theoretical papers based on a non-Markovian (NM) equation of motion [5, 9, 16, 17, 33–42] as well as experimental works which investigate NMB. The experiments range from an investigation of NM dynamics with classical and quantum correlations [94] and measuring the non-Markoviantiy of a process [95], to controlling the transition from Markov to NMB [96] and recovering entanglement by local operations [97]. Moreover there has been research into the role of structured environments and non-Markovianity in quantum metrology [98], quantum key distribution [99], quantum teleportation [100], entanglement generation [101], optimal control [102] and quantum biology [103, 104], all of which, once again, underline the significance of NMB.

In this thesis we focus on the sub-field of non-Markovianity dedicated to the definition and quantification of the degree of NMB present in an OQS and the parameters that effect it. This is still very much an active field of research with differing views, which has led to several proposals that discuss the definition, witnessing and measurement of NMB. These ideas have been reviewed by Breuer [105] and, more recently, by Rivas et. al. [92]. The first NM measure was developed for Gaussian channels by Wolf et. al. [106] by considering the deviation of the quantum map from Lindblad form (see Chapter 1). Since then the measurement of NMB has prompted several unique proposals which utilise quantities such as entanglement, trace distance, fidelity, Fisher information and quantum mutual information [91, 107–110].

This chapter covers the main body of the work contained in our first research paper 'Affecting non-Markovian behaviour by changing bath structures' [111]. The aim of the work was to gain a better understanding of the factors which determine the quantification of NMB. The two forms of quantification considered were an entanglement-based proposal by Rivas et. al. [107] which is covered in this chapter and a fidelity-based approach by Vasile et. al. [91], covered in Chapter 4.

3.1 Definition and quantification

To obtain a *quantifier* for the degree of NMB in an OQS we make use of a sufficient condition based on entanglement [107] (and fidelity [91] in Chapter 4). Before illustrating the quantifier in detail, we initially concentrate on the definition of Markovianity we adopt throughout this chapter, which is the one used in Ref. [107]. Note that there are measures which utilise other definitions and are outlined in the recent review of non-Markovianity by Rivas et. al. [92].

3.1.1 Definition

There are a few ways to define Markovian evolution, the definition we adopt is the *divisibility* definition of Markovianity.

The quantum divisibility definition of Markovianity is often used because of its analogy to the classical case. As described in Ref. [92], the classical Markov case, where the dynamics are driven by a stochastic process, the evolution can be detailed through conditional probabilities.

Thus the following definition of a Markovian processes can be given

$$\mathbb{P}\left(x_n, t_n | x_{n-1}, t_{n-1}; \ldots ; x_0, t_0\right) = \mathbb{P}\left(x_n, t_n | x_{n-1}, t_{n-1}\right) \ \forall \ \ t_n \geq t_{n-1} \geq \ldots \geq t_0 \tag{3.1}$$

where x_n is the value at time t_n of a random variable X associated with the stochastic process [112]. This is the origin of the memoryless interpretation of a Markov processes as the evolution has no history of the past values of X. Moreover, a composition law for the linear maps (transition matrices) which take the probability distribution from one time to another can be derived. This allows for the classical definition of divisibility, which essentially states that a transition matrix that takes a distribution from a time t_1 to a time t_3 can be divided into two maps; one from t_1 to t_2 and one from t_2 to t_3. This divisibility property is analogous to Markovian evolution when one-point probabilities are considered.

The problem with a simple extension of a classical Markov definition (Eq. 3.1) to a quantum description is that a quantum theory contains the measurement problem. If one were to probe a quantum system the measurement would have an effect on the subsequent probability distributions. Therefore the conditional probability $\mathbb{P}\left(x_n, t_n | x_{n-1}, t_{n-1}; \ldots ; x_0, t_0\right)$ is then difficult to construct as it would be dependent on the dynamics and the measurements, resulting in a complex definition of quantum Markovianity. Instead if one were to focus on one-time probabilities $\mathbb{P}\left(x, t\right)$, which negates the measurement problem, the divisibility definition becomes analogous to a Markovian process and all that remains is to find the quantum definition of divisibility.

The dynamics of a quantum system is, in general, described via a completely positive, trace-preserving map (CPT map) $\mathcal{E}_{\left(t_f, t_i\right)}$, such that if a state ρ_i is prepared at an initial time t_i, the corresponding state at a later time t_f is given by

$$\rho_f \equiv \mathcal{E}_{\left(t_f, t_i\right)}\left(\rho_i\right). \tag{3.2}$$

If we fix a start time t_0 and a final time t_2 the map $\mathcal{E}$ is *Markovian* between t_0 and t_2 iff, for any t_1 in the interval $t_0 \leq t_1 \leq t_2$, the following composition law holds

$$\mathcal{E}_{(t_2, t_0)} = \mathcal{E}_{(t_2, t_1)} \circ \mathcal{E}_{(t_1, t_0)} \tag{3.3}$$

where $\mathcal{E}_{(t_1, t_0)}$ and $\mathcal{E}_{(t_2, t_1)}$ are CPT. As before, this divisibility property attempts to formalise the memoryless interpretation of Markovianity. Explicitly, the implications of Eq. (3.3) can

be understood via the following simple example. Consider an initial state ρ_0 and define $\rho_1 \equiv \mathcal{E}_{(t_1,t_0)}(\rho_0)$ and $\rho_2 \equiv \mathcal{E}_{(t_2,t_0)}(\rho_0)$. Eq. (3.3) would suggest that there exists a CPT map $\mathcal{E}_{(t_2,t_1)}$ that takes the state ρ_1 to a state ρ_2 without knowledge of the history prior to t_1. This illustrates that it does not matter *how* the system has evolved between t_0 and t_1 and only the knowledge of the system at time t_1 is required to determine its evolution between t_1 and t_2.

From here on, we take the violation of Eq. (3.3) as our definition of non-Markovianity.

3.1.2 Entanglement-based non-Markovian behaviour quantifier

We now introduce the NMB quantifier that is initially employed for our investigations by considering the entanglement-based NMB sufficient measure proposed by Rivas et. al. [107]. They consider a bipartite system comprising of an OQS under investigation plus an ancilla. The two are initially prepared in a two mode squeezed state $\rho_{\mathrm{SA}}(0)$, and their entanglement is tracked as a function of time. Keeping in mind that no LOCC operation can increase entanglement [73], any system evolution satisfying the divisibility property (Eq. (3.3)) dictates that a system-ancilla entanglement would monotonically decrease with time

$$E[\rho_{\mathrm{SA}}(t)] \leq E[\rho_{\mathrm{SA}}(0)]. \tag{3.4}$$

If instead an increase in entanglement is detected, Eq. (3.3) must necessarily be violated, ergo the dynamics has to be NM.

Choosing an appropriate entanglement measure E, one may quantify NMB by summing all the entanglement increases detected during the time interval of interest. Hence, the NM quantifier is defined as

$$\mathcal{I}^{(E)} \equiv E[\rho_{\mathrm{SA}}(t_f)] - E[\rho_{\mathrm{SA}}(t_0)] + \int_{t_0}^{t_f} \left| \frac{dE[\rho_{\mathrm{SA}}(t)]}{dt} \right| dt. \tag{3.5}$$

Throughout this chapter we use logarithmic negativity as the entanglement measure since it is easily computable for a GS (see Section 2.6.1).

It is important to note at this point that $\mathcal{I}^{(E)} > 0$ defines only a *sufficient* condition for non-Markovianity, as NMB resulting in a decrease of entanglement would not be detected. Hence the above quantity should be interpreted as an NMB *quantifier* (NMBQ), rather than a full-fledged measure. A full measure can be gained if the full dynamical map is known (as shown in Ref. [107] with the use of the Choi - Jamiolkowski isomorphism) but this would require state

tomography. We choose to use an entanglement-based NMBQ (ENMBQ) because it is easy to calculate and we can directly understand how NMB could be utilised to control the flow of entanglement, a useful resource in quantum information.

3.2 Analysing coupled oscillators

Our aim here is to understand what factors of a particular model affect the ENMBQ. To this end, we begin with the simplest scenario involving a single 'bath' oscillator to understand the basic parameters which will determine the degree of NMB predicted by the ENMBQ.

We then proceed to open systems where we consider models which include a large, but finite number of oscillators in the environment. This allows us to use the CM formalism to simulate these models. This gives us a distinct advantage over the standard master equation approach (Chapter 1) by allowing an analysis of the features of the bath oscillators. The master equation approach requires one to trace out the environment before we analyse the density matrix of the system but the CM approach has no such restriction. We apply the ENMBQ to four different models in order to see the effects of changing bath structures on NMB. The downside to this approach is that we are restricted to the timescale we can accurately simulate an OQS. This is due to Poincaré recurrence [113, 114], i.e. the return of the system to its initial state due to the finite state space, with the timescale determined by the number of oscillators in the bath and their respective frequencies and couplings to the system.

3.2.1 Single bath oscillator

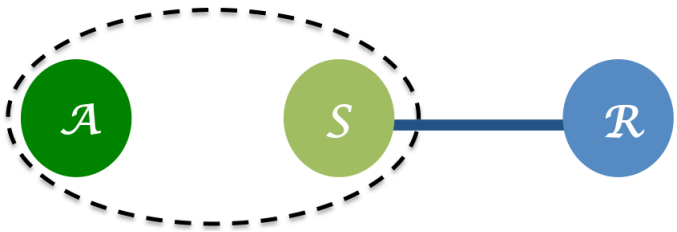


Figure 3.1: Diagram of single 'bath' mode model. An ancilla (A) is entangled with the system (S) (represented by the dotted oval). The system is then coupled to a single 'bath' oscillator (R).

Let us consider a two mode (ancilla (A) and system (S)) squeezed state defined as $\hat{U}_{AS}(\zeta)|00\rangle_{AS}$ [62], where $\hat{U}_{AS}(\zeta)$ is the two mode squeezing operator with the squeezing parameter ζ as described in Section 2.5.3.3. It is well-known that the two mode squeezed state is entangled for

any $\zeta \neq 0$ [65]. If we assume that the system mode of this squeezed state interacts with a single bosonic 'bath' mode in a thermal state with temperature $T = 1$ and the ancilla is left intact, we are left with a Hamiltonian of the form

$$H = \omega_a a^\dagger a + \omega_s s^\dagger s + \omega_r r^\dagger r + g\left(s^\dagger r + s r^\dagger\right). \tag{3.6}$$

where g is the system - 'bath' mode coupling strength and a, s and r (and their adjoints) are the annihilation (and creation) operators for the ancilla, system and the 'bath' mode respectively. Note that the ancilla is not coupled to any oscillator and only undergoes free evolution. The ancilla-system construct is a tool to witness the non-divisibility of the system's dynamics. Given that we arrange the symplectic basis as the following

$$R^T = (\hat{x}_a, \hat{x}_s, \hat{x}_r, \hat{p}_a, \hat{p}_s, \hat{p}_r) \tag{3.7}$$

the initial state of the model is given by the following CM

$$\gamma = \begin{pmatrix} \cosh(\zeta) & \sinh(\zeta) & 0 & 0 & 0 & 0 \\ \sinh(\zeta) & \cosh(\zeta) & 0 & 0 & 0 & 0 \\ 0 & 0 & \varpi & 0 & 0 & 0 \\ 0 & 0 & 0 & \cosh(\zeta) & -\sinh(\zeta) & 0 \\ 0 & 0 & 0 & -\sinh(\zeta) & \cosh(\zeta) & 0 \\ 0 & 0 & 0 & 0 & 0 & \varpi \end{pmatrix} \tag{3.8}$$

where

$$\varpi = \frac{2}{\exp(\omega_r/T) - 1} + 1. \tag{3.9}$$

3.2.1.1 Entanglement dynamics of a single oscillator

In this model the entanglement can be calculated using the methods detailed in Section 2.6.1. We find that the entanglement will oscillate between the system and the single mode (r) during the time evolution. The frequency of the ancilla-system entanglement oscillation (EO) is representative of the speed at which information travels between the system and the oscillator. If g is increased then the information travels back and forth faster, i.e. an increase in EO frequency. We also have to consider ω_r in relation to ω_s. For resonant interactions ($\omega_r = \omega_s$) we find that

the entanglement is shared maximally regardless of g. If the oscillator is detuned ($\omega_r \neq \omega_s$) we find that the EO increases in frequency but the magnitude of the EO decreases as seen by comparing the green and red lines in Figure 3.2. For detuned modes increasing the coupling strength also increases the magnitude of the EO and this behaviour is clearly shown by the blue and red lines in Figure 3.2.

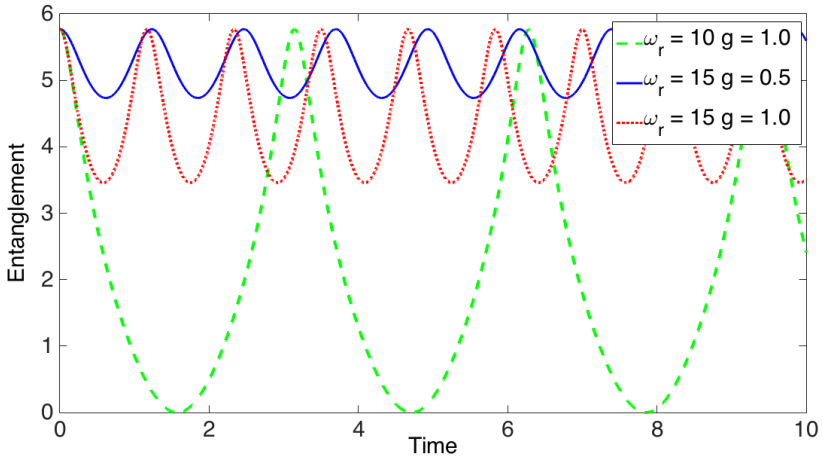


Figure 3.2: Entanglement dynamics for a system-ancilla state, with $\omega_s = 10$, coupled to an oscillator (r) with the properties; Green - [$\omega_r = 10$, $g = 1$], Blue - [$\omega_r = 15$, $g = 0.5$], Red - [$\omega_r = 15$, $g = 1$]. The squeezing parameter $\zeta = 4$. The single mode (r) is in a thermal state with temperature, T=1.

3.2.1.2 Analytical expression of entanglement for the large detuning case

Finding an understandable analytical expression for the EO for this model is difficult due to long-winded expression that arises from the diagonalisation process, but for the case of large detuning ($\omega_r - \omega_s = \Delta \gg g$) an analytic expression for the EO can be found. We begin by moving Eq. (3.6) into the interaction picture by making rotation of e^{-iAt} on the wavefunction to make it time dependent. This new wavefunction, $\Psi(t) = e^{-iAt}\Psi$, is then inserted into the Schrödinger equation

$$i\frac{\partial \Psi}{\partial t} = \left(A + e^{-iAt} H e^{iAt}\right)\Psi = \widetilde{H}\Psi. \tag{3.10}$$

Choosing $A = -\omega_s\left(a^\dagger a + s^\dagger s + r^\dagger r\right)$ and using the Hadamard Lemma we get the interaction picture Hamiltonian

$$\widetilde{H} = \Delta r^\dagger r + g\left(sr^\dagger + s^\dagger r\right) \tag{3.11}$$

where we have used the fact that $\omega_a = \omega_s$ for all our models and that the detuning $\Delta = (\omega_r - \omega_s)$. The next step is to find the eigenvalues and eigenvectors of the Hamiltonian. To this end, we define normal modes of the form $q_i = v_i s + w_i r$ where v and w are factors to be determined by enforcing the commutation relation $[q_i, q_i^\dagger] \equiv 1$. Finding the eigenvectors and eigenvalues of the normal modes, we arrive at the following set of equations expressed in matrix form

$$\begin{pmatrix} q_1 \\ q_2 \end{pmatrix} = \begin{pmatrix} A & B \\ C & D \end{pmatrix} \begin{pmatrix} s \\ r \end{pmatrix}. \tag{3.12}$$

$$\begin{aligned} A &= \sqrt{\tfrac{2g^2}{E_q(E_q+\Delta)}} \quad B = \sqrt{\tfrac{E_q+\Delta}{2E_q}} \\ C &= \sqrt{\tfrac{2g^2}{E_q(E_q-\Delta)}} \quad D = -\sqrt{\tfrac{E_q-\Delta}{2E_q}} \end{aligned} \tag{3.13}$$

$$E_q = \sqrt{\Delta^2 + 4g^2} \tag{3.14}$$

To find the time dependence of the system and 'bath' oscillator mode operators we utilise the knowledge that the normal q modes evolve in the following way

$$\frac{\partial q_i}{\partial t} = -i\left[q_i, H\right] = -iE_i q_i \tag{3.15}$$

therefore

$$q_i\left(t\right) = q_i e^{-iE_i t}. \tag{3.16}$$

This allows us to write the following time evolutions

$$s\left(t\right) = s\left(\cos\left(\frac{E_q t}{2}\right) + \frac{i\Delta}{E_q}\sin\left(\frac{E_q t}{2}\right)\right)e^{\frac{-i\Delta t}{2}} - r\left(\frac{2ig}{E_q}\right)\left(\sin\left(\frac{E_q t}{2}\right)\right)e^{\frac{-i\Delta t}{2}} \tag{3.17}$$

$$r\left(t\right) = -s\left(\frac{2ig}{E_q}\right)\left(\sin\left(\frac{E_q t}{2}\right)\right)e^{\frac{-i\Delta t}{2}} + r\left(\cos\left(\frac{E_q t}{2}\right) - \frac{i\Delta}{E_q}\sin\left(\frac{E_q t}{2}\right)\right)e^{\frac{-i\Delta t}{2}}. \tag{3.18}$$

In matrix form the time evolution of all the modes can be expressed as

$$R\left(t\right) = LR\left(0\right) \tag{3.19}$$

$$\begin{pmatrix} a(t) \\ s(t) \\ r(t) \\ a^{\dagger}(t) \\ s^{\dagger}(t) \\ r^{\dagger}(t) \end{pmatrix} = \begin{pmatrix} 1 & 0 & 0 & 0 & 0 & 0 \\ 0 & \varphi_{1-} & \varphi_{2-} & 0 & 0 & 0 \\ 0 & \varphi_{2-} & \varphi_{3-} & 0 & 0 & 0 \\ 0 & 0 & 0 & 1 & 0 & 0 \\ 0 & 0 & 0 & 0 & \varphi_{3+} & \varphi_{2+} \\ 0 & 0 & 0 & 0 & \varphi_{2+} & \varphi_{1+} \end{pmatrix} \begin{pmatrix} a(0) \\ s(0) \\ r(0) \\ a^{\dagger}(0) \\ s^{\dagger}(0) \\ r^{\dagger}(0) \end{pmatrix} \tag{3.20}$$

where

$$\begin{aligned} \varphi_{1\pm} &= e^{\pm\frac{i\Delta t}{2}} \left(\cos\left(\frac{E_q t}{2}\right) + \frac{i\Delta}{E_q} \sin\left(\frac{E_q t}{2}\right) \right) \\ \varphi_{2\pm} &= e^{\pm\frac{i\Delta t}{2}} \left(\pm\frac{2ig}{E_q} \sin\left(\frac{E_q t}{2}\right) \right) \\ \varphi_{3\pm} &= e^{\pm\frac{i\Delta t}{2}} \left(\cos\left(\frac{E_q t}{2}\right) - \frac{i\Delta}{E_q} \sin\left(\frac{E_q t}{2}\right) \right). \end{aligned} \tag{3.21}$$

If we express the initial state of the above model in the CM formalism and use the time evolution of the above modes in the correct basis, we can construct a matrix which acts on the initial CM. The first step is to transform matrix L from the ladder basis to the position-momentum basis in which the initial CM is constructed (Eq. 3.8), which we achieve by acting on it with the transformation matrix Ω (Eq. 2.28)

$$L^{(c)} = \Omega^{-1} L \Omega. \tag{3.22}$$

To find out how the state of the model is changing in time we express the time evolution of the CM as

$$\gamma(t) = L^{(c)} \gamma(0) L^{(c)T} \tag{3.23}$$

where $\gamma(0)$ is given in Eq. 3.8. Below is the time dependent CM for the ancilla-system state where we have left out the matrix components of the 'bath' mode.

$$\gamma(t) = \begin{pmatrix} V_{1+} & V_2 \\ V_2 & V_{1-} \end{pmatrix} \tag{3.24}$$

$$V_{1\pm} = \begin{pmatrix} \cosh(\zeta) & \pm\Xi \sinh(\zeta) \\ \pm\Xi \sinh(\zeta) & \cosh(\zeta) + \Phi \end{pmatrix} \tag{3.25}$$

$$V_{\not 2} = \begin{pmatrix} 0 & \Pi \sinh(\zeta) \\ \Pi \sinh(\zeta) & 0 \end{pmatrix} \tag{3.26}$$

$$\begin{aligned} \Xi &= \left(\cos\left(\frac{E_q t}{2}\right) \cos\left(\frac{\Delta t}{2}\right) + \frac{\sin\left(\frac{E_q t}{2}\right) \sin\left(\frac{\Delta t}{2}\right) \Delta}{E_q} \right) \\ \Pi &= \left(-\cos\left(\frac{E_q t}{2}\right) \sin\left(\frac{\Delta t}{2}\right) + \frac{\sin\left(\frac{E_q t}{2}\right) \cos\left(\frac{\Delta t}{2}\right) \Delta}{E_q} \right) \\ \Phi &= \frac{2g^2 \left(\cos(E_q t) - 1\right)}{E_q^2} \left(\cosh(\zeta) - \coth\left(\frac{\omega_r}{2}\right) \right) \end{aligned} \tag{3.27}$$

From this matrix we can calculate the evolution of the system-ancilla entanglement by finding the symplectic eigenvalues (from which we can calculate the logarithmic negativity) as detailed in Section 2.6.1.

The resulting expression for the symplectic eigenvalues γ_k is extremely long and therefore it is not exactly clear what the behaviour of the entanglement is. To simplify the expression we can consider cases where g/Δ is small, i.e. cases where we have a large detuning. To achieve this we consider g as a function of Δ, explicitly $f\Delta$ and perform a Taylor expansion around the value $f = 0$ (Maclaurin series)

$$\gamma_k = e^{-\zeta} + \frac{2\sin^2\left(\frac{\Delta t}{2}\right)\left(1 + e^{-\zeta} + e^{\omega_r}\left(1 - e^{-\zeta}\right)\right)}{e^{\omega_r} - 1} f^2 + \mathcal{O}\left(f^4\right). \tag{3.28}$$

By making the substitution $f = g/\Delta$, we just take terms up to the second order expansion of f under the large detuning approximation. This gives the following expression for the symplectic eigenvalues

$$\begin{aligned} \gamma_k &= \frac{e^{-\zeta}\left(-g^2 e^{\zeta}\left(e^{\omega_r} + 1\right)\left(\cos(\Delta t) - 1\right) + \left(e^{\omega_r} - 1\right)\left(\Delta^2 - g^2 + g^2\cos(\Delta t)\right)\right)}{\left(e^{\omega_r} - 1\right)\Delta^2} \\ &= \frac{\Delta^2 e^{-\zeta} + 2g^2\left(\coth\left(\frac{w_r}{2}\right) - e^{-\zeta}\right)\sin^2\left(\frac{\Delta t}{2}\right)}{\Delta^2}. \end{aligned} \tag{3.29}$$

Which essentially gives us the form of the entanglement as

$$E = \log_2\left(\frac{\Delta^2 e^{-\zeta} + 2g^2\left(\coth\left(\frac{w_r}{2}\right) - e^{-\zeta}\right)\sin^2\left(\frac{\Delta t}{2}\right)}{\Delta^2} \right). \tag{3.30}$$

The graphs below show the validity of the approximation for two different values of g/Δ. Figure 3.3 shows that the approximation is valid for the case where $g/\Delta = 0.01$, whereas Figure 3.4

shows that it starts to breaks down for higher values of this factor, in this case $g/\Delta = 0.1$.

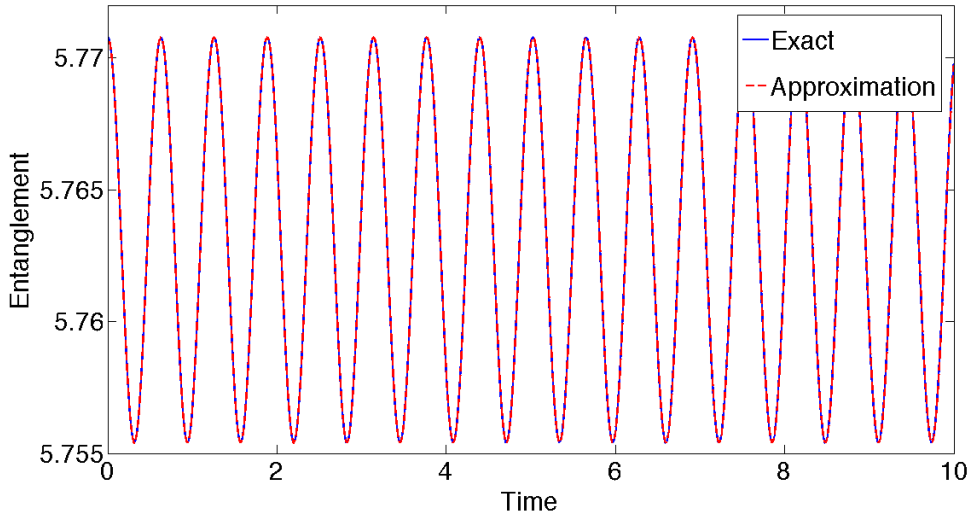


Figure 3.3: Entanglement dynamics for a system-ancilla state, with $\omega_s = 10$, $\omega_r = 20$ and $g = 0.1$. The squeezing parameter $\zeta = 4$. The single mode (r) is in a thermal state with temperature $T = 1$. The blue line indicates the exact entanglement obtained by using the CM of the model. The red dotted line is the approximation of the entanglement given by Eq. 3.30.

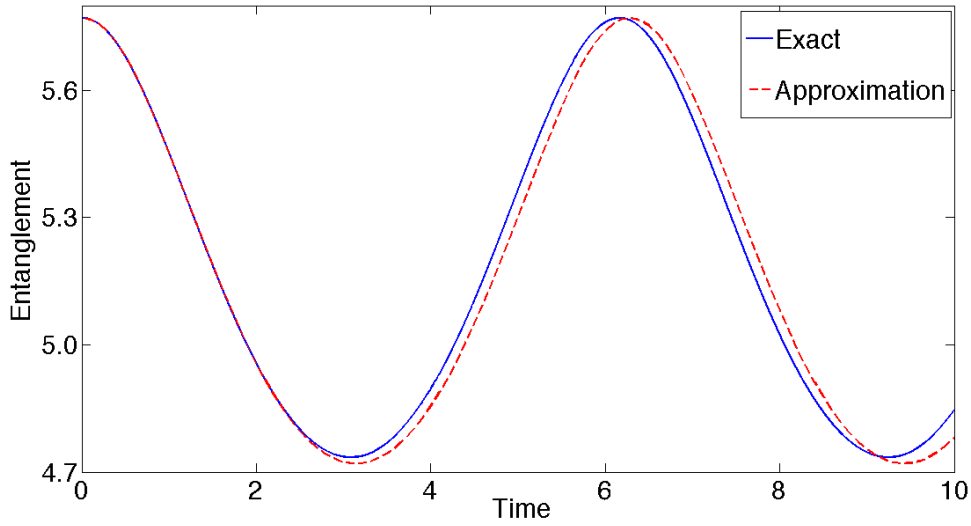


Figure 3.4: Entanglement dynamics for a system-ancilla state, with $\omega_s = 10$, $\omega_r = 11$ and $g = 0.1$. The squeezing parameter $\zeta = 4$. The single mode (r) is in a thermal state with temperature $T = 1$. The blue line indicates the exact entanglement obtained by using the CM of the model. The red dotted line is the approximation of the entanglement given by Eq. 3.30.

3.2.1.3 ENMBQ and the single oscillator

From the single oscillator model we can gain an insight into the predictions of the ENMBQ for a multiple oscillator bath. It is important to note that we can only gain an intuition for the

dynamics at play since adding even a single oscillator to the 'bath' complicates the dynamics significantly, as we have shown analytically in the next subsection. The ENMBQ sums up all entanglement increases and therefore will depend on two aspects of the EO, the magnitude and the frequency. At a low coupling strength a near-resonant mode would yield more NMB than an off-resonant mode. This is due to the much larger EO magnitude of a near-resonant mode. But as g is pushed past a specific value for a particular detuning, the detuned mode would yield more NMB due to a combination of the high frequency and increased magnitude of the EO. This is shown in Figure 3.5 where at low coupling strengths we get a higher ENMBQ value for the resonant frequency of 10 but as coupling is increased the off-resonant modes produce a greater value.

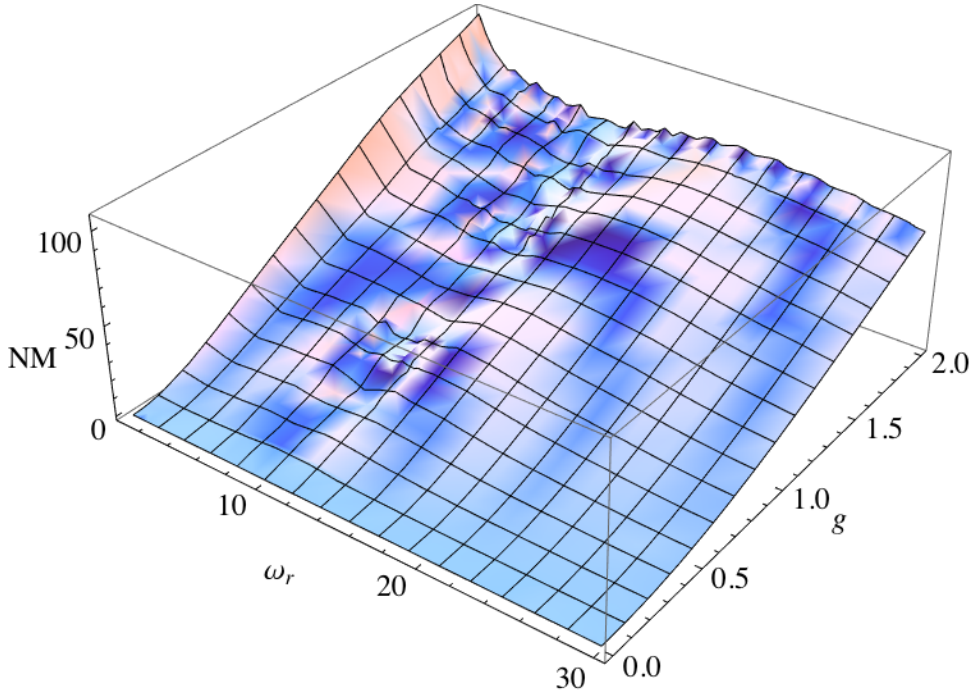


Figure 3.5: ENMBQ for the single 'bath' oscillator model. The coupling g and the frequency of the r mode is varied to show the transition of when off-resonant modes would yield more ENMBQ. The following parameters are fixed, the ancilla and system frequencies $\omega_a = \omega_s = 10$, the squeezing parameter $\zeta = 4$ and the single mode (r) is in a thermal state with temperature $T = 1$. The roughness seen in the figure is due to numerical resolution.

Keeping this in mind, we now investigate the behaviour when there are more oscillators coupled to the system in order to see how the ENMBQ is affected.

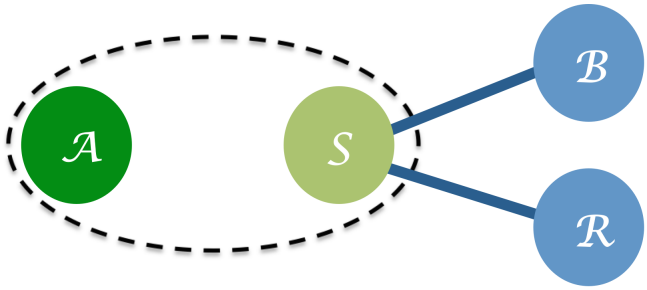


Figure 3.6: Diagram of the two 'bath' mode model. An ancilla (A) is entangled with the system (S) (represented by the dotted oval). The system is then coupled to two 'bath' oscillators (B and R) which are in a thermal state with temperature T.

3.2.2 Analytics for two 'bath' oscillators

The next step in the comprehension of an OQS problem is to expand the number of modes the system interacts with. The simplest extension of this is to add another mode to the 'bath' as shown in Figure 3.6. The problem of three coupled oscillators is a complicated one in the sense that it has no compact, easily understood analytic solution. The reason being that the diagonalisation of the problem leads to long-winded expressions for the eigenvalues and eigenvectors. What can be found however are effective Hamiltonians for certain scenarios which should give us insight into the behaviour.

3.2.2.1 Resonant modes

The simplest of these cases is when 'bath' modes b and r are resonant with the system, the Hamiltonian of which is given below

$$H = \omega\left(a^\dagger a + s^\dagger s + b^\dagger b + r^\dagger r\right) + g\left(sb^\dagger + s^\dagger b\right) + h\left(sr^\dagger + s^\dagger r\right). \tag{3.31}$$

First we rotate the Hamiltonian by moving into the interaction picture (as shown in Section 3.2.1.2) by $-\omega\left(a^\dagger a + s^\dagger s + b^\dagger b + r^\dagger r\right)$, leaving only the interaction terms of the Hamiltonian.

$$\widetilde{H} = g\left(sb^\dagger + s^\dagger b\right) + h\left(sr^\dagger + s^\dagger r\right) = s\left(gb^\dagger + hr^\dagger\right) + s^\dagger\left(gb + hr\right) \tag{3.32}$$

Then by defining a normal mode

$$q = \frac{gb + hr}{\sqrt{g^2 + h^2}} \tag{3.33}$$

we can transform the Hamiltonian as shown below

$$H_{eqv} = \sqrt{g^2 + h^2}\left(sq^\dagger + s^\dagger q\right) \tag{3.34}$$

where the new coupling strength is gained by the asserting the bosonic canonical commutation relations on the normal modes. This equivalent Hamiltonian shows that one of the normal modes couples to the system and the other decouples and is now a dark mode which only undergoes free evolution. Therefore the model can be reduced to a one 'bath' mode model with a new coupling strength as shown in Figure 3.7.

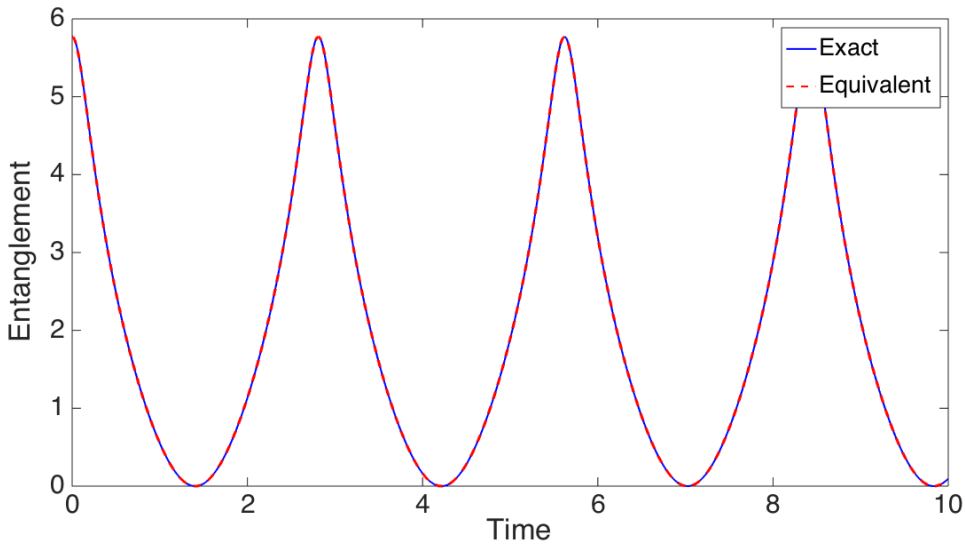


Figure 3.7: Entanglement when all oscillators are resonant. The oscillator frequencies are set at 10, i.e. $\omega_a = \omega_s = \omega_b = \omega_r = 10$. The squeezing parameter is $\zeta = 4$ and the 'bath' is in a thermal state with temperature $T = 1$.

In fact, it can be shown that this is true regardless of the number of coupled resonant modes, where the new normal mode would be

$$q = \sum_i^N \frac{g_i a_i}{g'} \tag{3.35}$$

where a_i are the annihilation operators for the resonant modes and the new coupling strength would be given by

$$g'^2 = \sum_i^N g_i^2 \tag{3.36}$$

where N is the number of resonant bath modes. In this case all but one of the normal modes would have effectively decoupled from the system. Figure 3.8 shows that is indeed true. In

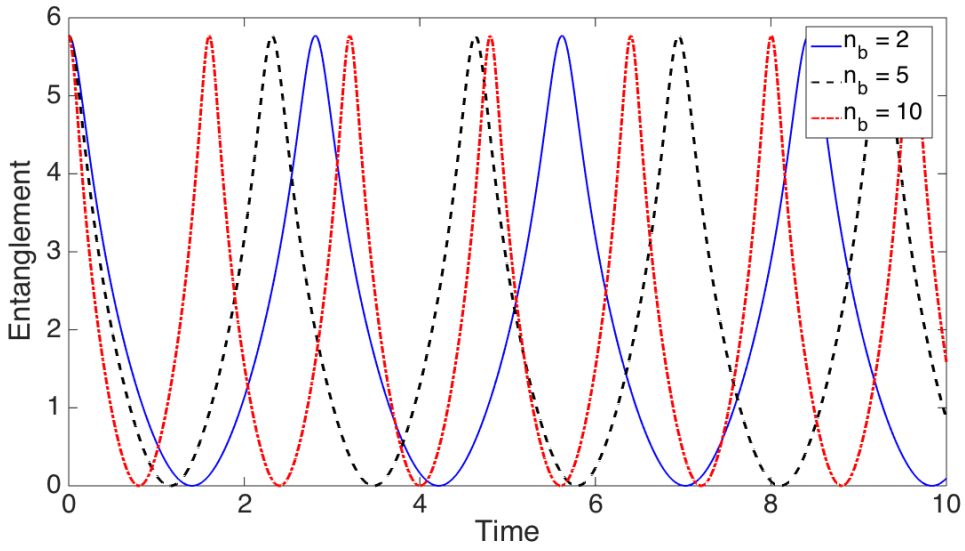


Figure 3.8: Entanglement when all the bath oscillators, n_b, are resonant. The oscillator frequencies are set at $\omega_a = \omega_s = \omega_{b_i} = 10$. The squeezing parameter is $\zeta = 4$ and the 'bath' is in a thermal state with temperature, $T = 1$. The couplings are set as follows, Blue line - [0.5, 1.0], Black line - [0.1, 0.3, 0.5, 0.7, 1.0] and Red line - [0 - 1.0, 0.1 splitting].

terms of how this analysis improves our understanding of the ENMBQ, we see that we will get an unperturbed, smooth oscillation of the entanglement regardless of the number of resonant bath modes we attach to the system. As we attach these modes to the 'bath' the ENMBQ will predict an increase in NMB because the dynamics are the same as a single resonant oscillator but with an increased effective coupling strength which we have seen in Section 3.2.1 increases EO frequency (as shown in Figure 3.8) and therefore NMB.

3.2.2.2 A resonant mode and an off-resonant mode

The simplest extension to the resonant case is to detune one of the 'bath' modes, i.e. we have one resonant (b) and one off-resonant (r) 'bath' mode with the Hamiltonian given by

$$H = \omega \left(a^\dagger a + s^\dagger s + b^\dagger b\right) + \omega_r r^\dagger r + g\left(sb^\dagger + s^\dagger b\right) + h\left(sr^\dagger + s^\dagger r\right). \tag{3.37}$$

As before we choose to rotate this Hamiltonian into the interaction picture by a rotation of $-\omega(a^\dagger a + s^\dagger s + b^\dagger b + r^\dagger r)$

$$H = \Delta r^\dagger r + g\left(sb^\dagger + s^\dagger b\right) + h\left(sr^\dagger + s^\dagger r\right). \tag{3.38}$$

where Δ is the detuning between the system and the off-resonant 'bath' mode r, specifically $\omega_r - \omega_s$.

Firstly we consider the large detuning case and perform an additional rotation by $-\Delta r^\dagger r$ and thus the new interaction Hamiltonian can be expressed as

$$\widetilde{H} = g\left(sb^\dagger + s^\dagger b\right) + h\left(s^\dagger r e^{-i\Delta t} + s r^\dagger e^{i\Delta t}\right). \tag{3.39}$$

In this form we can utilise a time-averaging technique outlined by Gamel and James [115] to obtain an effective Hamiltonian for the model. The basic premise is that by time-averaging the evolution, high frequency terms can be filtered out. For our Hamiltonian this implies that

$$\begin{aligned} \overline{e^{\pm i\Delta t}} &= 0 \\ \overline{e^{\pm 2i\Delta t}} &= 0 \end{aligned} \tag{3.40}$$

where the over-bar indicates time-averaging. Therefore under the large detuning assumption it becomes valid to use their method and by taking the standard form of the effective Hamiltonian given in paper we arrive at

$$\widetilde{H}_{eff} = g\left(sb^\dagger + s^\dagger b\right) + \frac{h^2}{\Delta}\left[sr^\dagger, s^\dagger r\right] = -\frac{h^2}{\Delta}s^\dagger s + \frac{h^2}{\Delta}r^\dagger r + g\left(sb^\dagger + s^\dagger b\right). \tag{3.41}$$

Rotating back out of the interaction picture by $\Delta r^\dagger r$, we get

$$H_{eff} = -\frac{h^2}{\Delta}s^\dagger s + \left(\Delta + \frac{h^2}{\Delta}\right)r^\dagger r + g\left(sb^\dagger + s^\dagger b\right). \tag{3.42}$$

If we rotate a further step, i.e. by $\omega_s\left(a^\dagger a + s^\dagger s + b^\dagger b + r^\dagger r\right)$ we get the following effective Hamiltonian

$$H_{eff} = \omega a^\dagger a + \omega^{'} s^\dagger s + \omega b^\dagger b + \omega_r^{'} r^\dagger r + g\left(sb^\dagger + s^\dagger b\right) \tag{3.43}$$

where

$$\begin{aligned} \omega &= \omega_a = \omega_s = \omega_b \\ \omega^{'} &= \omega - \frac{h^2}{\Delta} \\ \omega_r^{'} &= \omega_r + \frac{h^2}{\Delta}. \end{aligned} \tag{3.44}$$

This shows that the large detuned mode effectively decouples from, and introduces a frequency shift in, the system. The effective Hamiltonian clearly shows that for the case of large detuning

of one of the bath modes the entanglement dynamics can be modelled with just one 'bath' mode with a small detuning.

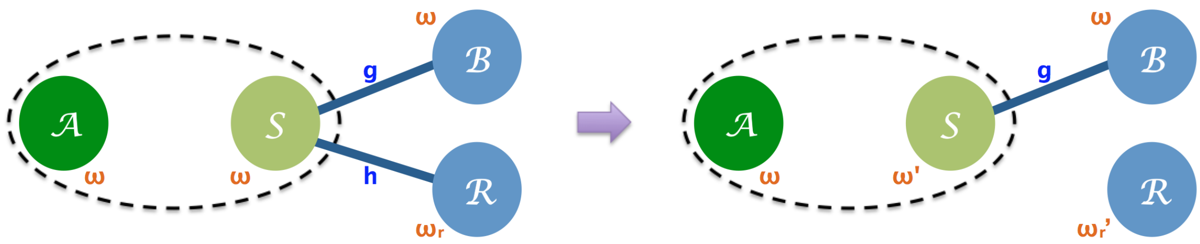


Figure 3.9: Effective model for the large detuning case.

To show the effectiveness of this approximation there are three cases to consider which involve the relative coupling strengths, i.e. roughly speaking when $g > h$, $g < h$ and $g = h$. We first note that it is clear that when the coupling to the detuned mode is weak in comparison to the resonant mode it will have little to no effect on the dynamics of the system as the resonant mode will dominate the interaction. This is shown in Figure 3.10 where we see that the approximation is accurate regardless of the amount of detuning because the resonant mode drives the dynamics.

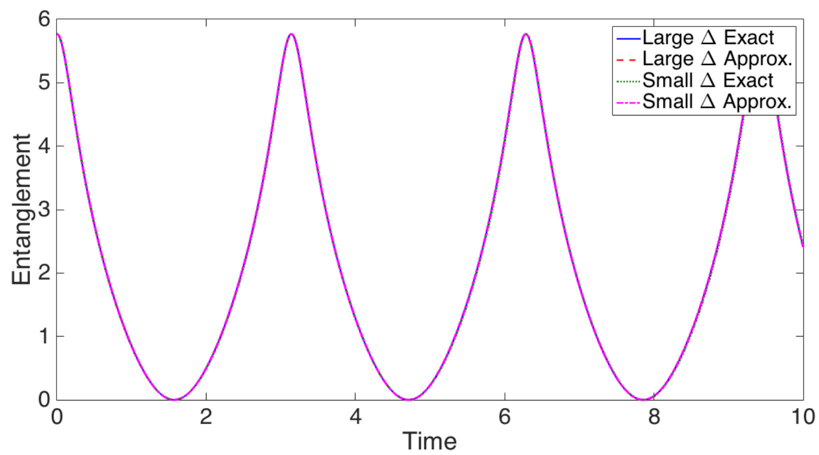


Figure 3.10: Entanglement dynamics of the system. The resonant oscillator frequencies are set at $\omega_a = \omega_s = \omega_b = 10$. $\omega_r = 40$ for the large detuning case and $\omega_r = 13$ for the small detuning case. The squeezing parameter is $\zeta = 4$ and the 'bath' is in a thermal state with temperature $T = 1$. The couplings are $g = 1.0$ and $h = 0.1$

Then for the cases where the off-resonant mode is more strongly coupled and therefore plays a more important role, we see that the approximation is good only for large detunings as shown in Figures 3.11 and 3.12.

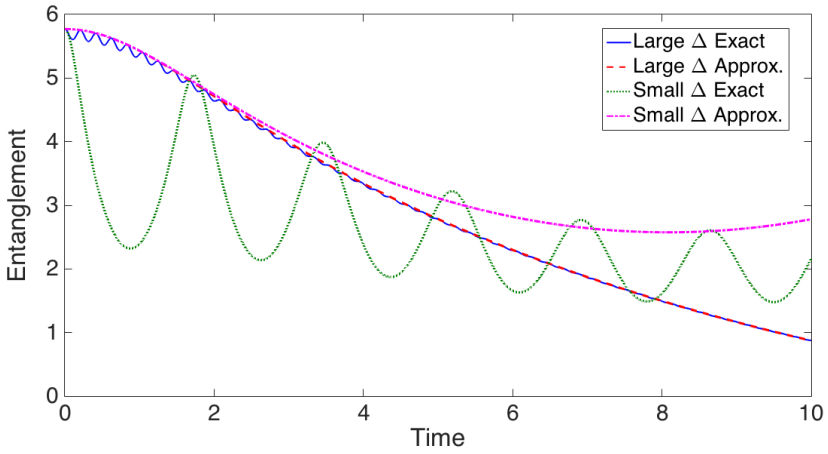


Figure 3.11: Entanglement dynamics of the system. The resonant oscillator frequencies are set at $\omega_a = \omega_s = \omega_b = 10$. $\omega_r = 40$ for the large detuning case and $\omega_r = 13$ for the small detuning case. The squeezing parameter is $\zeta = 4$ and the 'bath' is in a thermal state with temperature $T = 1$. The couplings are $g = 0.1$ and $h = 1.0$

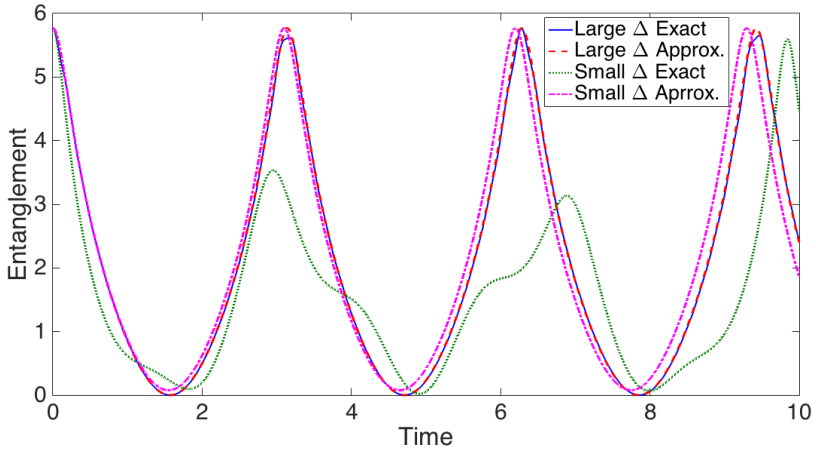


Figure 3.12: Entanglement dynamics of the system. The resonant oscillator frequencies are set at $\omega_a = \omega_s = \omega_b = 10$. $\omega_r = 40$ for the large detuning case and $\omega_r = 13$ for the small detuning case. The squeezing parameter is $\zeta = 4$ and the 'bath' is in a thermal state with temperature $T = 1$. The couplings are $g = 1.0$ and $h = 1.0$.

The procedure can be repeated for the case where the detuning is small in comparison to the coupling strength. We now rotate the Hamiltonian by $-g(sb^\dagger + s^\dagger b) - h(sr^\dagger + s^\dagger r)$ and average over the fast oscillating terms, i.e. all exponentials of the form shown below are set to zero.

$$\begin{aligned} \overline{e^{\pm\ i\ t\ \sqrt{g^2+h^2}}} &= 0 \\ \overline{e^{\pm\ 2i\ t\ \sqrt{g^2+h^2}}} &= 0 \end{aligned} \tag{3.45}$$

This is a valid assumption to make when we assume that the coupling strengths are strong in

comparison to the detuning. Then, as before, we rotate back away from the interaction picture to get to the effective Hamiltonian in the original picture

$$H_{eff} = \omega a^\dagger a + \omega_s^{'} s^\dagger s + \omega_b^{'} b^\dagger b + \omega_r^{'} r^\dagger r + g\left(sb^\dagger + s^\dagger b\right) + h\left(sr^\dagger + s^\dagger r\right) + c\left(br^\dagger + b^\dagger r\right) \tag{3.46}$$

where

$$\begin{aligned} \omega_s^{'} &= \omega + \frac{\Delta h^2}{2(g^2+h^2)} \\ \omega_b^{'} &= \omega + \frac{3\Delta g^2 h^2}{2(g^2+h^2)^2} \\ \omega_r^{'} &= \omega + \frac{\Delta(2g^4+h^4)}{2(g^2+h^2)^2} \\ c &= \frac{\Delta g h(h^2-2g^2)}{2(g^2+h^2)^2}. \end{aligned} \tag{3.47}$$

The Hamiltonian above suggests that frequency shifts are introduced in all modes and an effective coupling is gained between the two 'bath' modes.

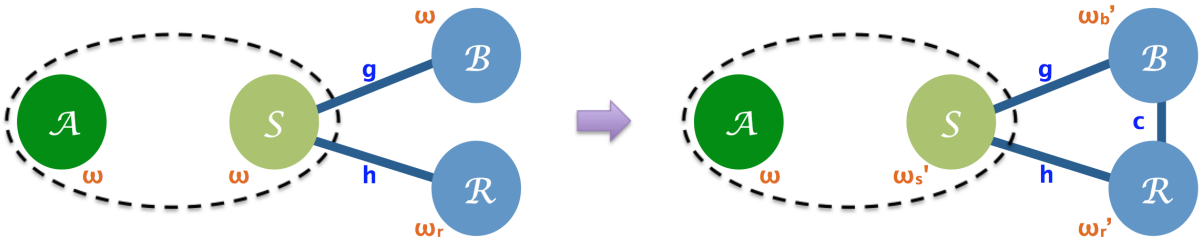


Figure 3.13: Effective model for the small detuning case.

This is understandable as the communication speeds to both 'bath' modes from the system would be similar (if the couplings are of the same order) due to the small detuning and so, an effective coupling is created. Note that these new features of the Hamiltonian would mean that rather complicated entanglement dynamics are at play because the 'bath' has the ability to hold on to the entanglement over time.

If we plot the entanglement dynamics for the three different coupling cases (Figures 3.14, 3.15 and 3.16) as we did for the large detuning case, we clearly see that the approximation is only valid for the small detuning cases, where the dynamics are matched exactly.

In terms of the effect this has on the ENMBQ, the large detuning case would be similar to the NMB observed in the one resonant 'bath' mode case (due to the small effective detuning). For small detuning we see that the NMB will depend on the relative coupling strengths between,

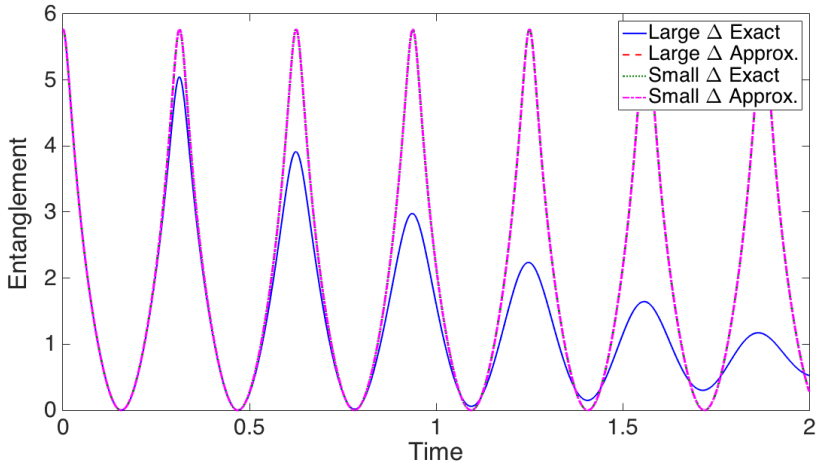


Figure 3.14: Entanglement dynamics of the system. The resonant oscillator frequencies are set at $\omega_a = \omega_s = \omega_b = 10$. $\omega_r = 20$ for the large detuning case and $\omega_r = 11$ for the small detuning case. The squeezing parameter is $\zeta = 4$ and the 'bath' is in a thermal state with temperature $T = 1$. The couplings are $g = 10.0$ and $h = 1.0$. Note that the red dashed, green dotted and pink dot-dash lines all follow a similar profile.

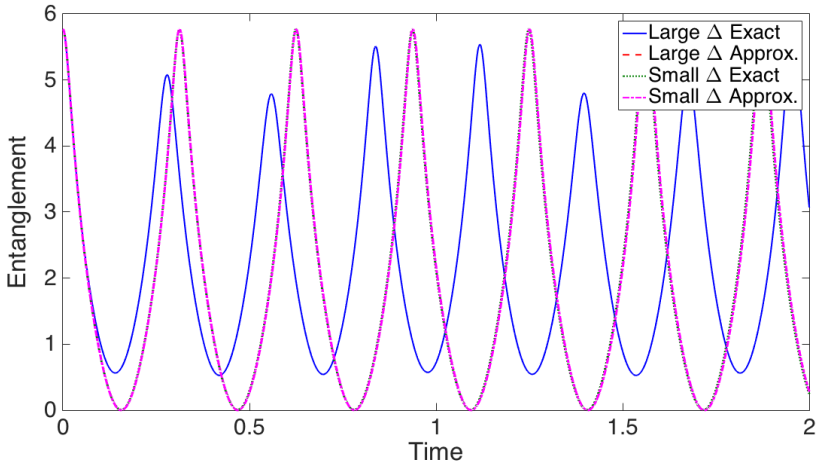


Figure 3.15: Entanglement dynamics of the system. The resonant oscillator frequencies are set at $\omega_a = \omega_s = \omega_b = 10$. $\omega_r = 20$ for the large detuning case and $\omega_r = 11$ for the small detuning case. The squeezing parameter is $\zeta = 4$ and the 'bath' is in a thermal state with temperature $T = 1$. The couplings are $g = 1.0$ and $h = 10.0$. Note that the red dashed, green dotted and pink dot-dash lines all follow a similar profile.

effectively, the three off-resonant modes.

3.2.3 Many bath oscillators

In this section we consider four different types of interaction between the OQS and the bath modes. These models show how bath structures can be manipulated in order to affect the

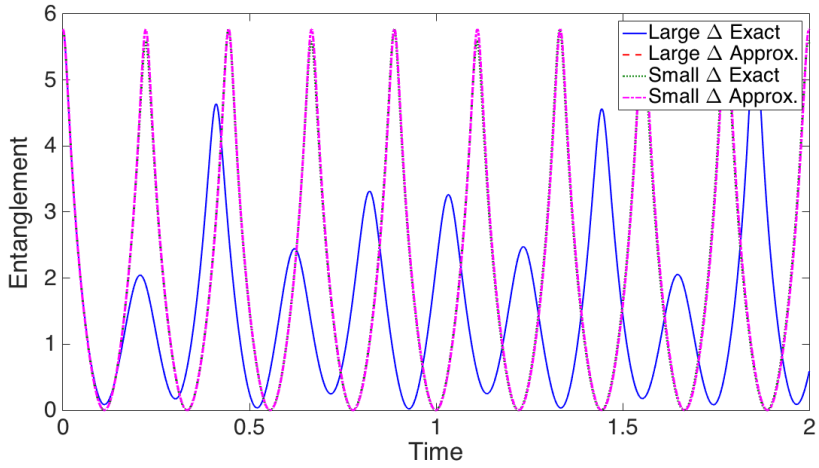


Figure 3.16: Entanglement dynamics of the system. The resonant oscillator frequencies are set at $\omega_a = \omega_s = \omega_b = 10$. $\omega_r = 20$ for the large detuning case and $\omega_r = 11$ for the small detuning case. The squeezing parameter is $\zeta = 4$ and the 'bath' is in a thermal state with temperature $T = 1$. The couplings are $g = 10.0$ and $h = 10.0$. Note that the red dashed, green dotted and pink dot-dash lines all follow a similar profile.

ENMBQ. Model 1 (Figure 3.17) shows the role of near-resonant and off-resonant modes in the bath and has the Hamiltonian given below

$$H = \omega_a a^\dagger a + \omega_s s^\dagger s + \sum_{i=1}^{N} \omega_{r_i} r_i^\dagger r_i + \sum_{i=1}^{N} g_i \left(s^\dagger r_i + s r_i^\dagger \right). \tag{3.48}$$

In Sections 3.2.3.6 and 3.2.3.7, Models 2 and 3 (Figures 3.27 and 3.30) display how adding a single strongly coupled resonant mode can affect the NMB.

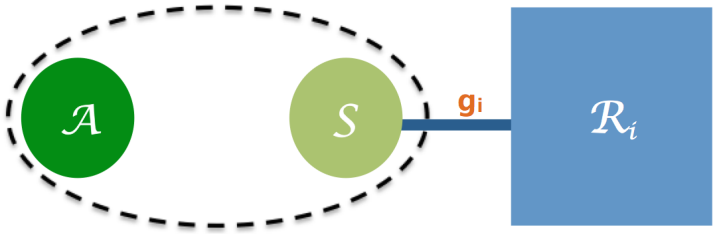


Figure 3.17: Diagram of Model 1. An ancilla (A) is entangled with the system (S) (represented by the dotted oval), i.e. a two mode squeezed state. The system is coupled to each bath mode (R_i) with respective coupling g_i. The bath is in a thermal state with temperature T.

3.2.3.1 Spectral densities

In the Hamiltonian given in Eq. (3.48) the coupling strengths of the bath modes g_i are determined by what is known as the spectral density function $J(\omega)$ [9, 40]. The spectral density

function essentially describes the distribution of frequencies in the bath and how strongly coupled these frequencies are to the system, mathematically it is given by

$$J(\omega) = \sum_{i}^{N} g_i^2 \delta(\omega_i - \omega). \tag{3.49}$$

In this thesis we only consider large finite systems of size N and therefore require a discretisation of the mode frequencies up to a maximum frequency ω_{max}. This is achieved by integrating both sides of Eq. (3.49) with respect to ω from 0 to ω_{max}, giving

$$\sum_{i}^{N} g_i^2 = \int_0^{\omega_{max}} J(\omega)\, d\omega \approx \lim_{N\to\infty} \sum_{i}^{N} J(\omega_{r_i})\, \Delta\omega \tag{3.50}$$

where

$$\begin{aligned} \Delta\omega &= \frac{\omega_{max}}{N} \\ \omega_{r_i} &= 0 + n_i \Delta\omega \end{aligned} \tag{3.51}$$

and n_i is the index number. The approximation comes from discretising the integral into a Riemann summation and therefore the approximation becomes more accurate as we choose a larger number of oscillators. Eq. (3.50) clearly shows that the coupling can be expressed as

$$g_i^2 \approx J(\omega_{r_i})\, \Delta\omega. \tag{3.52}$$

It is important to note that by choosing to use finite systems the model will undergo Poincaré recurrence [113, 114]. That is, after a finite time, the model will return to its original state because of the finite state space. The recurrence time, in this case, will be given by the number of oscillators, the frequencies and coupling strengths of these oscillators. Therefore by appropriately choosing the spectral density and the size of the bath we can ensure that we do not witness any recurrence in the time scale we simulate the model.

Different physical models are characterised by different forms of environmental spectra, which in turn directly affect how fast an OQS decays [116]. In this thesis we consider ohmic (Eq. (3.53)) and super ohmic (Eq. (3.54)) spectral densities [5, 9, 116]. The ohmic spectrum is perhaps the most commonly used density, especially in quantum brownian motion models and can be used, for example, to describe charged conductive electrons in metals [5]. An example of a super ohmic spectral density is to describe the effect of the interaction between a charged particle and its own electromagnetic field [117]. The spectral densities include a damping factor

(α) and an exponential cut-off which ensure that the high frequency couplings do not diverge.

$$J\left(\omega_{r_i}\right)_O = \alpha\omega_{r_i}e^{-\omega_{r_i}/\omega_c} \tag{3.53}$$

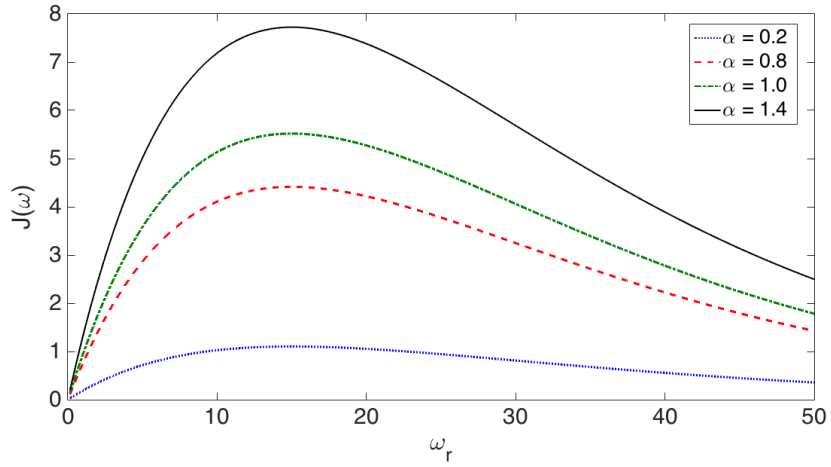


Figure 3.18: Form of an ohmic spectral density for various α values. The maximum frequency is 50 with a mode splitting of 0.1429 and the cut-off frequency is 15.

$$J\left(\omega_{r_i}\right)_{SO} = \alpha\omega_{r_i}^3 e^{-\omega_{r_i}/\omega_c} \tag{3.54}$$

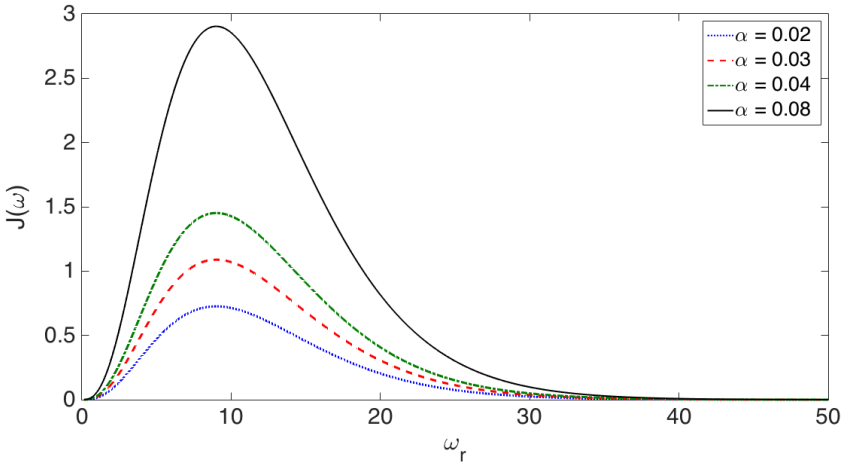


Figure 3.19: Form of an super ohmic spectral density for various α values. The maximum frequency is 50 with a mode splitting of 0.1429 and the cut-off frequency is 3.

The forms of these functions are shown in Figures 3.18 and 3.19. The cut-off frequencies, ω_c, for the ohmic and super ohmic baths are 15 and 3 respectively and we set the maximum frequency at 50 with a mode splitting of 0.1429.

3.2.3.2 Simulation details

To evaluate the ENMBQ we simulate the system coupled to a bath of 350 oscillators, in contrast to the master equation formalism, to avoid using approximations and to gain the ability to analyse the environment. The frequencies of the bath oscillators are distributed evenly up to a maximum frequency ω_{max} and therefore, the frequency splitting $\Delta\omega$ is given by $\omega_{max}/350$. The initial state of the bath for all the models is a thermal state with temperature T and the ancilla-system is a two mode squeezed state, the forms of which are given in Section 2.5. In Models 2 and 3 (see Sections 3.2.3.6 and 3.2.3.7 respectively), the additional bath and buffer modes are also initially in a thermal state with temperature T. We fix the system and ancilla frequencies ($\omega_s = \omega_a = 10$) the maximum bath mode frequency ($\omega_{max} = 50$) the temperature ($T = 1$) and the squeezing parameter ($\zeta = 4$) for Models 1, 2 and 3. Numerical results indicate that the squeezing parameter acts only to rescale the NMB without losing the qualitative features and so we choose ζ to exaggerate the observed effects (though not so high as to cause problems with the numerics) as shown in Figure 3.20. The equation that is simulated is given by Eq. 2.24 in Section 2.4.1.

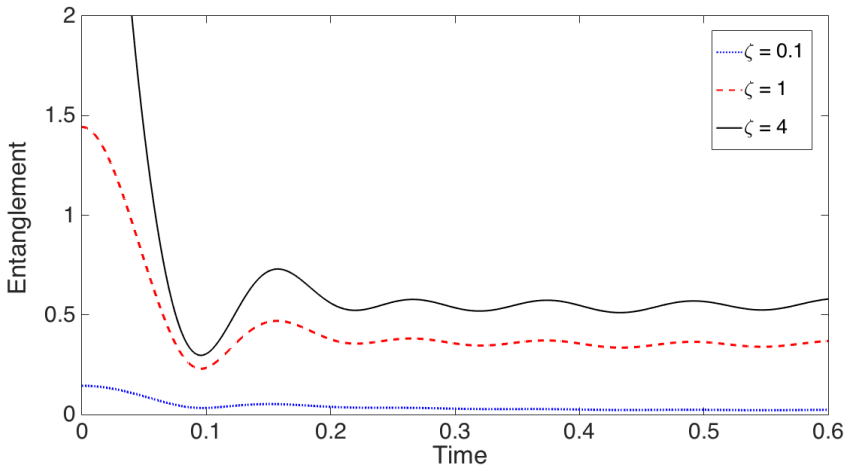


Figure 3.20: The entanglement dynamics of the system-ancilla state. We have used Model 1 with an ohmic spectral density to show the scaling effect of choosing a high squeezing parameter (ζ) value.

3.2.3.3 ENMBQ for ohmic baths

Figure 3.21 shows the predictions of the ENMBQ (Section 3.1.2) for Models 1-3 with an ohmic spectral density as a function of the spectral density damping factor α. The figure shows distinct regions of NMB. To understand the different regions for the multiple models we consider the

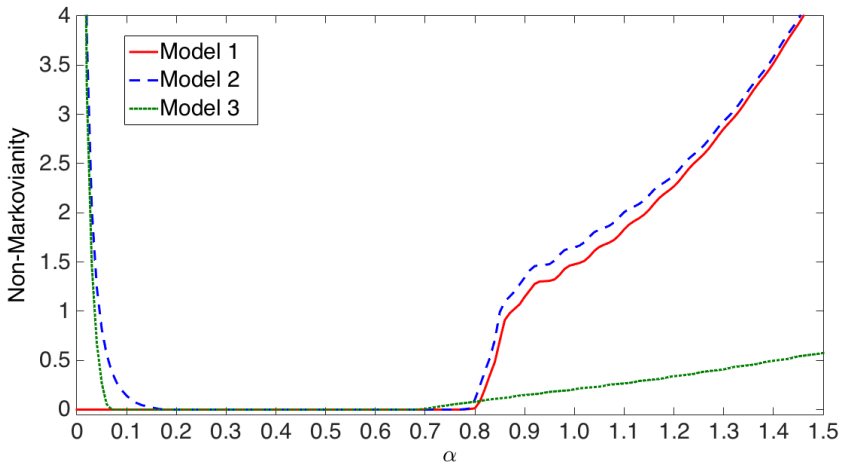


Figure 3.21: The figure shows the ENMBQ for the three models. We see that there is a high threshold α value for NMB and Models 2 and 3 display NMB for low α due to the strong coupling of the additional mode. The simulation is run from time $t_0 = 0$ to $t_f = 20$ in time intervals of $\Delta t = 0.001$.

entanglement dynamics for varying values of α. Using our knowledge of coupling strengths and by finding the occupation numbers of the bath modes with time, we can construct an interpretation of the processes involved when there are numerous modes coupled to the system.

As mentioned earlier, the first two types of interaction we consider are for Model 1 with a pair of spectral densities. The other two models add a single strongly coupled resonant mode to Model 1 in different configurations. The purpose of which is to understand how the NMB, as given by the ENMBQ, is affected by varying bath structures.

3.2.3.4 Model 1 with an ohmic bath

Beginning with an ohmic spectral density, Figure 3.22 shows the entanglement dynamics for Model 1 with varying α.

Furthermore we can also plot the occupancy of the bath modes against time. The occupancy is calculated by taking the $x_{r_i}^2$ and $p_{r_i}^2$ components from the CM. In our plots we have taken the $x_{r_i}^2 + p_{r_i}^2$ values of the bath mode r_i minus its initial thermal energy (i.e. the same value at t_0) as the occupancy. Removing the initial energy of the mode improves the clarity of the colour scale. The occupancy is intended to show how often and how much energy (up to a factor) a mode r_i has gained from the system and therefore is an indicator of the level of interaction between the system and bath mode. Figure 3.23 shows the occupancy of the bath modes for Model 1 with an ohmic spectrum and has a plot range of 1 to 30 for ω_r. The first few modes are ignored because they have a high initial thermal energy and so gain a negative value over time

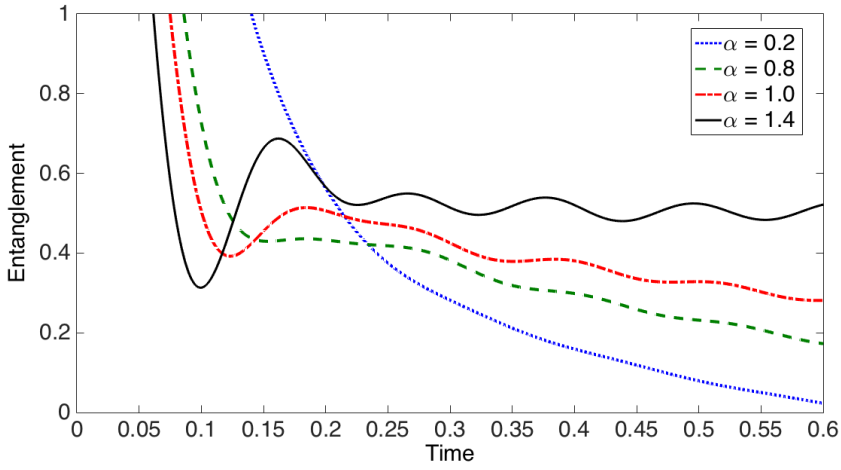


Figure 3.22: Entanglement dynamics for Model 1 with an ohmic bath. Coupling strengths to bath modes are varied by changing damping factor α in the spectral density function. We detect NMB after an α value of 0.8 and significant oscillations in the entanglement are seen after this value.

which skews the colour map on the surface plot. The high end is ignored because no significant dynamics take place in that region.

As time passes the entanglement is shared, unequally, to all the modes in the bath and sometimes this entanglement comes back to the system (if at all). The result of this dynamic depends on various parameters, which consequently decide the NMB of the model.

In the ohmic case, when the bath is weakly coupled with a scaling factor of $\alpha = 0.2$, the spectral density function (Figure 3.18) would suggest that the near-resonant bath modes have the strongest coupling and therefore the highest occupation and indeed we see that in Figure 3.23. At this stage the coupling strengths to the bath modes are too weak and we see decoherence which leads to dynamics that do not produce NM effects detectable by the ENMBQ. As α is increased the entanglement starts to decay faster due to a stronger coupling to the bath i.e. a faster transmission of information to the bath where it decoheres. For higher values of α however, EOs are increasingly found and NMB is detected by the ENMBQ.

The non-Markovianity of the model in this region of α values is influenced by a variety of factors including the strength of system-bath couplings, the occupation numbers of the bath modes and the ability of the system to induce oscillations in a bath mode's occupancy (which is an indicator of the level of interaction between them). If α is increased beyond a certain threshold initially a situation arises where the profile of the spectral density dictates that the system is *significantly* strongly coupled to near-resonant modes. Since the system shares more entanglement with the near-resonant modes, the stronger coupling increases the likelihood that

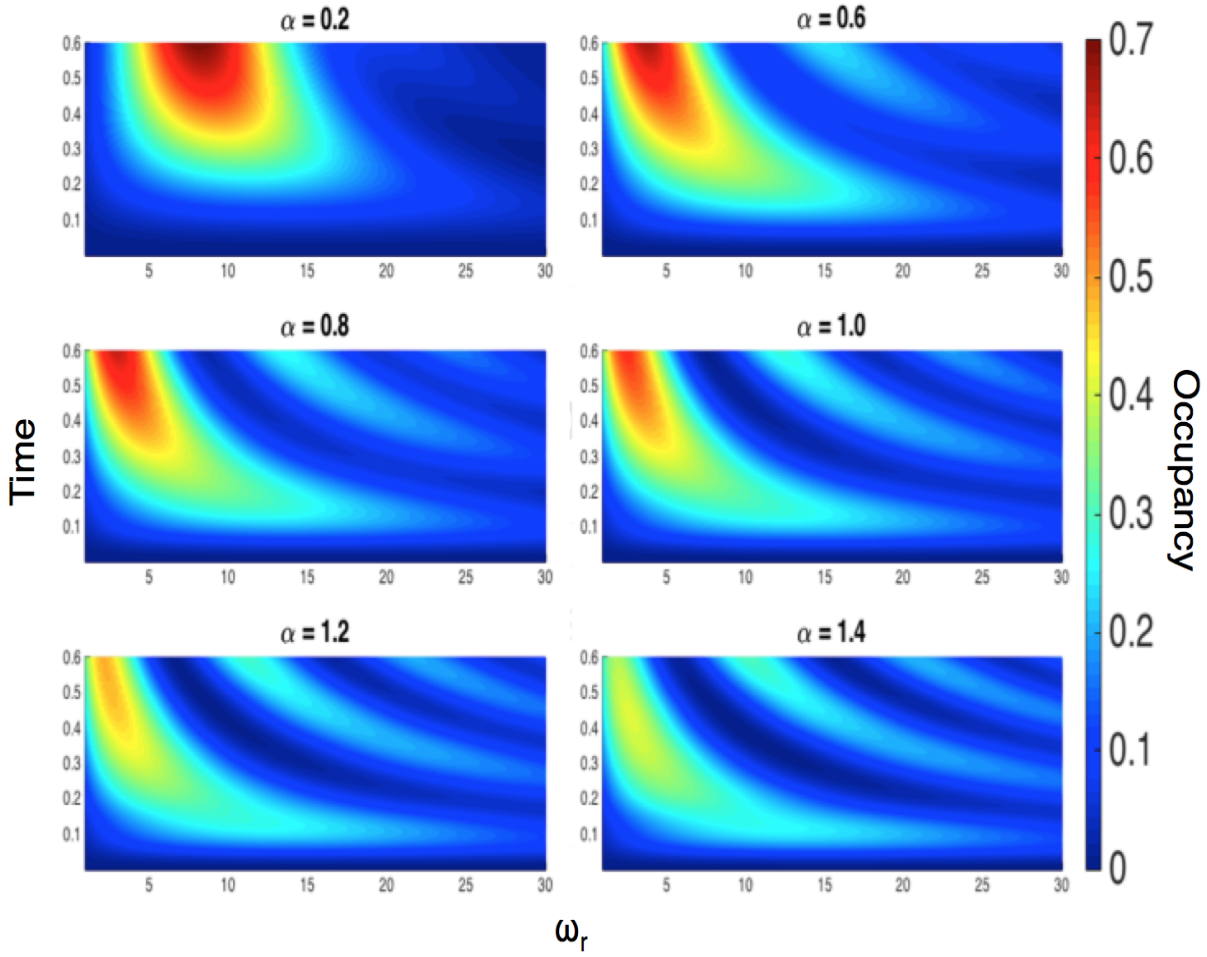


Figure 3.23: Occupancy of the bath modes for Model 1 with an ohmic bath. It shows that for low α the near-resonant modes ($\omega_{r_i} \approx 10$) interact more with system but as α increases the off-resontant modes start to play a more important role.

the dynamic results in an entanglement increase for the system-ancilla state. For now it is the near-resonant modes that are the main contributors to the NMB. This is due to the fact that at this coupling strength the combined frequency and magnitude of their EOs is more than that of the detuned modes, because the detuned modes have a very low EO magnitude thanks to the relatively weaker coupling they are allocated by the ohmic function.

As dictated by Eq. 3.53, when α is increased further, the detuned modes begin to couple more strongly to the OQS, resulting in an increased magnitude of their EOs. Our intuition is that if we include the fact that they have high frequency EOs (as a result of the detuning) and that they greatly outnumber the near-resonant modes, the combined entanglement increases of the detuned modes will be greater than the near-resonant modes. This now makes the detuned modes the important players in determining the NMB of the model.

The importance of detuned modes at stronger couplings is shown in Figure 3.23, where it

can be seen that an increase in α results in more occupancy and increased occupancy oscillations of these modes. This indicates that the system is interacting more with these modes. Moreover we notice at certain times the near-resonant modes are not occupied when we see an EO, e.g. at $\alpha = 1$ between times 0.45 and 0.5.

This transition between the importance of near-resonant/detuned modes is not easily seen for the ohmic case because the occupancy would suggest that it is only the detuned modes which are important. But as we will see in the other models, near-resonant modes do have a role to play.

3.2.3.5 Model 1 with a super ohmic bath

The next step is to investigate Model 1 with a super ohmic bath. Figure 3.24 shows the NMB for the model as given by the ENMBQ and the entanglement dynamics of the simulation is shown in Figure 3.25. The occupancy figure for this case also has a plot range of 1 to 30 for ω_r where again the high and low end are ignored for the same reasons as the ohmic scenario.

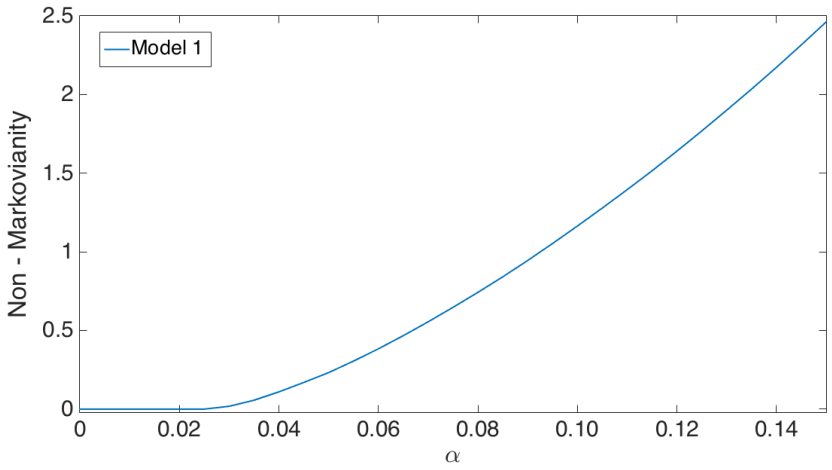


Figure 3.24: The ENMBQ for Model 1 with a super ohmic bath. We see that there is a lower threshold α value for NMB compared to the ohmic case. The simulation is run from time $t_0 = 0$ to $t_f = 20$ in time intervals of $\Delta t = 0.001$ and the α splitting is 0.005.

For Model 1 with a super ohmic spectrum, smaller values of α are needed for strong coupling strengths (see Eq. 3.54 and Figure 3.19). Therefore, as Figure 3.24 shows, a lower threshold α value was needed to observe NMB. Unlike the previous case Figure 3.26 shows that there is still a significant occupation in the near-resonant region when we initially witness NMB ($\alpha = 0.03$) and due to their naturally large EO magnitude, they play an important role. But as we saw in the ohmic case, when α is increased further the occupancy and occupancy oscillations of the

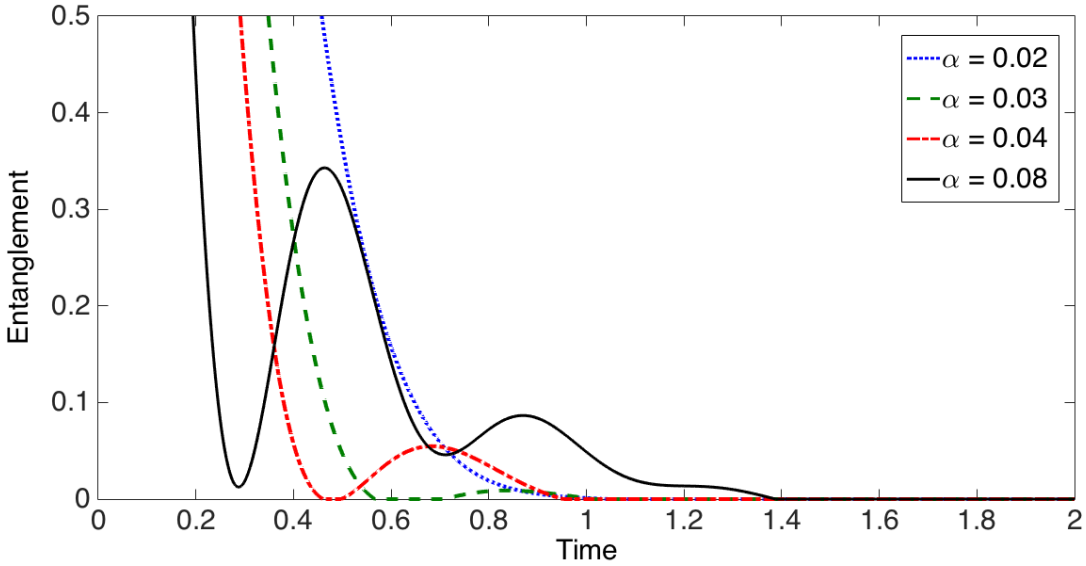


Figure 3.25: Entanglement dynamics for Model 1 with a super ohmic spectrum. NMB is detected after an α value of 0.03 and, as expected, we see EOs for those values.

detuned modes (Figure 3.26) become more significant and they will take the lead. This is again made clear when we see an entanglement increase between times 0.8 and 0.9 for $\alpha = 0.08$ and we see a low occupation of the resonant modes.

3.2.3.6 Model 2

Model 2 modifies Model 1 by adding a single strongly coupled resonant mode to the bath (see Figure 3.27), the Hamiltonian of this model is therefore of the following form

$$H = \omega_a a^\dagger a + \omega_s s^\dagger s + \omega_o o^\dagger o + h(so^\dagger + s^\dagger o) + \sum_{i=1}^{N} \omega_{r_i} r_i^\dagger r_i + \sum_{i=1}^{N} g_i (s^\dagger r_i + s r_i^\dagger) \tag{3.55}$$

where the coupling to the new bath mode o is h which is set to 1 for all investigations of this model. The entanglement dynamics for Model 2 are shown in Figure 3.28 and occupancy in Figure 3.29 where the low end frequencies are included because the dynamics are important in that region but the high end is still not significant so the plot range stops at $\omega_r = 30$. For Model 2 the ENMBQ suggests two regions of NMB which can be seen in Figure 3.21. The first region is for low α values where we get NMB due to the strongly coupled resonant extra mode in the bath. This can be seen from the EOs caused by the extra mode in Figure 3.28 and the lack of the occupancy in the resonant region of the bath (Figure 3.29), indicating that the extra mode is strongly interacting with the system. As α increases, the model behaves like Model 1 when

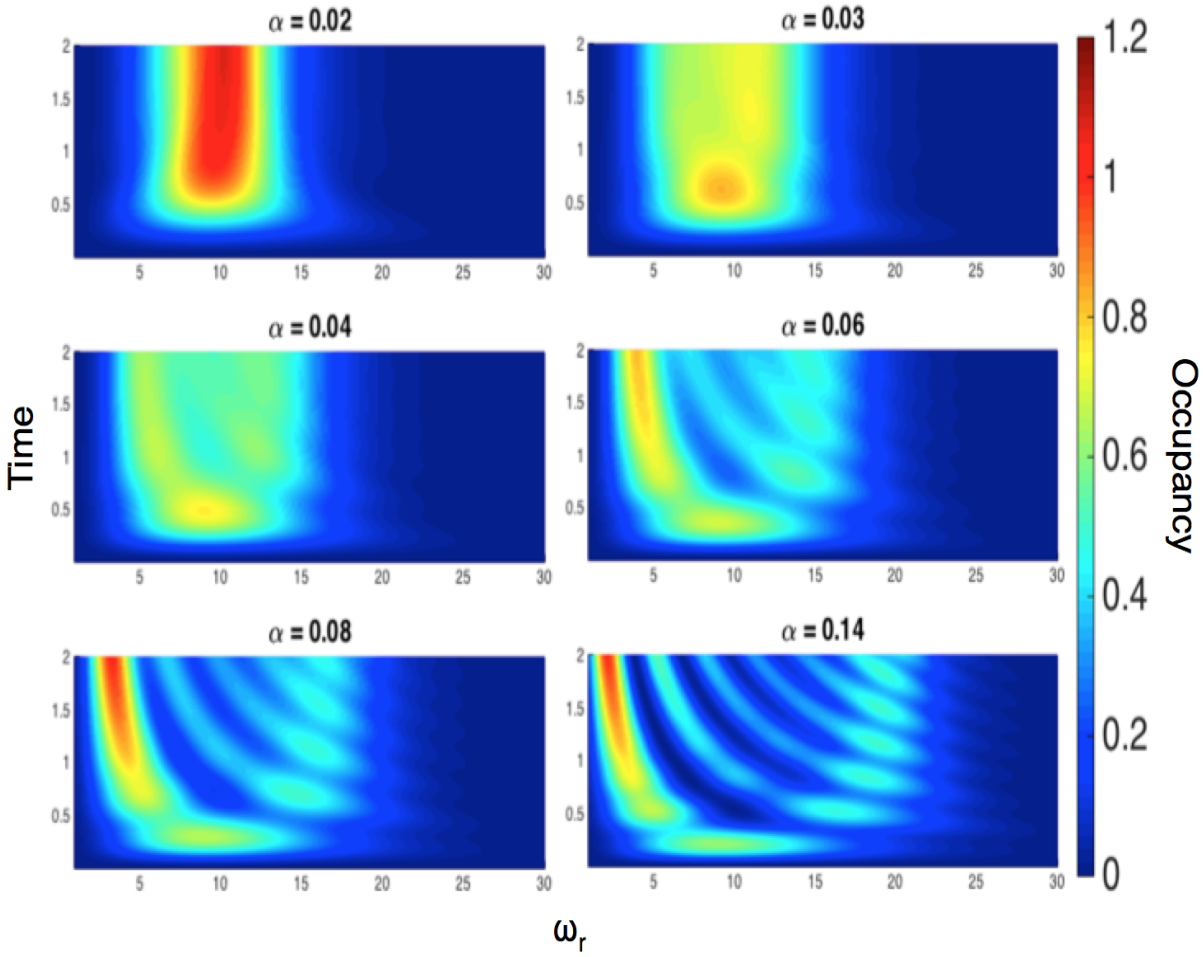


Figure 3.26: Occupancy of the bath modes for Model 1 with a super ohmic bath. It shows more clearly, in comparison to the ohmic case, that the near-resonant modes interact more with system for low α before the off-resonant modes take over.

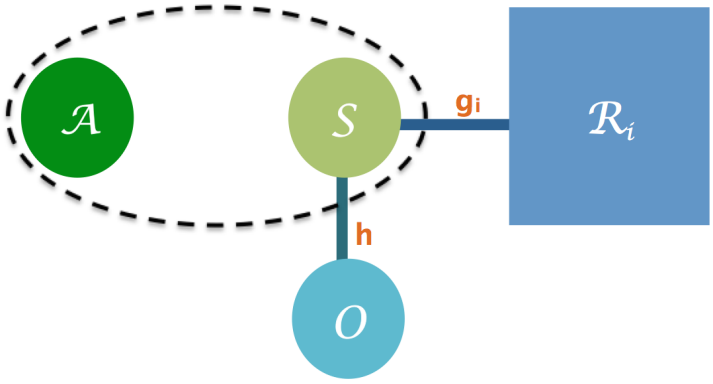


Figure 3.27: Diagram of Model 2. Model 2 is similar to Model 1 with a system (S) - ancilla (A) in an entangled state and the system coupled to all bath modes (R_i), but now there is an extra resonant mode (O) in the bath with a fixed coupling strength of $h = 1$. All bath modes and the extra mode are in a thermal state with temperature $T = 1$.

we enter a region where there is no NM dynamics as the rest of the bath is coupled strongly enough to kill the EOs from the extra mode. Then, as before, we see that when α is increased

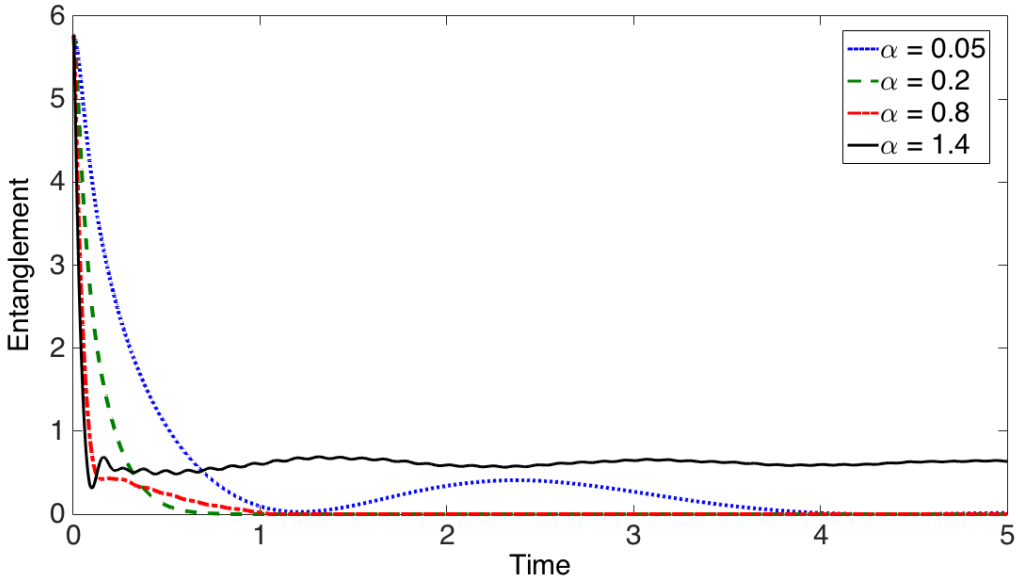


Figure 3.28: Entanglement dynamics for Model 2. It shows that for very low coupling we get EOs from the extra mode and as the coupling is increased this oscillation is suppressed. Then as α is increased further we see similar oscillations to Model 1 with an ohmic bath.

beyond a threshold we get NMB according to the same reasoning as in Model 1. Indeed it can be seen that the ENMBQ values follow a similar profile to that of Model 1 but with slightly more NMB. This is shown in the entanglement dynamics (Figure 3.28) and the occupancy of the bath modes (Figure 3.29). The additional NMB we notice is due to the extra strongly coupled mode, indicated again by the diminished occupancy in the resonant region compared to that of Model 1. Note that for Model 2, as we reach very high α values the occupancy in the resonant region of the bath increases and therefore Models 1 and 2 have increasingly similar ENMBQ values. This is because the resonant extra mode plays a less significant role since the off-resonant modes are the greatest contributors to the NMB in the high α region.

3.2.3.7 Model 3

Model 3 modifies Model 1 by adding a strongly coupled resonant 'buffer' mode in-between the system and the bath (see Figure 3.30), the Hamiltonian for this model is therefore of the following form

$$H = \omega_a a^\dagger a + \omega_s s^\dagger s + \omega_b b^\dagger b + h(sb^\dagger + s^\dagger b) + \sum_{i=1}^{N} \omega_{r_i} r_i^\dagger r_i + \sum_{i=1}^{N} g_i (b^\dagger r_i + b r_i^\dagger) \tag{3.56}$$

where the coupling between the system and buffer mode b is h which is set to 1 for all investigations of this model. The entanglement dynamics for this model is displayed in Figure 3.31

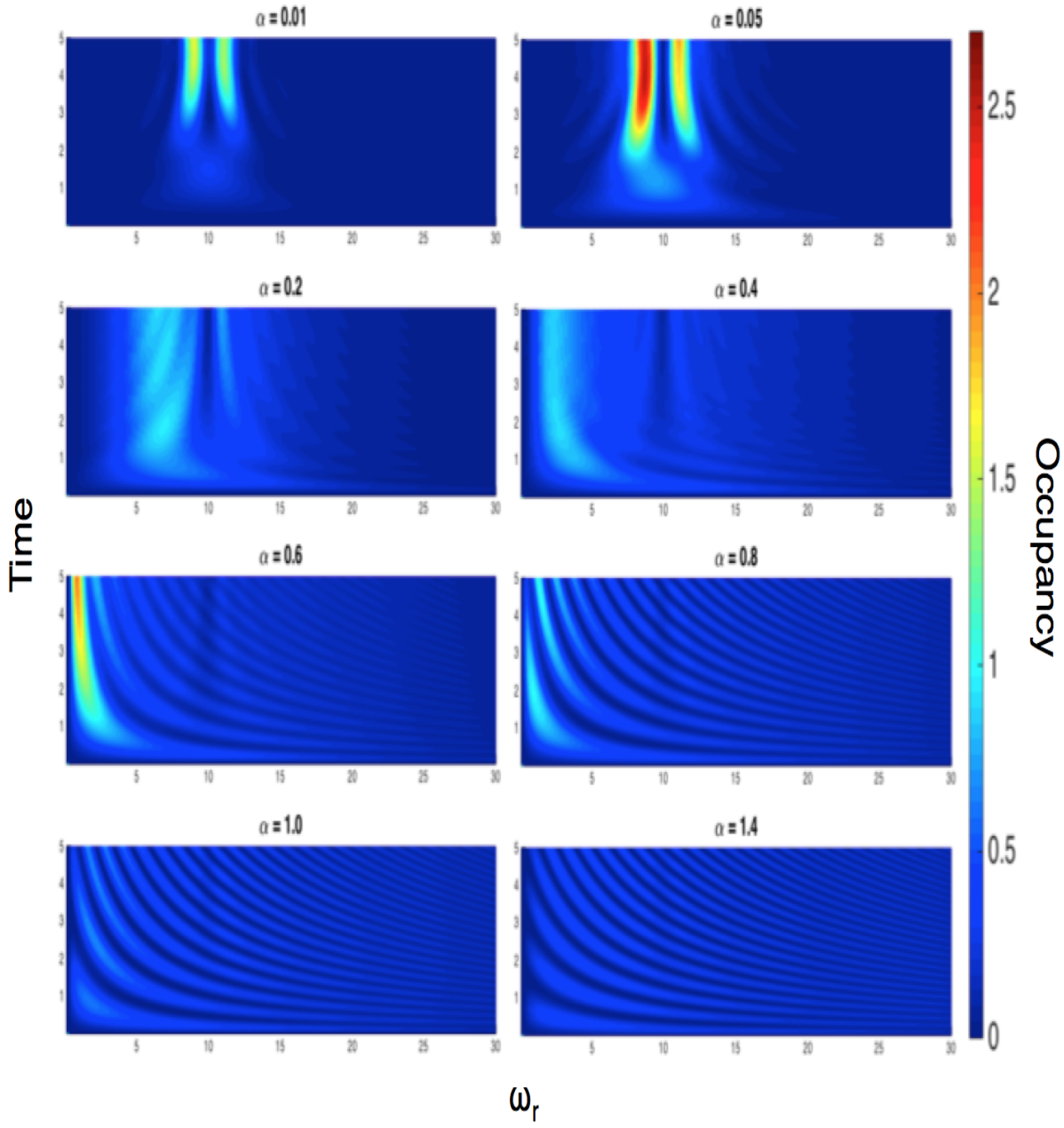


Figure 3.29: Occupancy of the bath modes for Model 2. It shows for very low α the resonant modes in the bath are unoccupied as resonant mode o has a stronger coupling than those in the bath. Then as α is increased the occupation reverts back to the Model 1 with an ohmic bath scenario since the bath coupling strengths are comparable to that of the extra mode.

and, as with Model 1, the occupancy figure (Figure 3.32) for this model has a plot range of 1 to 30 for ω_r i.e. it ignores both the high and low ends of the bath frequencies. Like Model 2, Model 3 also displayed two regions of NMB as shown in Figure 3.21. The first is for very low coupling strengths (i.e. low α) between the buffer and the bath. We witness NMB due to the 'reflections' of the entanglement from the strongly coupled resonant buffer mode (in similar fashion to Model 2) which can be clearly seen in Figure 3.31. As the buffer-bath coupling

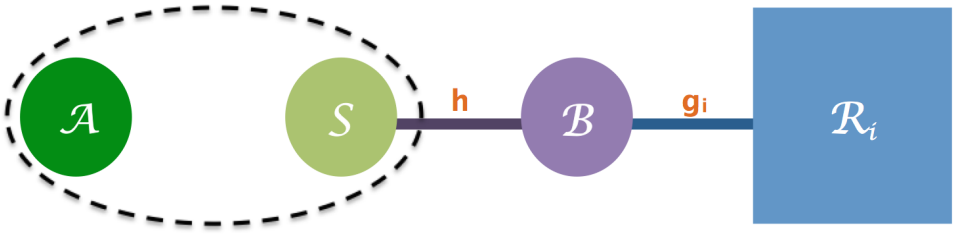


Figure 3.30: Diagram of Model 3. This model consists of the same parts as Model 2 but in a different configuration. The resonant extra mode is now a resonant 'buffer' (B) which is coupled to every bath mode (R_i) as well as the system (S). The buffer-system coupling strength is set to $h = 1$. The bath and buffer modes are in a thermal state with temperature T.

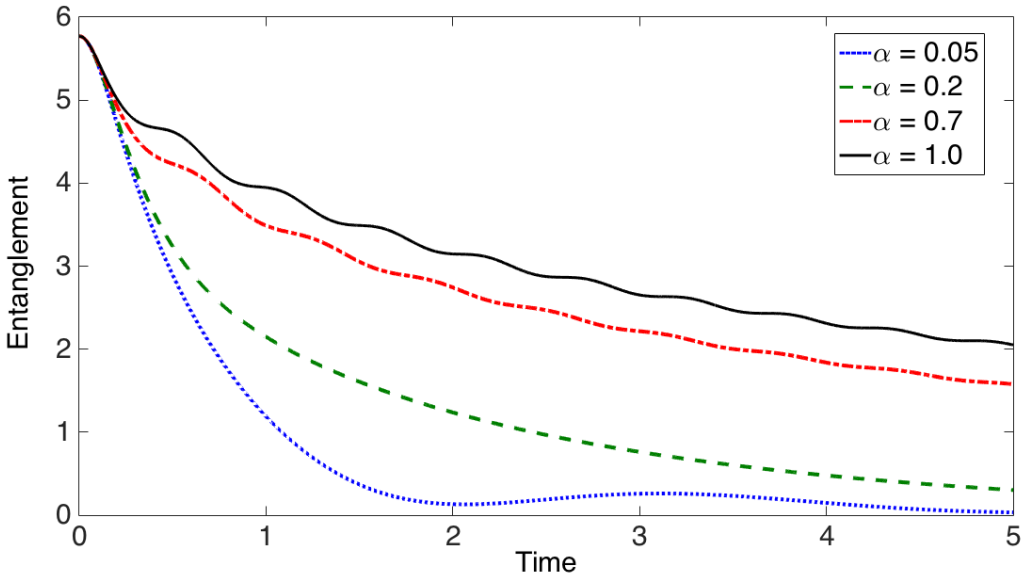


Figure 3.31: Entanglement dynamics for Model 3. It shows that for very low coupling we get EOs from the buffer mode and as the coupling is increased this oscillation is suppressed. Then as α is increased further we see oscillations due to the near-resonant bath modes.

strength is increased, NM dynamics is not detected because the buffer leaks the entanglement to the bath before it has a chance to return (i.e. Model 1 at low α and Model 2 in the Markov region). Note however, in comparison to Model 2, a smaller α is needed to see no NMB as the buffer leaks the entanglement to the near-resonant modes in the bath before it can give it back to the system mode.

As we have seen before, beyond a threshold, increasing α results in NMB. Note however that there are two key differences to Models 1 and 2; a lower threshold value of α and a lower value of non-Markovianity. The reasons for these differences can be seen from the occupancy (Figure 3.32). They show a large occupancy of the near-resonant frequency region indicating that the buffer is primarily interacting with the near-resonant modes which are now solely responsible for the NMB.

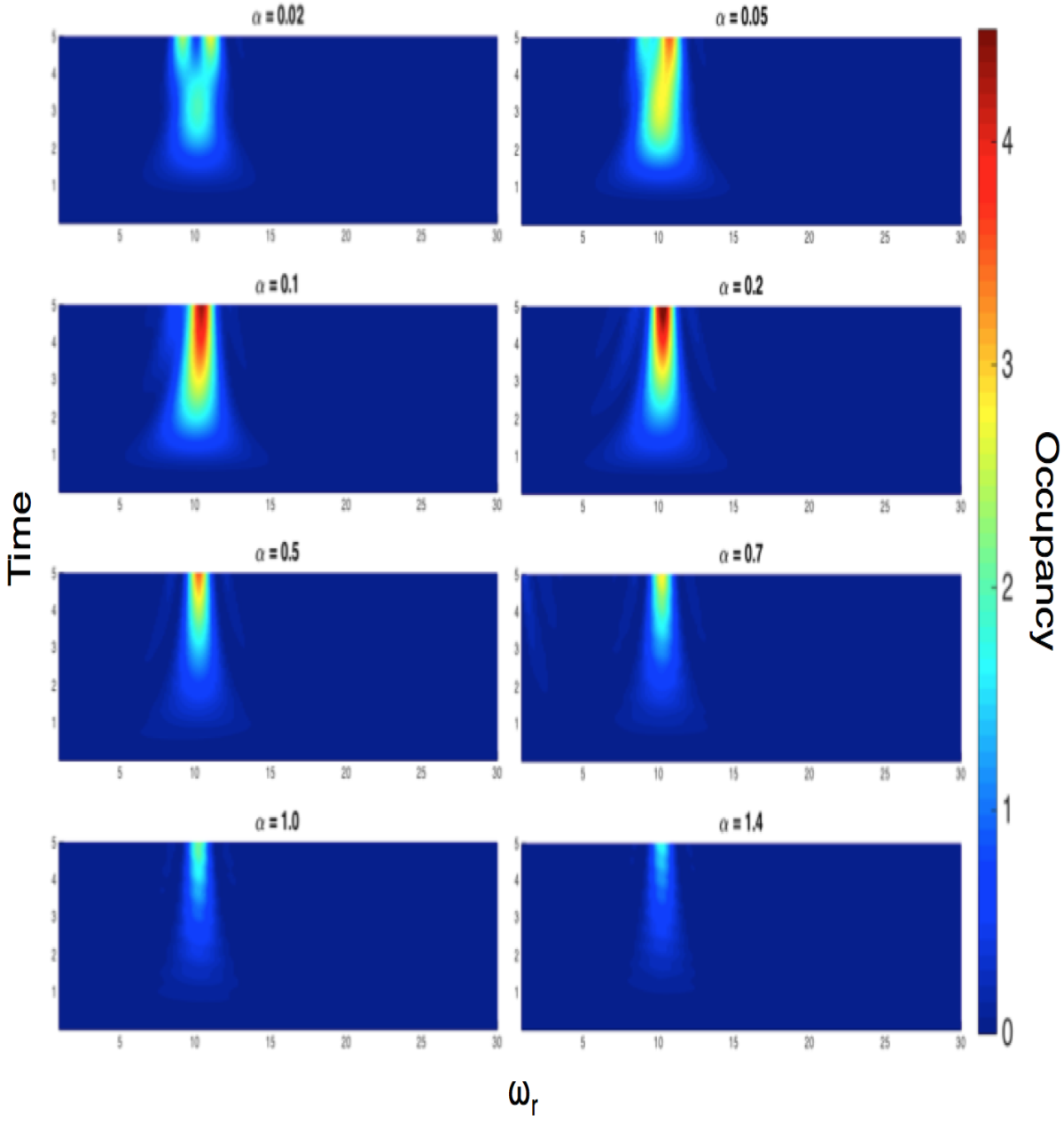


Figure 3.32: Occupancy of the bath modes for Model 3. It shows that the buffer mode has effectively reduced the size of the bath. As α is increased the number of modes in the bath which interact with the buffer reduces.

Figure 3.31 shows that the EOs at high α are significantly different to the other models. We can clearly see that there are fewer oscillations and a longer decay time. This, along with Figure 3.32, seem to indicate that the buffer has effectively reduced the size of the bath around the resonant region. For the chosen system-buffer coupling, we can hypothesise that the threshold is lower because of the reduced bath size. Also the value of the NMB is lower because the near-resonant modes have a lower EO frequency and are few when compared to the detuned modes.

3.3 Concluding remarks

In this chapter, using a series of coupled harmonic oscillators, we investigated the role resonant and off-resonant modes play in determining the NMB predicted by an entanglement-based quantifier of non-Markovianity, which we termed the ENMBQ. We began with an investigation of models with one and two 'bath' oscillators to get an intuition of the entanglement sharing between the system and the 'bath' modes. Understanding that detuning and coupling strength played a significant role in the flow of information, we analysed four OQS models.

The first two models considered a harmonic oscillator coupled to a bath (Model 1) with two different spectral density functions. The CM formalism allowed us to determine which modes in the bath played the important role in determining NMB, which would not be possible with a master equation approach. Roughly speaking, we found that when the coupling to the bath was sufficiently strong the near-resonant bath modes were primarily responsible for NMB, but for even stronger couplings it was the off-resonant modes that played a crucial role.

The other two models (Models 2 and 3) added a single strongly coupled resonant oscillator to the scheme in different configurations. This lead to NMB detected at lower couplings to the bath for both cases and diminished NMB for larger coupling values when the extra mode was a buffer between the system and the bath (Model 3).

It should be noted that models similar to Model 3 have been investigated in works on effective spectral densities and the structure of the bath which could be used to extend the model [118, 119]. These papers use techniques that transform the multiple oscillator bath model to a coupled chain. In a different vein of investigation, an analysis of the entanglement dynamics for coupled cavity fields in various baths using Feynman - Vernon influence functional theory [120] has been done, as well as EOs in a single qubit-bath model [121].

As mentioned in the introduction to this chapter, there has been recent interest in how structured environments can be used to exploit non-Markovianity to aid the control of a quantum system. Our methodology has allowed us to isolate the modes in the bath that play a significant role in determining NMB and therefore are better equipped to engineer environments to control the flow of quantum information. Here we noted the importance detuning and coupling strengths have on the flow of entanglement, but of course the ENMBQ is not the only witness/measure of NMB that exists in the field. In the next chapter we perform a brief inspection into another witness (based on fidelity) and note if the same factors play a role in its prediction of NMB.

Chapter 4

Fidelity-based non-Markovian behaviour quantifier

In the previous chapter the importance of NMB was made quite apparent, as was the significance of structured environments on quantum systems [98–104]. Chapter 3 highlighted the modes in the bath that play a significant role in determining NMB as given by the ENMBQ. Of course the ENMBQ is not the only witness/measure of NMB that exists in the field [92, 105], and entanglement is not the only quantum information that researchers are concerned with manipulating. Therefore it is relevant for us to verify whether the factors noted in the previous chapter apply to another quantifier of NMB.

This chapter considers a fidelity-based measure of NMB proposed by Vasile et. al. [91] as an extension of Breuer's NMB measure [108] for GSs. Breuer's measure is based on trace distance, a measure of the similarity of two states. We consider the fidelity (also a measure of distinguishability) based measure as it can be easily calculated for a GS (see Section 2.6.2). In their paper Vasile et. al. use a weak-coupling, secular non-Markovian master equation [9, 36, 122–124] to describe a model of a single mode squeezed state coupled to an ohmic bath of oscillators. Their analysis mostly attributes NMB to the time-dependent diffusion coefficient in the master equation. Our analysis however, avoids the use of the approximations used in the master equation by once again utilising a large finite bath to simulate this model via a CM approach, as seen in Chapter 3. The focus of this chapter is to better understand the factors that determine NMB as given by this measure in order to check whether there are any similarities with the ENMBQ. This work has been covered in our paper 'Affecting non-Markovian behaviour by changing bath structures' [111].

4.1 Definition and quantification

Based on the information back-flow definition of NMB, the measure proposed by Vasile et. al. [91] has the advantage of providing a necessary and sufficient condition for NMB (hence it is a proper *measure*); however, it relies on a maximisation step which makes it hard to compute. The measure is based on the distinguishability of two different initial states ρ_1 and ρ_2 under the action of a dynamical map $\mathcal{E}$. The distinguishability is given by

$$\mathcal{D}(\rho_1, \rho_2) \equiv 1 - F(\rho_1, \rho_2) \tag{4.1}$$

with

$$F(\rho_1, \rho_2) \equiv Tr\sqrt{\sqrt{\rho_1}\rho_2\sqrt{\rho_1}} \tag{4.2}$$

where F is the fidelity (see Section 2.6.2). Under the action of any CP map the distinguishability follows the contractive property

$$\mathcal{D}(\mathcal{E}\rho_1, \mathcal{E}\rho_2) \leq \mathcal{D}(\rho_1, \rho_2). \tag{4.3}$$

Hence, under Markovian evolution, the divisibility property (given in Eq. (3.3)) will ensure a monotonic decrease of distinguishability in analogy to what was observed for the system-ancilla entanglement (see Eq. (3.4)). Such irreversible loss of distinguishability may be understood as the leakage of 'quantum information' into the bath, which in turn is unable to transfer the information back to the system. Hence any increase in distinguishability can be interpreted as the environment returning part of the leaked information to the system, a signature of NMB. Similarly to the ENMBQ, a measure of non-Markovianity can be constructed by summing the distinguishability increases between pairs of quantum states. Restricting the analysis to GSs, the non-Markovianity is given by

$$\mathcal{N}_P = \max_P \left[- \int_{\dot{F}<0} \frac{d}{dt} F\left(P, t\right) dt \right] \tag{4.4}$$

where one maximises over all parameters, P, of the GS. These parameters are not bounded and therefore running this measure can become numerically challenging.

The fidelity relies on the states of the two systems and is therefore dependent on the energy of the states at any given time. Since the measure collects variations in fidelity, the energy

dynamics could have an impact on the NMB. As we will see later in this chapter, the energy dynamics of the system is dependent on the modes in similar fashion to that of entanglement. These dynamics are very dependent on the initial state of the system which is why the maximisation procedure is needed, and even if we restrict ourselves to squeezed states, a maximisation over both the squeezing parameter and the phase is necessary, making the measure numerically time-consuming. What can be done, however, is to understand the impact the modes would have on the predictions of this measure. Note that under the divisibility definition this measure, even with the maximisation, would only be a witness, as there exists non-divisible dynamics which can increase the fidelity.

In our analysis we investigate just one pair of initial states and this allows the fidelity to be used as a quantifier of NMB for this particular case under the information feedback definition of NMB, i.e. a fidelity-based NMBQ (FNMBQ).

4.2 Analysis

Once again the CM approach is utilised to simulate the model and the formula given in Section 2.6.2.1 is used to calculate the fidelity from the CM. We initially consider the simplest case of a system coupled to a single 'bath' mode and then move on to a model of a single mode squeezed thermal state coupled to an ohmic bath (i.e. the scenario considered by Vasile et. al. [91]).

4.2.1 Energy dynamics of two coupled oscillators

As in the previous chapter we initially investigate the simplest case of a single 'bath' mode. A single system mode (s) in a squeezed thermal state with squeezing parameter r and temperature T_s is coupled with a strength g to a 'bath' mode (b) in a thermal state with temperature T_b (see Figure 4.1).



Figure 4.1: Diagram of the single 'bath' mode model. The system (S) is in a squeezed thermal state. The system is then coupled to a single 'bath' oscillator (B) which is in a thermal state.

The Hamiltonian for this model is given as

$$H = \omega_s s^\dagger s + \omega_b b^\dagger b + g\left(s^\dagger b + s b^\dagger\right) \tag{4.5}$$

where ω_s and ω_b are the system and 'bath' mode frequencies respectively. The initial CM, γ, is given by

$$\gamma = \begin{pmatrix} (2\bar{n}_s+1)(\cosh(2r)+\sinh(2r)) & 0 & 0 & 0 \\ 0 & 2\bar{n}_b+1 & 0 & 0 \\ 0 & 0 & (2\bar{n}_s+1)(\cosh(2r)-\sinh(2r)) & 0 \\ 0 & 0 & 0 & 2\bar{n}_b+1 \end{pmatrix} \tag{4.6}$$

where

$$\begin{aligned} \bar{n}_s &= \frac{1}{(\exp(\omega_s/T_s)-1)} \\ \bar{n}_b &= \frac{1}{(\exp(\omega_b/T_b)-1)}. \end{aligned} \tag{4.7}$$

Note that we have set the phase of the squeezing ϕ to zero.

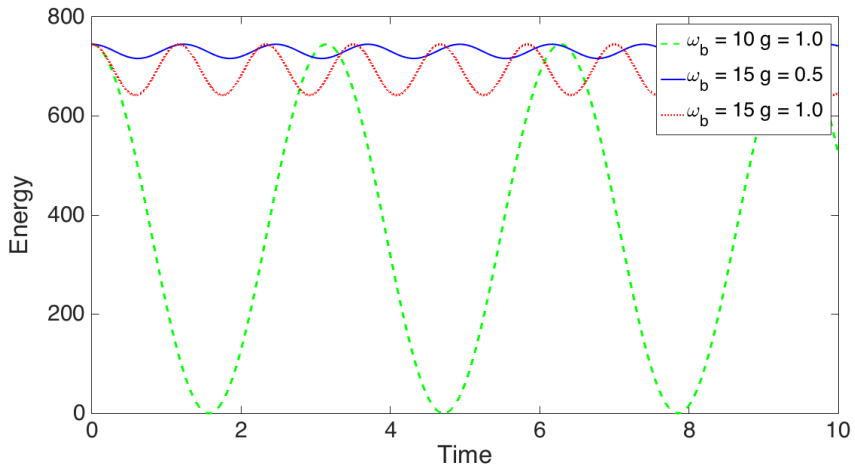


Figure 4.2: Energy dynamics of a single mode squeezed thermal state (with $r = 4$ and $T_s = 1$) coupled to a thermal mode with temperature $T_b = 1$. The three lines represent the energy dynamics of the system mode; Green - [$\omega_b = 10$, $g = 1$], Blue - [$\omega_b = 15$, $g = 0.5$], Red - [$\omega_b = 15$, $g = 1$].

Figure 4.2 shows the energy dynamics for this model for the case of $w_s = 10$, $r = 4$ and $T_s = T_b = 1$ for varying g and ω_b. The energy dynamics can be gained from the CM with the following equation

$$E = \langle s^\dagger s \rangle = \frac{1}{4}(\gamma_{11} + \gamma_{22}) - \frac{1}{2} \tag{4.8}$$

where we have used Eq. (2.25) to expand the ladder operator in the position-momentum basis and utilised the definition of the CM (Eq. (2.9)). The energy dynamics show that the system shares energy with the same dependence on coupling strength and frequency as in the single 'bath' mode case for the entanglement dynamics (see Section 3.2.1). As shown in Figure 4.2

the energy of the system is shared maximally when the 'bath' mode is resonant. The oscillation magnitude drops as the mode is further detuned from the system frequency. As before, when the coupling is strengthened there is an increase in frequency of any oscillation and the magnitude of an off-resonant oscillation.

4.2.2 Fidelity and energy dynamics of an open system

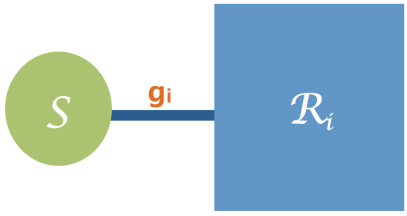


Figure 4.3: Diagram of the OQS used to investigate the FNMBQ. The system (S) is in a squeezed thermal state. The system is then coupled to each bath mode (R_i) with respective coupling g_i. The bath is in a thermal state with temperature T.

To investigate the FNMBQ we consider an OQS with temperature $T_s = 1$ and two different squeezing parameters, r. The system is then coupled to a bath in a thermal state with temperature $T = 1$ (see Figure 4.3). The spectral density of the bath is ohmic (see Section 3.2.3.1) and all associated frequency parameters are the same as the models in Chapter 3 with the frequency of the system mode kept at 10.

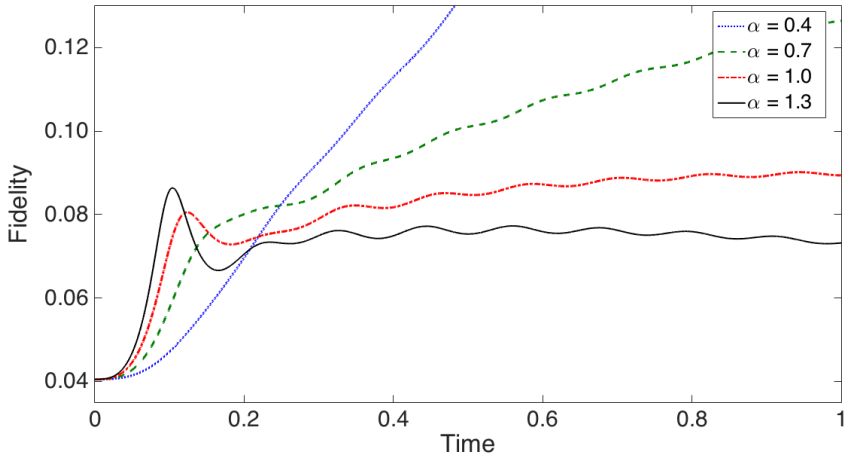


Figure 4.4: Fidelity dynamics between two different initial single mode squeezed thermal states. The two states have zero phase but they have different squeezing parameters, r, of 4 and 0.1. We find more oscillations in the fidelity as the damping factor, α, is increased.

Figure 4.4 shows the fidelity dynamics for a pair of initial states which vary only in the squeezing parameter, r, with values of 4 and 0.1 (the phase, ϕ, is set to zero in both cases). We

can clearly see that as α (and therefore the coupling to the environment) is increased we start to see oscillations in the fidelity between the two states, which indicates the presence of NMB. The oscillations in the fidelity seem to coincide with the oscillations in the energy dynamics for $r = 4$ (as shown in Figure 4.5), indicating that the energy dynamics do have a role to play in the NMB predicted by the FNMBQ. Figure 4.5 also shows that as the α value increases more oscillations are seen in the energy of the system. This is analogous to the ENMBQ where the NMB is caused by oscillations in the entanglement dynamics rather than the energy dynamics. From our analysis of the ENMBQ for Model 1 (see Section 3.2.3.4) we know that at low couplings the near-resonant modes receive the majority of the energy (which can essentially be seen, up to a factor difference, from the occupancy figure, Figure 3.23) and therefore affect the NMB. As the coupling is increased the detuned bath modes start to gain more energy from the system and become the driving force of the NMB. This is due to the high frequency of their energy oscillations, which we are aware of from our analysis of the simple single 'bath' mode scenario.

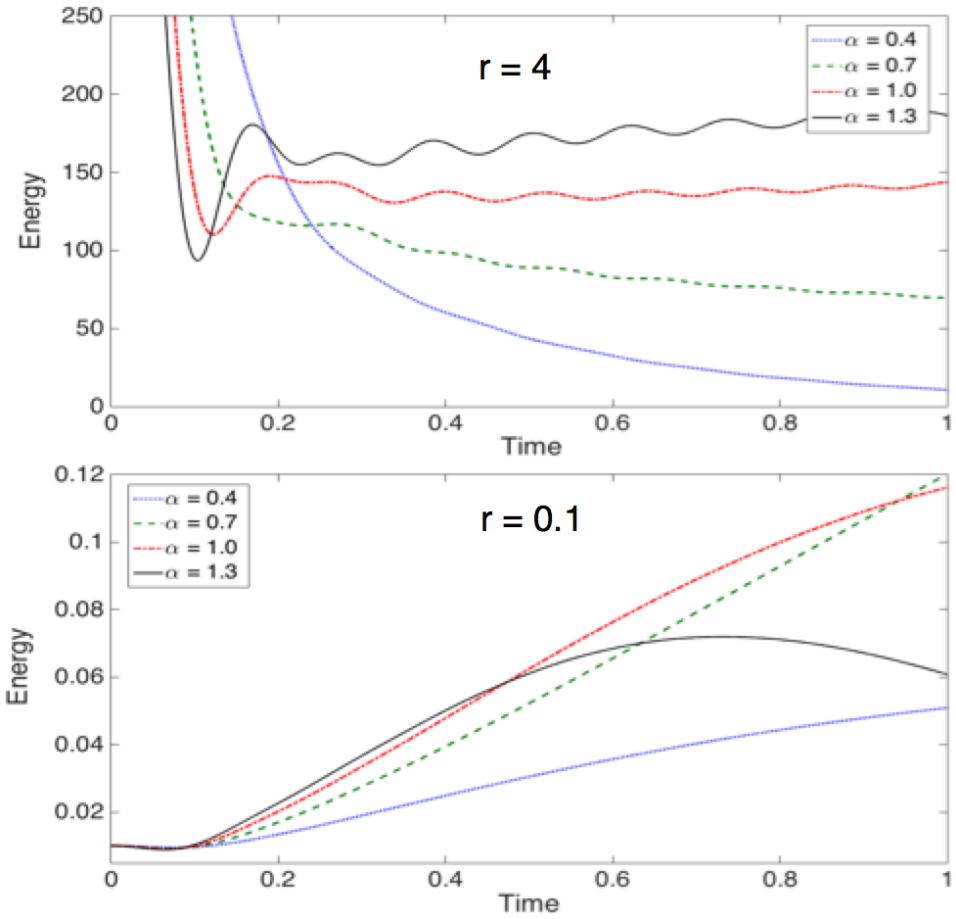


Figure 4.5: Energy dynamics of single mode squeezed states coupled to an ohmic bath. The initial squeezing parameter of the states, r, are 4 and 0.1. We find oscillations in the energy dynamics in a similar fashion to the EOs in the ENMBQ scenario as α is varied.

4.3 Concluding remarks

The purpose of this chapter was to determine the underlying factors which affect the FNMBQ and understand any similarities, if any, with the ENMBQ. Indeed the analysis has revealed that the FNMBQ is dependent on coupling strengths and detuning in similar fashion to the ENMBQ. By analysing the energy dynamics of a simple single 'bath' mode model and a pair of squeezed thermal states, we found that the same basic principles are responsible for energy oscillations as they were for the entanglement oscillations in the ENMBQ. Therefore, this would lead us to believe that it is likely that the interplay between coupling strengths and off-resonance is responsible for the oscillations that are utilised in other witnesses/measures of non-Markovianity.

The usefulness of this knowledge is highlighted in the manipulation of environments in various quantum models [98–104]. Whereas the previous chapter allowed one to isolate the modes that played a crucial role in the flow of entanglement in a particular model, here we are shown the bath modes that are responsible for the energy dynamics. Armed with this knowledge, one could better engineer environments to maintain and control the flow of energy in an OQS. Moreover it suggests that the properties of the modes that determine the oscillations are the same for both cases and quite possibly for other forms of quantum information. Therefore it is our hope that this methodology could be utilised to better structure environments to aid the controlled quantum dynamics of multiple forms of quantum information.

The next chapter tackles another approximation, namely the Rotating-Wave approximation, and its effects on the predictions of the ENMBQ.

Chapter 5

Role of counter rotating terms on the entanglement-based non-Markovian behaviour quantifier

All models considered so far in this thesis have Hamiltonians which have applied to them what is known as the Rotating-Wave approximation (RWA). The RWA modifies the interaction Hamiltonian by removing the fast oscillating counter rotating (CR) terms. The theory of the RWA and its applicability to various models has been discussed in many works, e.g. the books given in Refs. [6, 9, 63]. As with all other approximations the RWA's validity has been scrutinised in multiple situations, for example the study by Agarwal on the effect of the RWA on spontaneous emission [125–127]. For our particular interests, it is worthy to note work that questions the validity of the RWA for open systems [43, 48] and non-Markovianity [44].

Usually the RWA loses its validity when there are strong couplings involved, as the fast oscillating terms start to become more significant. With recent advances in quantum technologies stronger interactions are being observed and subsequently there has been interest in the application of the RWA in open quantum systems [43, 45–48, 128–130]. Usually when one considers an OQS the system-environment coupling applies a RWA since a weak coupling to the environment is assumed [6, 9, 63]. Some early work by Walls [128] and subsequently Cresser [129] has shown that when considering a strongly coupled system a weak coupling approximation to the environment may not accurately describe the model. They show that the stationary solution for the density operator of the system is inconsistent with the expected form given by the sta-

tistical mechanics of a system in thermal equilibrium. This suggests that applying the RWA to the system-environment interaction in this scenario may not be correct and has prompted work that includes both the RWA and CR terms when investigating a strongly coupled system [130, 131].

The effect of the RWA on the trace-distance-based measure of non-Markovianity was researched by Mäkelä and Möttönen [44]. They show that the application of the RWA reduces the non-Markovianity, as given by the trace distance, for a two-level atom coupled to an environment.

From our analysis of the ENMBQ we observed NMB either when a threshold value of α is passed, or from a strongly coupled resonant mode. At this threshold of α, the coupling strengths to the bath modes become relatively strong as given by the spectral density (Section 3.2.3.1). Therefore, we note that the ENMBQ predicts the presence of NMB when there are strong couplings involved. The studies on the validity of the RWA for strong couplings and non-Markovianity would suggest that it is warranted to consider the effect of CR terms on the ENMBQ. Thus this chapter is dedicated to an investigation of the ENMBQ for Hamiltonians which include both the RWA and CR terms, also known as an x-x coupling, to see if the predictions of NMB are affected.

5.1 Counter rotating terms

We begin by briefly showing how the $a^\dagger b + ab^\dagger$ interaction we have utilised so far can be gained by applying a RWA to x-x couplings. The terms that are excluded by the RWA are called the CR terms. A Hamiltonian which includes the full x-x coupling between two oscillators has the form

$$H = H_0 + H_I = \omega_a a^\dagger a + \omega_b b^\dagger b + g\left(a + a^\dagger\right)\left(b + b^\dagger\right) \tag{5.1}$$

where we have split the Hamiltonian into two components; the free Hamiltonian, H_0 which includes the free oscillating terms of mode a and b and the interaction between them given by the interaction Hamiltonian H_I. The most famous usage of the RWA in quantum optics is the Jaynes-Cummings model [132] of a two-level atom in a cavity as shown by the Hamiltonian below

$$H_{JC} = \omega_{cav} c^\dagger c + \omega_{atm}\frac{\sigma_z}{2} + \frac{\Omega}{2}\left(c\sigma_+ + c^\dagger\sigma_-\right) \tag{5.2}$$

where ω_{cav}, ω_{atm}, $\sigma_{\pm}$, σ_z, c and Ω are the cavity field and atom frequencies, the atomic ladder, atomic inversion and cavity annihilation operators, and the atom-cavity coupling strength respectively. The RWA has also been used for many other models [6, 9, 63]. To perform the RWA we take the above Hamiltonian (Eq. (5.1)) and perform a rotation, similar to the ones shown in Section 3.2.1.2, by $-H_0$.

$$\begin{aligned}\widetilde{H} &= -H_0 + e^{iH_0t} H e^{-iH_0t} \\ &= -H_0 + e^{iH_0t} \left(H_0 + H_I\right) e^{-iH_0t} \\ &= e^{iH_0t} H_I e^{-iH_0t}\end{aligned} \tag{5.3}$$

where we have used the fact that when the Hadamard Lemma (Eq. (2.52)) is applied to perform a rotation on the free Hamiltonian it leaves it unchanged as clearly H_0 commutes with itself. The rotation on the interaction part of the Hamiltonian gives

$$\widetilde{H} = g\left(abe^{-i(\omega_a+\omega_b)t} + a^\dagger be^{i(\omega_a-\omega_b)t} + ab^\dagger e^{-i(\omega_a-\omega_b)t} + a^\dagger b^\dagger e^{i(\omega_a+\omega_b)t}\right). \tag{5.4}$$

The RWA argues that when $\omega_a \approx \omega_b$ the terms of the form $e^{\pm i(\omega_a+\omega_b)t}$ oscillate rapidly in comparison to the other terms in the Hamiltonian and so can be averaged to zero [6, 9, 63] while the terms containing $e^{\pm i(\omega_a-\omega_b)t}$ will remain. This gives us the final form of the RWA Hamiltonian, which we have used in Chapter 3, as shown in Eq. (5.5) below.

$$\widetilde{H} = g\left(a^\dagger b + ab^\dagger\right) \tag{5.5}$$

The terms that have been removed from the Hamiltonian, i.e. $a^\dagger b^\dagger$ and ab, are known as the CR terms.

5.2 Adapted models

For the rest of the chapter we will investigate the models in Chapter 3 but now we include the CR terms to see if the predictions of NMB are affected. We use the same parameters as those mentioned in Chapter 3 for all the models with the exception of the final time of the simulation which is now set to one (i.e. one tenth of ω_s), for most of the plots, for reasons explained later in this section, but is sufficient to see the dynamics that we are interested in.

5.2.1 Model 4 - Model 1 with counter rotating terms

The Hamiltonian for Model 4, i.e. Model 1 with CR terms included, is given by

$$H = \omega_a a^\dagger a + \omega_s s^\dagger s + \sum_{i=1}^{N} \omega_{r_i} r_i^\dagger r_i + \sum_{i=1}^{N} g_i \left(s r_i + s^\dagger r_i + s r_i^\dagger + s^\dagger r_i^\dagger \right). \tag{5.6}$$

We now analyse the NMB predictions by the ENMBQ for this model for both ohmic and super ohmic baths.

5.2.1.1 Ohmic bath

Figure 5.1 shows the results of the ENMBQ for Models 1 and 4 with an ohmic bath.

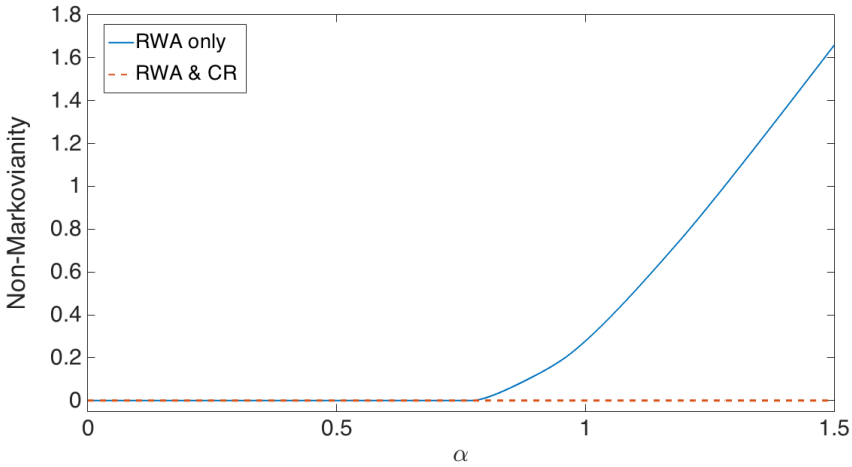


Figure 5.1: ENMBQ for Models 1 and 4 with an ohmic bath. Note that the final time of the simulations is now 1. The addition of the CR terms removes any trace of NMB predicted by the ENMBQ. The model parameters are the same as Model 1 with an ohmic bath, i.e. $\omega_s = \omega_a = 10$, $\zeta = 4$, $\omega_{max} = 50$, $\omega_c = 15$, $\Delta\omega = 0.1429$ and $T = 1$.

It is important to note that the final time of the simulation is now reduced to one. The reason for this can be seen in Figure 5.2 where we can see that the addition of the CR terms results in a fast decay rate for the entanglement. The simulation time for the ENMBQ is restricted to the point where we do not see numerical errors. These errors arise when the entanglement is zero for an extended period. We choose to find the final simulation time for an α value of 1.5 as we expect the entanglement to be destroyed at the fastest rate when the coupling to the bath is at its strongest. The reduced time limit means that we see lower NMB for the RWA-only case in Figure 5.1 when compared to Figure 3.21 because the EOs from time 1-20 are no longer included.

The data shows that the inclusion of the CR terms result in the ENMBQ predicting no

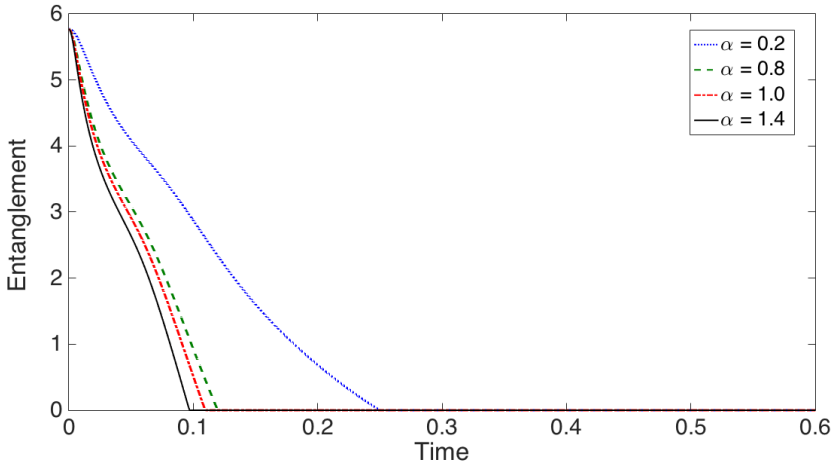


Figure 5.2: Entanglement dynamics for Model 4 with an ohmic bath for various α values. It shows that the addition of the CR terms results in the entanglement being destroyed at a fast rate. When compared with Figure 3.22 we can see that there are no more EOs. The model parameters are the same as Model 1 with an ohmic bath.

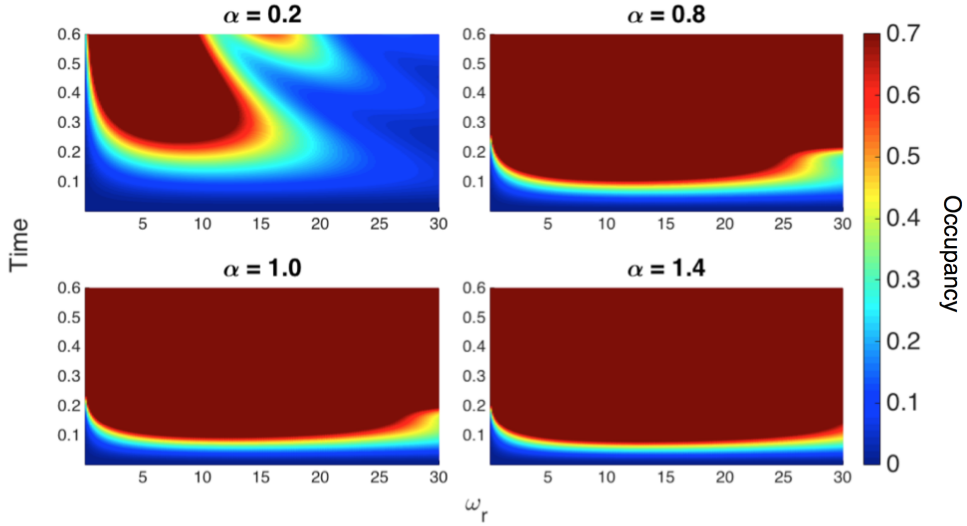


Figure 5.3: Occupancy of the bath modes for Model 4 with an ohmic bath. We use the same axis scales as the occupancy graph for Model 1 with an ohmic bath (Figure 3.23) for an easier comparison. The addition of the CR terms has caused more modes to have a higher occupation for all couplings. For high α values we see that the modes become highly occupied after the entanglement has been destroyed.

NMB. We have seen that the entanglement is destroyed at such a fast rate that there are no EOs present (Figure 5.2) and therefore no NMB. The difference with the entanglement dynamics can be clearly seen by comparing Figure 5.2 with Figure 3.22. The intuition is that the addition of the CR terms results in the inclusion of the fast oscillating terms which suppresses any feedback of the entanglement from any of the bath modes. We can see from the the occupancy of the bath modes in Figure 5.3 that the CR terms has caused more modes to become occupied in comparison to the RWA only case (Figure 3.23). When α is 0.2 we notice a higher occupation

of the off-resonant modes but the coupling to the bath is still weak and so do not see any NMB. For higher values of α where NMB was observed for Model 1 due to the off-resonant modes, we see that the occupation of the modes only becomes high after the entanglement has been destroyed. Moreover we see that there are no longer any oscillations in the occupancy (for each mode frequency) indicating that all the modes are interacting with system similarly, the end result of which is that no entanglement is returned to the system-ancilla state. Mathematically speaking, this can be understood as the CR terms connecting more elements of the CM together, effectively spreading the information in a greater region making it more difficult for it to be returned to the OQS. Simply speaking Model 1 displayed NMB where Model 4 does not because it required coupling strengths at which CR terms play a significant role.

5.2.1.2 Super ohmic bath

We can see from Figure 5.4 that, in similar fashion to the ohmic spectrum, the addition of CR terms removes all presence of NMB as predicted by the ENMBQ for the super ohmic case. Again, we have restricted the simulation time for the ENMBQ to unity for the same reasons as in the previous subsection.

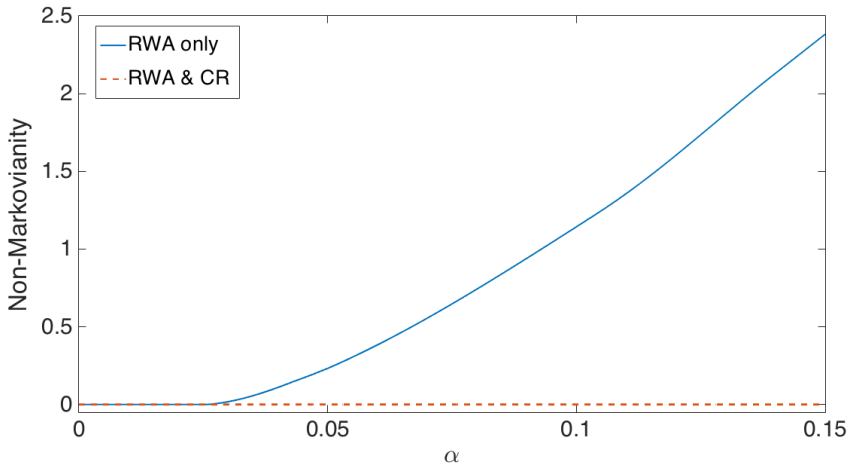


Figure 5.4: ENMBQ for Models 1 and 4 with a super ohmic bath. Note that the final time of the simulations is now 1. The addition of the CR terms removes any trace of NMB predicted by the ENMBQ. The model parameters are the same as Model 1 with a super ohmic bath, i.e. $\omega_s = \omega_a = 10$, $\zeta = 4$, $\omega_{max} = 50$, $\omega_c = 3$, $\Delta\omega = 0.1429$ and $T = 1$.

Comparing Figure 5.5 with Figure 3.25 we can again see that the addition of the CR terms suppresses any EO. The occupancy of the modes is shown in Figure 5.6. In the RWA case, when α was 0.03, 0.04 and 0.08, NMB was predicted by the ENMBQ and for these values we observe that when CR terms are included, the modes only become significantly populated after the

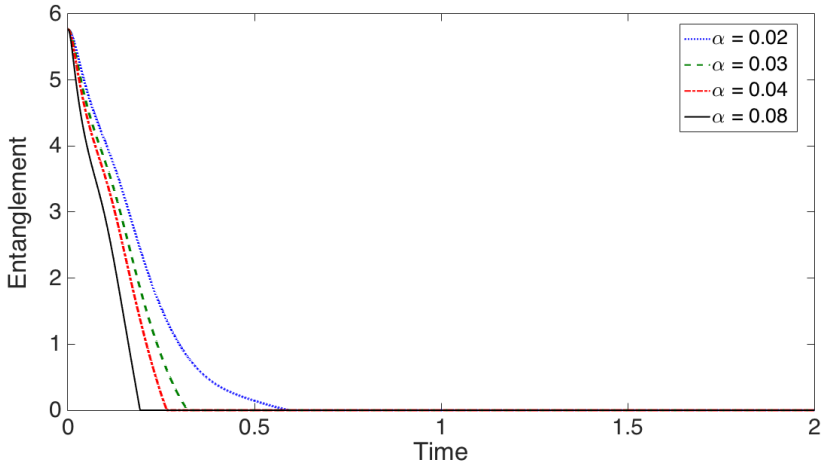


Figure 5.5: Entanglement dynamics for Model 4 with a super ohmic bath for various α values. It shows that the addition of the CR terms results in the entanglement being destroyed at a fast rate. When compared with Figure 3.25 we can see that there are no more EOs. The model parameters are the same as Model 1 with a super ohmic bath.

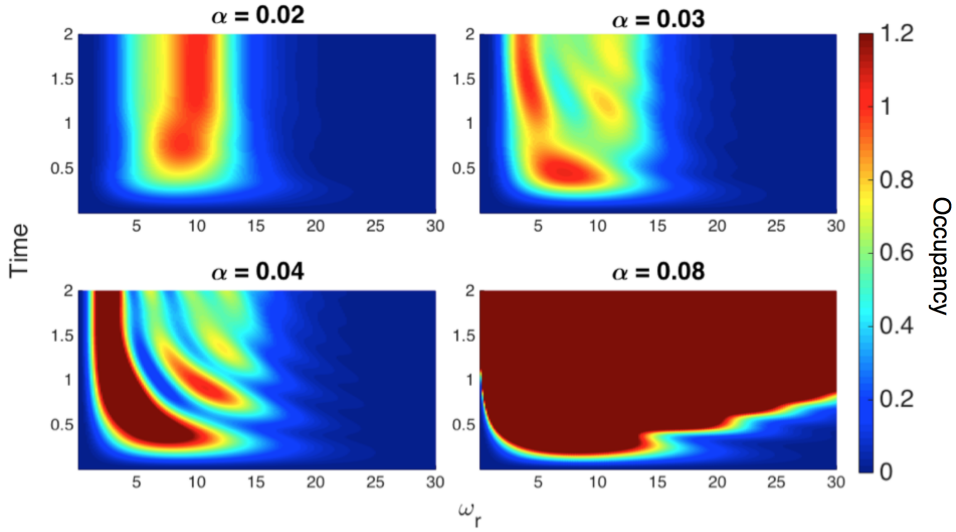


Figure 5.6: Occupancy of the bath modes for Model 4 with a super ohmic bath. We use the same axis scales as the occupancy graph for Model 1 with a super ohmic bath (Figure 3.26) for an easier comparison. The addition of the CR terms has caused most modes to have a higher occupation for all couplings which occurs roughly after the destruction of the entanglement.

entanglement has been killed. We can see that in general more modes are occupied, indicating that a greater number of modes are interacting with the system. Combining this with the fact that they all have different coupling strengths for the various α values, results in dynamics which is unable to resurrect the entanglement.

5.2.2 Model 5 - Model 2 with counter rotating terms

We adapt Model 2 by adding CR terms to all the bath modes as well as the strongly coupled extra 'o' mode, so that the Hamiltonian of Model 5 is given by

$$\begin{aligned} H = \omega_a a^\dagger a + \omega_s s^\dagger s + \omega_o o^\dagger o + h\left(so + so^\dagger + s^\dagger o + s^\dagger o^\dagger\right) \\ + \sum_{i=1}^{N} \omega_{r_i} r_i^\dagger r_i + \sum_{i=1}^{N} g_i \left(s r_i + s^\dagger r_i + s r_i^\dagger + s^\dagger r_i^\dagger\right). \end{aligned} \tag{5.7}$$

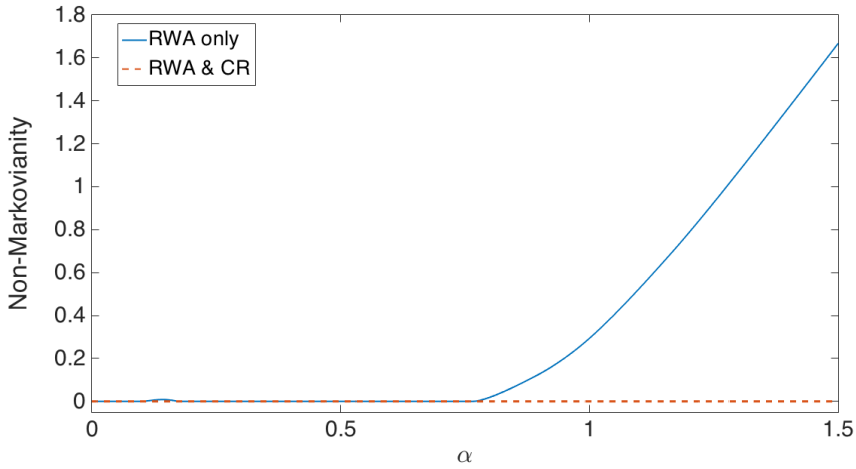


Figure 5.7: ENMBQ for Models 2 and 5. Note that the final time of the simulations is now 1. The addition of the CR terms removes the NMB predicted by the ENMBQ for Model 2. The model parameters are the same as Model 2, i.e. $\omega_s = \omega_a = \omega_o = 10$, $\zeta = 4$, $\omega_{max} = 50$, $\omega_c = 15$, $\Delta\omega = 0.1429$, $T = 1$ and $h = 1$.

Figure 5.7 shows the ENMBQ for the range of α from 0 to 1.5 with a final simulation time of one for Models 2 and 5. The short simulation time is needed to run the simulation without numerical errors for the entire alpha range. This short time results in no NMB for low α for both models as the entanglement increases caused by the extra mode happen after a simulation time of one (as seen in Figures 3.28 and 5.9). Therefore we perform a secondary ENMBQ plot for α, up to a value of 0.2 with a longer simulation time of 10 as shown in Figure 5.8.

With the longer simulation time we see that the NMB caused by the o - mode is restored for Model 2, as expected, but also for Model 5, albeit with a reduction in NMB from the extra mode for low α due to the CR terms. For larger α we can clearly see from Figure 5.7 that the CR terms suppress any NMB caused by the bath modes as we saw in the preceding subsections.

Both of these results are displayed in the entanglement dynamics for Model 5 (Figure 5.9)

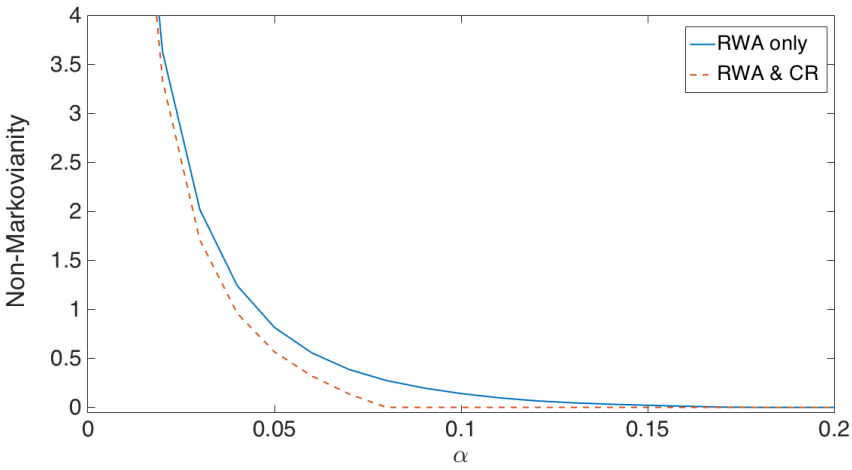


Figure 5.8: ENMBQ for Models 2 and 5 for smaller values of α. The final time of the simulations is now 10. The addition of the CR terms affects the NMB for low α.

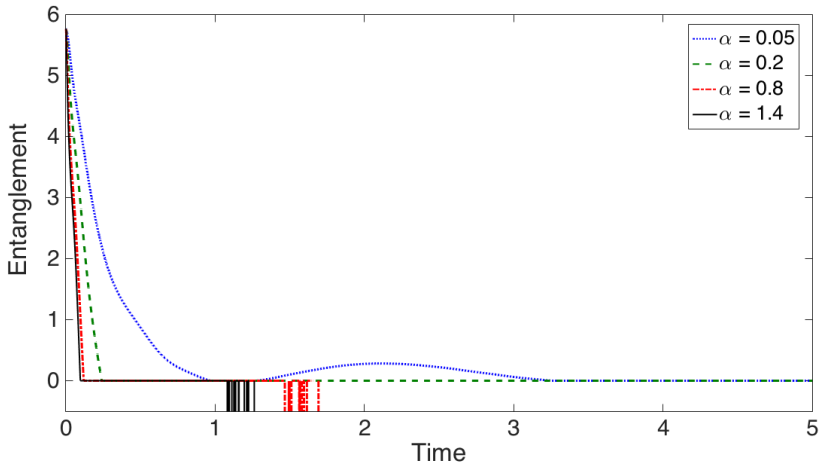


Figure 5.9: Entanglement dynamics for Model 5 for various α values. Comparing with Figure 3.28 we can see that the CR terms for low α affects the dynamics slightly but when α is increased it stops any EOs from the bath or the extra mode. Furthermore we can see for $\alpha = 0.8, 1.4$ that the numerical simulation fails after times ~ 1.5 and ~ 1.0 respectively for reasons explained in Section 5.2.1.1. The model parameters are the same as Model 2.

and comparing it with that of Model 2 (Figure 3.28). They show that the CR terms for low α affects the dynamics slightly but when α is increased it destroys entanglement at a fast rate and stops any EOs from the bath or the extra mode. The occupancy of the modes for Model 5 (Figure 5.10), for $\alpha = 0.05$, is very similar to that of Model 2 (Figure 3.29) with a vacancy in the resonant region of the bath, indicating again that the NMB is from the strongly coupled resonant extra mode. For higher α, we see once again that the addition of the CR terms causes more modes to have a higher occupation for all couplings only after the entanglement has been destroyed, just as in Model 4. Note that in Figure 5.9, for $\alpha = 0.8, 1.4$, the numerical simulation

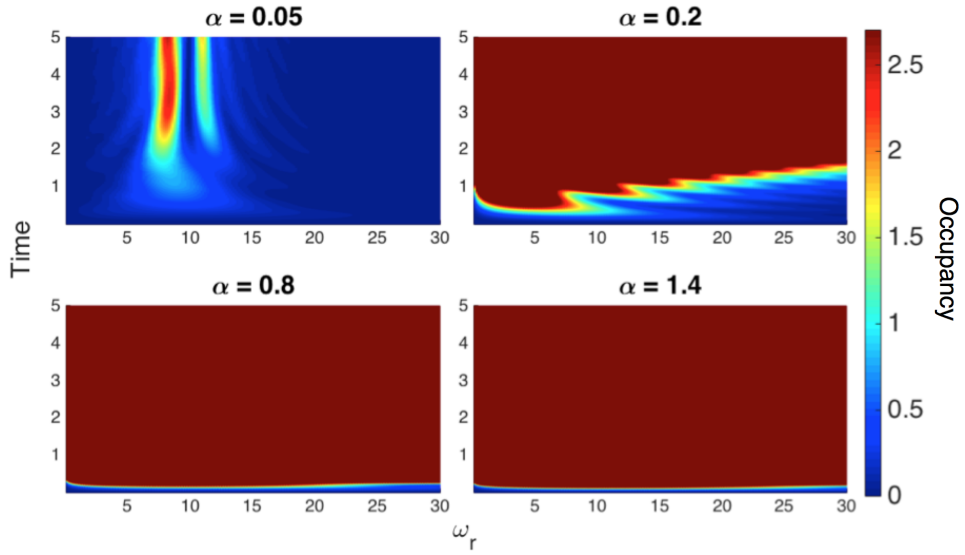


Figure 5.10: Occupancy of the bath modes for Model 5. We use the same axis scales as the occupancy graph for Model 2 (Figure 3.29) for an easier comparison. For $\alpha = 0.05$ the occupancy graph is very similar with a vacancy in the resonant region of the bath due to the strongly coupled extra mode. For higher α we observe once again that the addition of the CR terms causes more modes to have a higher occupation for all couplings after the entanglement has been destroyed.

fails after times ~ 1.5 and ~ 1.0 respectively for reasons explained in Section 5.2.1.1 but a final simulation time of one is sufficient to see all the relevant dynamics for these couplings.

5.2.3 Model 6 - Model 3 with counter rotating terms

The Hamiltonian for Model 6 is given below

$$\begin{aligned} H = \omega_a a^\dagger a + \omega_s s^\dagger s + \omega_b b^\dagger b + h\left(sb + sb^\dagger + s^\dagger b + s^\dagger b^\dagger\right) \\ + \sum_{i=1}^{N} \omega_{r_i} r_i^\dagger r_i + \sum_{i=1}^{N} g_i \left(b r_i + b^\dagger r_i + b r_i^\dagger + b^\dagger r_i^\dagger\right) \end{aligned} \tag{5.8}$$

where we have added CR terms to all the bath modes as well as the strongly coupled 'buffer' mode, b. Figure 5.11 displays the ENMBQ for a range of α from 0 to 1.5 with a final simulation time of one, which again results in no NMB for low α as the entanglement increases caused by the buffer mode happen after a simulation time of one (seen in Figures 3.31 and 5.13).

Therefore we perform a secondary ENMBQ plot for α, up to a value of 0.2 with a longer simulation time of 10 as shown in Figure 5.12.

With the longer simulation time, the NMB caused by the buffer mode is noted for Models 3 and 6, but as before it shows that the CR terms slightly reduces the NMB from the buffer mode

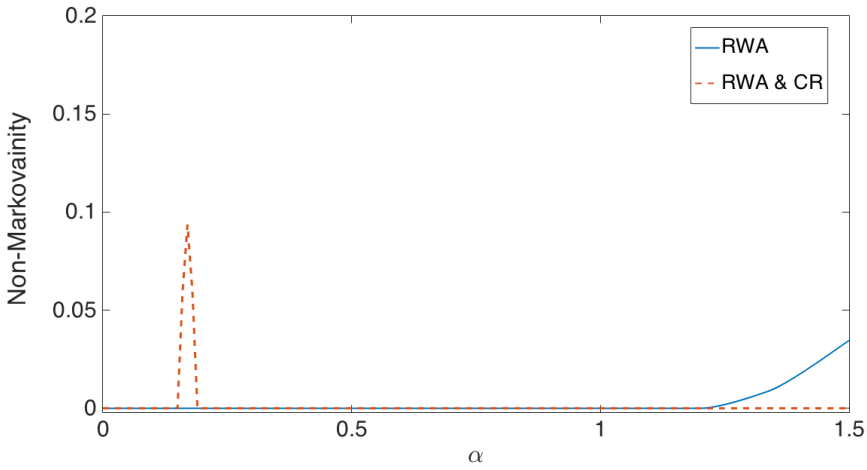


Figure 5.11: ENMBQ for Models 3 and 6. Note that the final time of the simulations is now 1. The addition of the CR terms affects the NMB for low α and removes any trace of NMB predicted by the ENMBQ for high α. The model parameters are the same as Model 3, i.e. $\omega_s = \omega_a = \omega_b = 10$, $\zeta = 4$, $\omega_{max} = 50$, $\omega_c = 15$, $\Delta\omega = 0.1429$, $T = 1$ and $h = 1$.

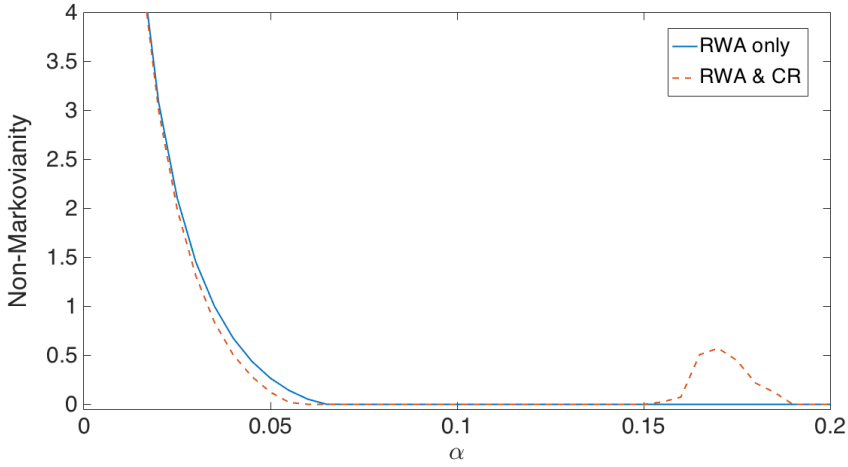


Figure 5.12: ENMBQ for Models 3 and 6 for smaller values of α. The final time of the simulations is now 10. The addition of the CR terms affects the NMB for low α but some NMB is seen for $\alpha = 0.16 - 0.2$ for Model 6 where Model 3 does not predict any NMB.

for low α. This is confirmed by the entanglement dynamics (Figure 5.14) and the occupancy (Figure 5.14 for $\alpha = 0.05$) with a similarity shown to Model 3 (Figure 3.31 and $\alpha = 0.05$ in Figure 3.32 respectively). After this point, Markovian behaviour is witnessed as the buffer leaks the entanglement to the bath before it has a chance to return.

Interestingly, Figures 5.11 and 5.12 show that for α between roughly 0.15 and 0.2 the addition of the CR terms has resulted in some NMB where Model 3 does not predict any. Looking at the entanglement dynamics in this region (Figure 5.15), EOs similar to that caused by the bath in Model 3 (Section 3.2.3.7) are seen but to a much smaller degree, this is especially true for

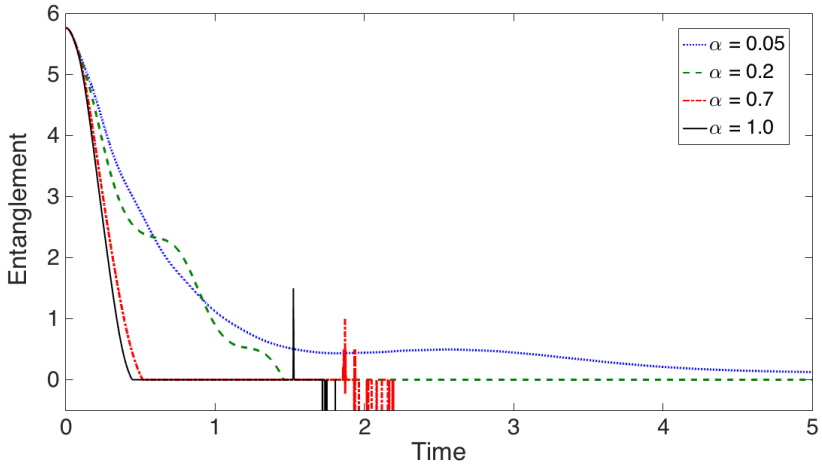


Figure 5.13: Entanglement dynamics for Model 6 for various α values. Comparing with Figure 3.31, we see that the CR terms for low α affect the dynamics slightly. For $\alpha = 0.2$ we see some EOs. When $\alpha = 0.7, 1.0$ the CR terms stops any EOs from the bath, also note that for these values the numerical simulation fails after times ~ 1.8 and ~ 1.5 respectively for reasons explained in Section 5.2.1.1. The model parameters are the same as Model 3.

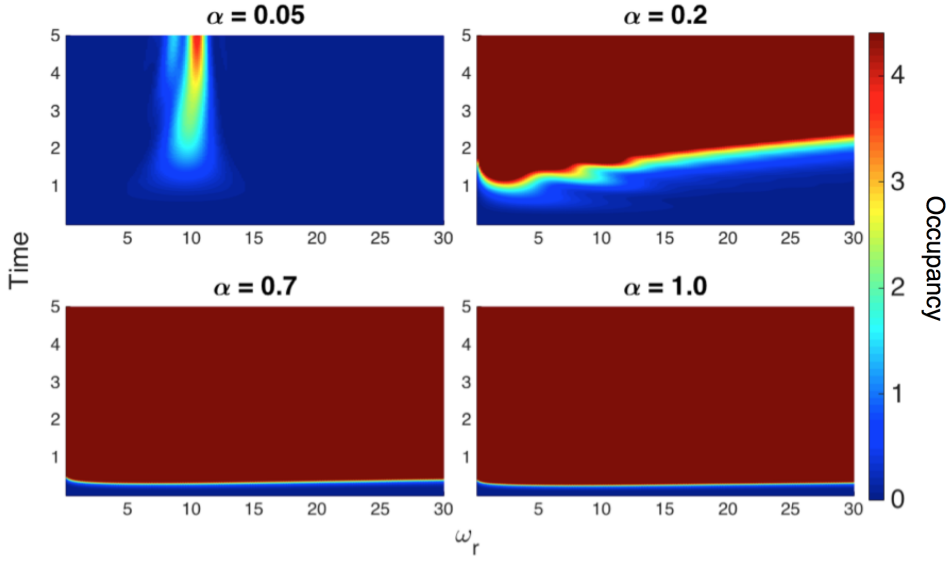


Figure 5.14: Occupancy of the bath modes for Model 6. We use the same axis scales as the occupancy graph for Model 3 (Figure 3.32) for an easier comparison. For $\alpha = 0.05$, a very similar occupancy graph is noted with the resonant region of the bath showing the highest occupation. For higher α, we see once again that the addition of the CR terms causes more modes to have a higher occupation for all couplings after the entanglement has been destroyed.

$\alpha = 0.16$. No EOs are observed for $\alpha = 0.14$ but as α is increased we see more oscillations for $\alpha = 0.16, 0.17$. The occupancy of the modes in this secondary NMB region (Figure 5.16) show that when α is 0.14 and 0.16 we have an effective reduced bath size. Therefore, only the near-resonant modes in the bath are interacting with the system, this is supported by the longer decay time of the entanglement which is what we witnessed in Section 3.2.3.7.

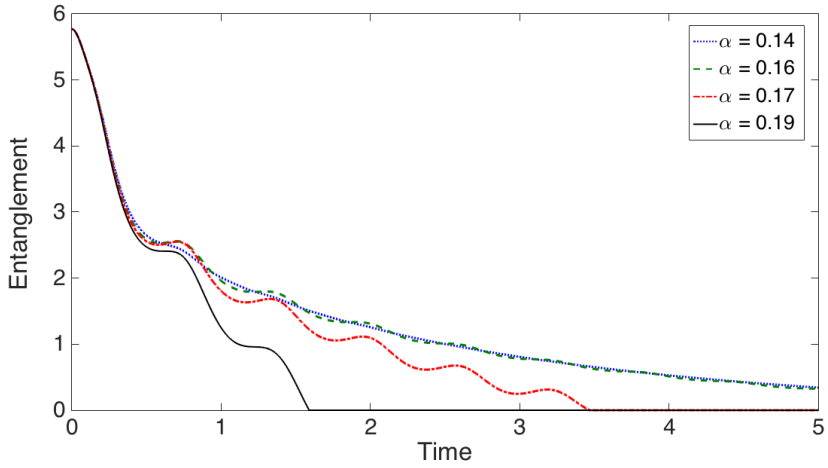


Figure 5.15: Entanglement dynamics for Model 6 for α values in the secondary NMB region. We see EOs most likely caused by the resonant modes in the bath. As α is increased further we see a faster decay rate which reduces the amount of NMB.

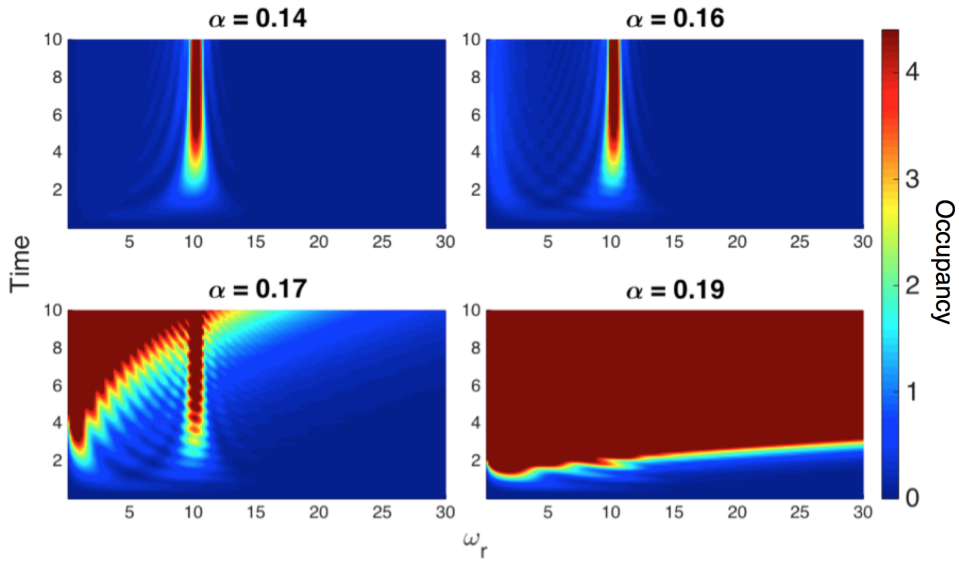


Figure 5.16: Occupancy of the bath modes for Model 6 in the secondary NMB region. For $\alpha = 0.14, 0.16$, we see a high occupancy in the resonant regions only. In the $\alpha = 0.17$ case, more modes come in to play and for $\alpha = 0.19$ the addition of the CR terms has caused the majority of the modes to have a higher occupation after the entanglement has been destroyed.

The ENMBQ predicts NMB when α is 0.16, the intuition for the reason behind this being that the near-resonant modes in the bath feed some entanglement back to the system before it is destroyed. Essentially, this is the $\alpha = 0.7$ threshold that existed for Model 3. Due to the faster decay of entanglement we note very few EOs, resulting in a low NMB prediction and we see this taking effect for $\alpha = 0.17$ and 0.19. Unlike Model 3 we observe that increasing α does not indefinitely increase NMB, in fact when α is 0.17 the occupancy shows that the CR terms bring the off-resonant modes into play and the 'addition' of these modes causes the entanglement to

decay at a faster rate. There are two main things to take note of, the first being that there is still occupation in the resonant region of the bath when we see EOs indicating that the NMB is likely due to these modes as well as the buffer (since there is low occupation for the first few EOs). The second thing to notice is that we start to see a high occupation of the off-resonant modes once the entanglement has been destroyed, just like the other models in this chapter. The likely reason why we see NMB for these α values in this model and not for the others is probably due to the reduced bath size, which we saw for Model 3 in Section 3.2.3.7. For $\alpha = 0.19, 0.2$ we still see a few EOs before the bath destroys the entanglement, indeed we start to see that the decay time of the entanglement decrease and the occupancy looks similar to the previous models in this chapter for high α.

For large α, Figure 5.11 clearly shows that the CR terms suppresses any NMB due to bath modes as we saw in the previous subsections. The entanglement dynamics (Figure 5.13) and the occupancy (Figure 5.14) show that the CR terms cause the entanglement to be destroyed at a fast rate and stops any EOs from the bath or the buffer mode. Also more modes get a higher occupation after the entanglement has been destroyed just like the large α cases for the other models in this chapter. Note that we see for $\alpha = 0.7, 1.0$ that the numerical simulation fails after times ~ 1.8 and ~ 1.5 respectively for reasons explained in Section 5.2.1.1 but a final simulation time of one is sufficient to see all the relevant dynamics for these couplings.

5.3 Concluding remarks

This aim of this chapter, in light of the various works on the validity of the RWA with regards to strong couplings and non-Markovianity, was to investigate the predictions of NMB as given by the ENMBQ if the RWA is not applied.

By adding the CR terms to the Hamiltonians of Models 1, 2 and 3 we noted that it had a largely destructive effect on the non-Markovianity detected. For large coupling strengths to the bath (essentially α), all the modified models (Models 4, 5 and 6) showed no NMB where previously we noted contributions from the bath modes. This was attributed to the rapid decay rates of the entanglement caused by the fast oscillating terms. Model 5 and 6 showed, for low α, that the CR terms diminish the NMB detected due to the extra mode. In the buffer model, the addition of the CR terms resulted in a new region of NMB which was not witnessed in Models 1-5. The conjecture was that it was caused by the extra mode and the near-resonant

bath modes, i.e. the CR terms lowered the threshold value of α (in comparison to Model 3) that needed to be crossed for the bath/buffer to cause EOs.

It is worth noting that although the analysis in this chapter shows the addition of the CR terms has a significant effect on the predictions of NMB by the ENMBQ, other witnesses or measures may not be as significantly affected by these terms. Indeed, Mäkelä and Möttönen noted that the CR terms increased the non-Markovianity, as given by the trace distance, for their model [44].

Seeing the possible effects CR terms can have on a model, it has become clear that one should ask the question as to when it is appropriate to make a RWA, which is the basis of the investigation in the next chapter.

Chapter 6

Finding the limits of the Rotating-Wave approximation

The introduction to Chapter 5 showed that the validity of the RWA has been questioned in many scenarios [43, 44, 48, 125–129]. We especially highlighted works which focused on the legitimacy of the RWA with respect to non-Markovianity and strong couplings in OQSs. The previous chapter showed that the presence of CR terms had a significant effect on the non-Markovianity of a model when strong couplings were involved. Early works by Walls [128] and Cresser [129] demonstrated that the presence of strong coupling in an OQS may invalidate the an application of the RWA to the environment coupling.

Therefore, the aim of this chapter is to gain a better understanding of when and if the RWA can be accurately applied to a weakly coupled oscillator if there is a strong coupling present in a model. To this end, we investigate the simplest possible scenario, a three oscillator model with a strongly coupled pair of oscillators and a single weakly coupled oscillator. Moreover we describe a methodology that could be applied to any model (including OQSs) to understand whether a RWA coupling would be valid for the parameter regime used for the interest of the investigator.

There has been significant work which display 'strong' [130, 131, 133, 134] and 'ultra-strong' coupling [45, 135–138] including studies on coupled harmonic oscillators [45–47, 130, 131, 135]. As highlighted by Sudhir et. al. [135], the definition of 'strong' coupling has changed throughout the years and refers to a coupling up to the order of roughly half the strength of the resonant frequency of the system and 'ultra-strong' coupling referring to one that is roughly greater than or equal to the natural frequency. The model we consider in this chapter concentrates on the

classic x-x coupling, also referred to as the spring coupling and this precludes any use of the 'ultra-strong' regime which requires the full 'Hookian' coupling to remain stable [135].

The contents of this chapter covers the work in our second research paper (as yet untitled) which is in the process of publication.

6.1 Three oscillator model

The model under investigation consists of three quantum harmonic oscillators (Figure 6.1), a, b and c, the coupling between modes b and c is in a strong coupling regime and the interaction Hamiltonian between them is described by an x-x coupling, i.e. the RWA cannot be applied to describe the model accurately. The question becomes whether a model containing a weak coupling between an additional mode a and mode b could be understood properly with a RWA when there is a strong interaction in play between modes b and c.

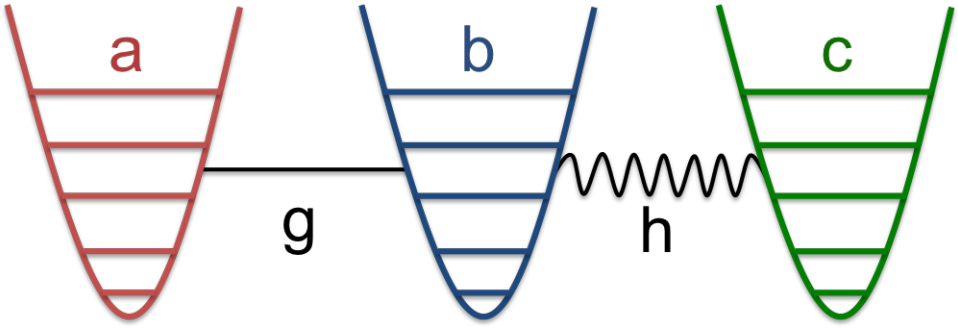


Figure 6.1: Red - Mode a, Blue - Mode b, Green - Mode c. Coupling between modes a and b is varied between a RWA coupling and the spring coupling with a weak coupling strength g. The coupling between modes b and c is always a x-x coupling with a strong coupling h.

To this end we consider two models, model one (M1) has a RWA applied between a and b and model two (M2) has the full x-x coupling as shown by the equations below

$$\begin{aligned} H &= H_0 + H_{AB} + H_{BC} \\ &= \omega_a a^\dagger a + \omega_b b^\dagger b + \omega_c c^\dagger c + h\left(b + b^\dagger\right)\left(c + c^\dagger\right) + H_{AB} \end{aligned} \tag{6.1}$$

where for model M1

$$H_{AB} = g\left(a^\dagger b + a b^\dagger\right) \tag{6.2}$$

and for model M2

$$H_{AB} = g\left(a + a^\dagger\right)\left(b + b^\dagger\right). \tag{6.3}$$

We compare M1 against M2 by considering the fidelity (Section 2.6.2), F, between the two states that describe them. Once again a CM formalism is applied to simulate the models and the single and two mode fidelities can be calculated in a straightforward manner as shown in Sections 2.6.2.1 and 2.6.2.2. All the oscillators are resonant with a frequency of 1 and, unless stated otherwise, we begin with mode a in the vacuum state and a single thermal photon in each of the b and c modes. The symplectic basis we have chosen for the simulation is of the form

$$R^T = (\hat{x}_a, \hat{x}_b, \hat{x}_c, \hat{p}_a, \hat{p}_b, \hat{p}_c) \tag{6.4}$$

which contains the position and momentum operators for modes a, b and c respectively. We have shown in Section 2.5 that in this basis, the initial CM for this model is given by

$$\gamma_0 = \begin{pmatrix} 1 & 0 & 0 & 0 & 0 & 0 \\ 0 & 2\bar{n_b}+1 & 0 & 0 & 0 & 0 \\ 0 & 0 & 2\bar{n_c}+1 & 0 & 0 & 0 \\ 0 & 0 & 0 & 1 & 0 & 0 \\ 0 & 0 & 0 & 0 & 2\bar{n_b}+1 & 0 \\ 0 & 0 & 0 & 0 & 0 & 2\bar{n_c}+1 \end{pmatrix} \tag{6.5}$$

where $\bar{n_b}$ and $\bar{n_c}$ refer to the number of thermal photons in modes b and c respectively. For most of this chapter $\bar{n_b} = \bar{n_c} = 1$. Using this CM we can calculate the one and two mode fidelities using the formulae given in Sections 2.6.2.1 and 2.6.2.2.

6.2 Effects of the strong coupling limit

We first consider the origin of the strong coupling limit, i.e. the limit where the RWA coupling between a and b is invalidated. In our case this would mean that past this limit M1 would not accurately describe the dynamics. We begin by investigating the normal modes of oscillators b and c.

Modes b and c can be expressed in terms of normal modes p_1 and p_2, with p_1 and p_2 obeying the canonical commutation relation

$$\left[p_i, p_i^\dagger\right] \equiv 1 \tag{6.6}$$

such that the symplectic matrix σ remains the same as shown in Eq. (2.3). If we consider

normal modes, a new symplectic basis (the R vector) needs to be defined to simulate the model via the CM and it is arranged as follows

$$R_{NM}^{T} = (\hat{x}_a, \hat{x}_{p_1}, \hat{x}_{p_2}, \hat{p}_a, \hat{p}_{p_1}, \hat{p}_{p_2}) \tag{6.7}$$

which contains the position and momentum operators for modes a, p_1 and p_2 respectively. For convenience we now use the term 'bare modes' to describe the un-transformed modes, usually modes b and c. To find the normal modes we begin by defining p_i

$$p_i = C_{i1}b + C_{i2}c + C_{i3}b^{\dagger} + C_{i4}c^{\dagger} \tag{6.8}$$

where C_{ij} are coefficients that need to be determined. To find these coefficients we acquire a few simulations equations; the first of which is gained by substituting the expansion of the normal mode (Eq. (6.8)) into the canonical commutation relation shown in Eq. (6.6)

$$1 \equiv |C_{i1}|^2 + |C_{i2}|^2 - |C_{i3}|^2 - |C_{i4}|^2 \tag{6.9}$$

where we have used the standard bosonic canonical commutation relations between modes b and c. Additionally, more equations are gained by taking the commutator between the normal mode and H, the Hamiltonian of the model given in Eq. (6.1).

$$\begin{aligned}
[p_i, H] = &\left(C_{i1}\omega_b + C_{i2}g - C_{i4}g\right) b \\
&+ \left(C_{i1}g + C_{i2}\omega_c - C_{i3}g\right) c \\
&+ \left(C_{i2}g - C_{i3}\omega_b - C_{i4}g\right) b^{\dagger} \\
&+ \left(C_{i1}g - C_{i3}g - C_{i4}\omega_c\right) c^{\dagger} \\
= &\, E_i p_i
\end{aligned} \tag{6.10}$$

where in the last line we utilise the fact that if p_i is a normal mode that diagonalises the system, then it will have an associated eigenfrequency E_i. Comparing coefficients of either side of Eq.

(6.10) results in the four simultaneous equations below

$$\begin{aligned}
\omega_b C_{i1} + gC_{i2} - gC_{i4} &= E_i C_{i1} \\
gC_{i1} + \omega_c C_{i2} - gC_{i3} &= E_i C_{i2} \\
gC_{i2} - \omega_b C_{i3} - gC_{i4} &= E_i C_{i3} \\
gC_{i1} - gC_{i3} - \omega_c C_{i4} &= E_i C_{i4}.
\end{aligned} \tag{6.11}$$

With Eqs. (6.9) and (6.11) one can solve for C_{ij} and E_i and express p_i in terms of bare modes b and c

$$\begin{pmatrix} p_1 \\ p_2 \\ p_1^\dagger \\ p_2^\dagger \end{pmatrix} = \begin{pmatrix} C_{11} & C_{12} & C_{13} & C_{14} \\ C_{21} & C_{22} & C_{23} & C_{24} \\ C_{13} & C_{14} & C_{11} & C_{12} \\ C_{23} & C_{24} & C_{21} & C_{22} \end{pmatrix} \begin{pmatrix} b \\ c \\ b^\dagger \\ c^\dagger \end{pmatrix} \tag{6.12}$$

where C_{ij} are given by

$$\begin{aligned}
C_{i1} &= \frac{h\omega_c \left(E_i + \omega_b\right)}{D_i} \\
C_{i2} &= \frac{\left(E_i^2 - \omega_b^2\right)\left(E_i + \omega_c\right)}{2D_i} \\
C_{i3} &= \frac{h\omega_c \left(E_i - \omega_b\right)}{D_i} \\
C_{i4} &= \frac{\left(E_i^2 - \omega_b^2\right)\left(E_i - \omega_c\right)}{2D_i}
\end{aligned} \tag{6.13}$$

with

$$D_i = \sqrt{E_i \omega_c \left(4h^2 \omega_b \omega_c + \left(\omega_b^2 - E_i^2\right)^2\right)} \tag{6.14}$$

and

$$\begin{aligned}
E_1 &= \sqrt{\frac{\left(\omega_b^2 + \omega_c^2\right) + \sqrt{\left(\omega_b^2 - \omega_c^2\right)^2 + 16h^2\omega_b\omega_c}}{2}} \\
E_2 &= \sqrt{\frac{\left(\omega_b^2 + \omega_c^2\right) - \sqrt{\left(\omega_b^2 - \omega_c^2\right)^2 + 16h^2\omega_b\omega_c}}{2}}.
\end{aligned} \tag{6.15}$$

Therefore the relationship between the bare modes and the normal modes can be shown in a

matrix given below

$$\begin{pmatrix} b \\ c \\ b^\dagger \\ c^\dagger \end{pmatrix} = \begin{pmatrix} C_{11} & C_{21} & -C_{13} & -C_{23} \\ C_{12} & C_{22} & -C_{14} & -C_{24} \\ -C_{13} & -C_{23} & C_{11} & C_{21} \\ -C_{14} & -C_{24} & C_{12} & C_{22} \end{pmatrix} \begin{pmatrix} p_1 \\ p_2 \\ p_1^\dagger \\ p_2^\dagger \end{pmatrix} \tag{6.16}$$

where we have used the fact that the matrix is of symplectic form to invert it in a simple fashion, as shown in Ref. [139]. Using the normal modes we rewrite the Hamiltonians for models M1 and M2, shown in Eqs. (6.1). The Hamiltonian for model M1 is given by

$$\begin{aligned} H =& \omega_a a^\dagger a + E_1 p_1^\dagger p_1 + E_2 p_2^\dagger p_2 + gC_{11}\left(a^\dagger p_1 + a p_1^\dagger\right) \\ & - gC_{13}\left(a^\dagger p_1^\dagger + a p_1\right) + gC_{21}\left(a^\dagger p_2 + a p_2^\dagger\right) \\ & - gC_{23}\left(a^\dagger p_2^\dagger + a p_2\right) \end{aligned} \tag{6.17}$$

and for model M2 it is given by

$$\begin{aligned} H =& \omega_a a^\dagger a + E_1 p_1^\dagger p_1 + E_2 p_2^\dagger p_2 \\ & + \frac{2gh\omega_b\omega_c}{D_1}\left(a + a^\dagger\right)\left(p_1 + p_1^\dagger\right) \\ & + \frac{2gh\omega_b\omega_c}{D_2}\left(a + a^\dagger\right)\left(p_2 + p_2^\dagger\right). \end{aligned} \tag{6.18}$$

Since a new symplectic basis has been defined using the normal modes, R_{NM} (Eq. (6.7)), the initial CM has to be adapted. Section 2.5.2 shows that the new initial CM will be given by

$$\gamma_{ij} = 2Re \sum_n \frac{1}{1+\bar{n}} \left(\frac{\bar{n}}{1+\bar{n}}\right)^n \langle n_a n_b n_c | R_{NM(i)} R_{NM(j)} | n_a n_b n_c \rangle \tag{6.19}$$

where we begin with a generic thermal state with n_a, n_b and n_c representing the number basis of modes a, b and c respectively. As the new position and momentum operators, $\hat{x}_{p_i}$ and $\hat{p}_{p_i}$, are expressed in terms of the creation and annihilation operators (Eq. (6.20)), we need to know how the normal mode ladder operators act on the number states of the modes.

$$\hat{x}_{p_i} = \frac{p_i^\dagger + p_i}{\sqrt{2}} \qquad \hat{p}_{p_i} = \frac{i\left(p_i^\dagger - p_i\right)}{\sqrt{2}} \tag{6.20}$$

The expansion of the normal modes given in Eq. (6.12) is used to calculate their action on the

state

$$
\begin{aligned}
p_i|n_a,n_b,n_c\rangle &= C_{i1}\sqrt{n_b}|n_a,n_b-1,n_c\rangle + C_{i2}\sqrt{n_c}|n_a,n_b,n_c-1\rangle \\
&\quad + C_{i3}\sqrt{n_b+1}|n_a,n_b+1,n_c\rangle + C_{i4}\sqrt{n_c+1}|n_a,n_b,n_c+1\rangle \\
p_i^\dagger|n_a,n_b,n_c\rangle &= C_{i3}\sqrt{n_b}|n_a,n_b-1,n_c\rangle + C_{i4}\sqrt{n_c}|n_a,n_b,n_c-1\rangle \\
&\quad + C_{i1}\sqrt{n_b+1}|n_a,n_b+1,n_c\rangle + C_{i2}\sqrt{n_c+1}|n_a,n_b,n_c+1\rangle
\end{aligned}
\tag{6.21}
$$

where we have used the usual operation of the creation (annihilation) operators $b^\dagger$, $c^\dagger$ (b,c) on their respective number states. Utilising Eq. (6.21) every term of the CM (Eq. (6.19)) can be evaluated in the same fashion shown in Section 2.5.2

$$
\gamma_0 = \begin{pmatrix}
1 & 0 & 0 & 0 & 0 & 0 \\
0 & \iota_{11} & \iota_{12} & 0 & 0 & 0 \\
0 & \iota_{21} & \iota_{22} & 0 & 0 & 0 \\
0 & 0 & 0 & 1 & 0 & 0 \\
0 & 0 & 0 & 0 & \iota_{33} & \iota_{34} \\
0 & 0 & 0 & 0 & \iota_{44} & \iota_{44}
\end{pmatrix}
\tag{6.22}
$$

where the ι_{xy} are given by

$$
\begin{aligned}
\iota_{11} &= (2\bar{n_b}+1)\left(C_{11}+C_{13}\right)^2 + (2\bar{n_c}+1)\left(C_{12}+C_{14}\right)^2 \\
\iota_{12} = \iota_{21} &= (2\bar{n_b}+1)\left(C_{11}+C_{13}\right)\left(C_{21}+C_{23}\right) \\
&\quad + (2\bar{n_c}+1)\left(C_{12}+C_{14}\right)\left(C_{22}+C_{24}\right) \\
\iota_{22} &= (2\bar{n_b}+1)\left(C_{21}+C_{23}\right)^2 + (2\bar{n_c}+1)\left(C_{22}+C_{24}\right)^2 \\
\iota_{33} &= (2\bar{n_b}+1)\left(C_{11}-C_{13}\right)^2 + (2\bar{n_c}+1)\left(C_{12}-C_{14}\right)^2 \\
\iota_{34} = \iota_{43} &= (2\bar{n_b}+1)\left(C_{13}-C_{11}\right)\left(C_{21}-C_{23}\right) \\
&\quad + (2\bar{n_c}+1)\left(C_{14}-C_{12}\right)\left(C_{22}-C_{24}\right) \\
\iota_{44} &= (2\bar{n_b}+1)\left(C_{21}-C_{23}\right)^2 + (2\bar{n_c}+1)\left(C_{22}-C_{24}\right)^2 .
\end{aligned}
\tag{6.23}
$$

Note that we have set mode a to be in the vacuum state i.e. $\bar{n_a}=0$. To simplify this model we consider the resonant case, i.e. $\omega_a=\omega_b=\omega_c=\omega$, this results in Eqs. (6.13), (6.14) and (6.15)

becoming

$$\begin{aligned} C_{i1} &= \frac{h\omega\left(E_i+\omega\right)}{D_i} \\ C_{i2} &= \frac{\left(E_i^2-\omega^2\right)\left(E_i+\omega\right)}{2D_i} \\ C_{i3} &= \frac{h\omega\left(E_i-\omega\right)}{D_i} \\ C_{i4} &= \frac{\left(E_i^2-\omega^2\right)\left(E_i-\omega\right)}{2D_i} \end{aligned} \tag{6.24}$$

with

$$D_i = \sqrt{E_i\omega\left(4h^2\omega^2+\left(\omega^2-E_i^2\right)^2\right)} \tag{6.25}$$

and the eigenfrequencies of the normal modes p_1 and p_2 are given by

$$\begin{aligned} E_1 &= \sqrt{\frac{\left(\omega^2+\omega^2\right)+\sqrt{16h^2\omega^2}}{2}} \\ E_2 &= \sqrt{\frac{\left(\omega^2+\omega^2\right)-\sqrt{16h^2\omega^2}}{2}}. \end{aligned} \tag{6.26}$$

The eigenfrequencies can clearly be simplified to

$$E_{1,2} = \sqrt{\omega^2 \pm 2h\omega} \tag{6.27}$$

which simplifies D_i

$$D_i = 2h\omega\sqrt{2\omega\sqrt{\omega^2 \pm 2h\omega}}. \tag{6.28}$$

Concentrating on the eigenfrequencies (Eq. (6.27)), it is clear that although E_1 will always remain positive and real, E_2 will become imaginary when $h > 0.5\ \omega$ which invalidates the normal mode transformation. This effectively limits the strength of the b - c coupling.

Eqs. (6.17) and (6.18) show that there is an effective coupling created between mode a and the normal modes p_1 and p_2 which, naturally, depends on h, g and the nature of the a - b coupling. An analytic study reveals how this effective coupling is scaled as h approaches the limit of the strong coupling regime. Expressing h in terms of a parameter ϵ

$$h = \frac{\left(1-\epsilon\right)\omega}{2} \tag{6.29}$$

we find the following scaled couplings in M1 for the RWA terms; given by gC_{11} for the p_1 mode

$$gC_{11} = \frac{gh\omega\left(E_1+\omega\right)}{D_1} = \frac{g\left(\sqrt{2-\epsilon}+1\right)}{2\sqrt{2\sqrt{2-\epsilon}}} \tag{6.30}$$

and gC_{21} for the p_2 mode

$$gC_{21} = \frac{gh\omega\left(E_2+\omega\right)}{D_2} = \frac{g\left(\sqrt{\epsilon}+1\right)}{2\sqrt{2}\epsilon^{\frac{1}{4}}}. \tag{6.31}$$

The CR terms in M1 are given by gC_{13} for the p_1 mode

$$gC_{13} = \frac{gh\omega\left(E_1-\omega\right)}{D_1} = \frac{g\left(\sqrt{2-\epsilon}-1\right)}{2\sqrt{2\sqrt{2-\epsilon}}} \tag{6.32}$$

and gC_{23} for the p_2 mode

$$gC_{23} = \frac{gh\omega\left(E_2-\omega\right)}{D_2} = \frac{g\left(\sqrt{\epsilon}-1\right)}{2\sqrt{2}\epsilon^{\frac{1}{4}}}. \tag{6.33}$$

For M2 the scaled couplings are the same for both the RWA and CR terms. The coupling between mode a and the p_1 mode is given by

$$\frac{2gh\omega^2}{D_1} = \frac{2gh\omega^2}{2h\omega\sqrt{2\omega\sqrt{\omega^2+2h\omega}}} = \frac{g}{\sqrt{2\sqrt{2-\epsilon}}} \tag{6.34}$$

and for the p_2 mode it is given by

$$\frac{2gh\omega^2}{D_2} = \frac{2gh\omega^2}{2h\omega\sqrt{2\omega\sqrt{\omega^2-2h\omega}}} = \frac{g}{\sqrt{2}\epsilon^{\frac{1}{4}}}. \tag{6.35}$$

In both models, as ϵ is diminished, the coupling between mode a and the p_2 mode will be scaled up, whereas the coupling to the p_1 mode will be largely unaffected in comparison. This is shown in Figures 6.2 and 6.3.

Juxtaposing the interaction Hamiltonians of the p_2 mode for both models we notice that the coupling in M1 will be scaled more than M2, as ϵ is not taken to the power of a quarter in one of the terms (shown in Eqs. (6.36) and (6.37)). The interaction Hamiltonian between mode a and p_2 for M1 is given by

$$\begin{aligned} H_{a-p_2} = &\frac{g}{2\sqrt{2\epsilon}}\left(a^\dagger - a\right)\left(p_2 - p_2^\dagger\right) \\ &+ \frac{g}{2\sqrt{2}\epsilon^{1/4}}\left(a^\dagger + a\right)\left(p_2 + p_2^\dagger\right) \end{aligned} \tag{6.36}$$

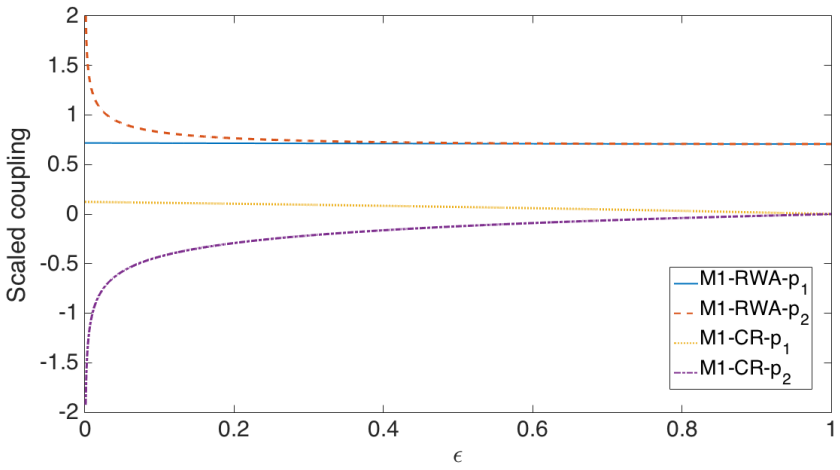


Figure 6.2: M1 coupling terms scaling. This figure shows how the coupling to the different terms in the Hamiltonian for M1 scale as ϵ is varied between 0 and 1. It clearly shows that as ϵ approaches zero the couplings to the p_2 mode increases.

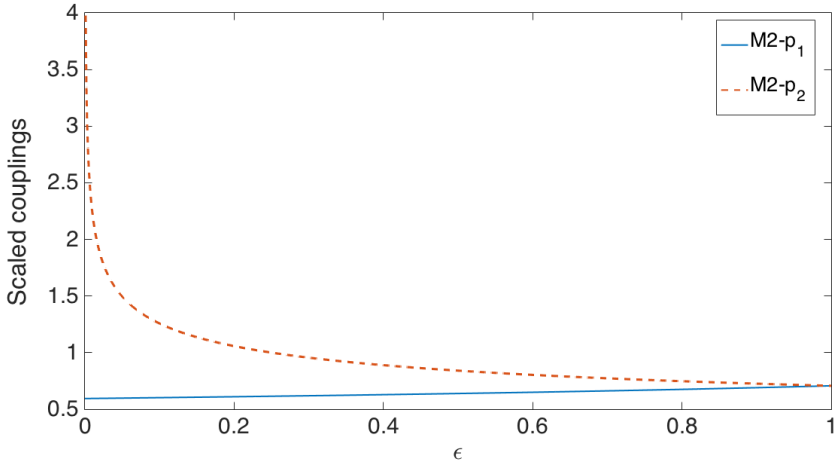


Figure 6.3: M2 coupling terms scaling. This figure shows how the coupling to the different terms in the Hamiltonian for M2 scale as ϵ is varied between 0 and 1. It clearly shows that as ϵ approaches zero the coupling to the p_2 mode increases.

and for M2

$$H_{a-p_2} = \frac{g}{\sqrt{2}\epsilon^{1/4}} \left(a^\dagger + a\right) \left(p_2 + p_2^\dagger\right). \tag{6.37}$$

Ergo, if we were to test the fidelity between M1 and M2 we would expect to see a change on the time scale of roughly $2\sqrt{2\epsilon}/g$.

6.3 Fidelities and Uhlmann's theorem

To test the time scale prediction from the previous section we consider the fidelity between M1 and M2. We use the CM approach and choose parameters that ensures weak coupling, i.e. we

initially choose $g = \alpha\ \omega$ and fix $\omega = 1$ and $\alpha = 0.01$, where we can be confident that the RWA is usually valid between mode a and the adjoining mode. Using Eq. (2.77) we can plot the fidelity between M1 and M2 for modes a, b and c. Note that $F(m_i)$ represents the single mode fidelity of a mode m_i and $F(m_i, m_j)$ is the two mode fidelity of modes m_i and m_j. We notice that the estimated time scale is a reasonable indicator for a fidelity drop, as shown in Figures 6.4 and 6.5.

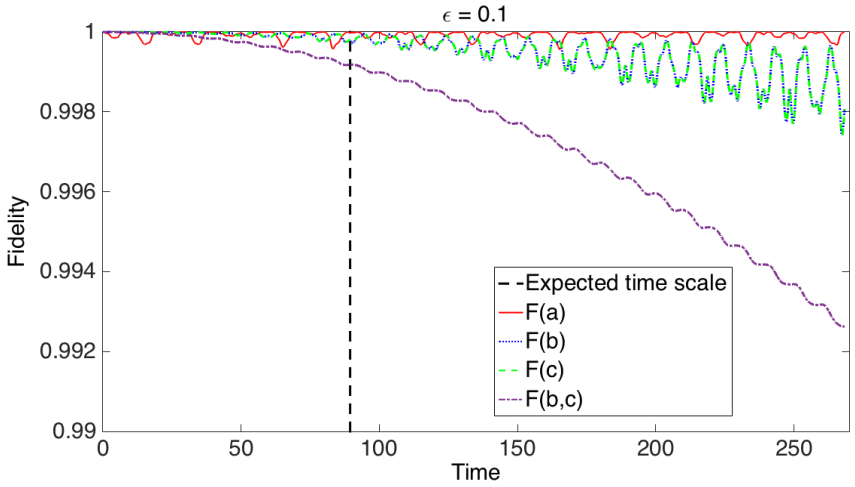


Figure 6.4: Plot of the fidelity, F, between M1 and M2 for bare modes a, b, c and the two mode b - c state against time for $\epsilon = 0.1$. Red line - $F(a)$, Blue dotted line - $F(b)$, Green dashed line - $F(c)$, Purple dot-dashed line - $F(b, c)$. The vertical dashed black line is the expected time scale for a decrease in fidelity. There is a small drop in fidelity of primarily of b and c modes on the order of the time scale, moreover $F(b, c)$ is significantly less than the individual fidelities of b and c.

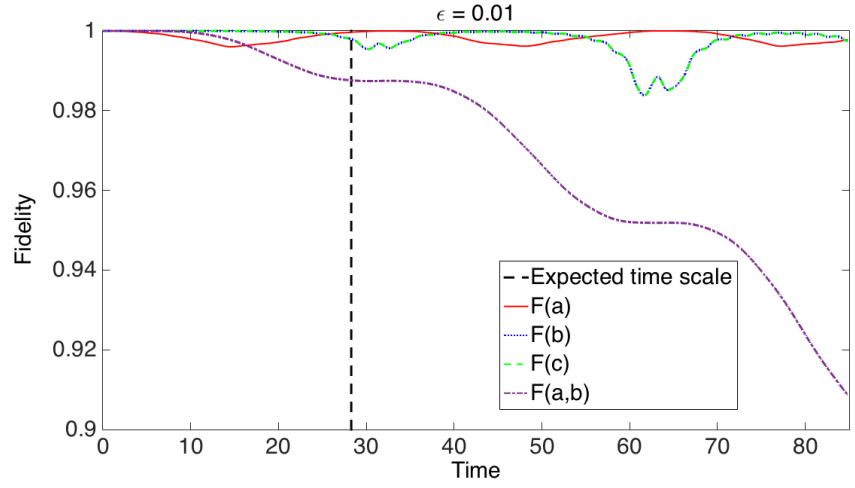


Figure 6.5: Plot of the fidelity, F, between M1 and M2 for bare modes a, b, c and the two mode b - c state against time for $\epsilon = 0.01$. Red line - $F(a)$, Blue dotted line - $F(b)$, Green dashed line - $F(c)$, Purple dot-dashed line - $F(b, c)$. The vertical dashed black line is the expected time scale for a decrease in fidelity. We see a similar behaviour to the $\epsilon = 0.1$ case but with a greater fall in fidelity especially for $F(b, c)$.

One can clearly see that in this parameter regime a high fidelity is maintained between the two models, indicating that the RWA is valid to make. However, a greater loss of fidelity of modes b and c is noticed in the long time limit and for smaller ϵ (i.e. closer to the strong coupling limit). It is interesting to note that $F(a)$ is more resistant to diminishing ϵ and long-time dynamics, therefore if the primary area of interest is the dynamics of mode a then, when $\alpha = 0.01$, a RWA is great to make until ϵ is on the order of 0.0001.

Note that the increases of fidelity at various moments in the dynamics can be understood as the return of quantum information in a finite state space. A three oscillator state space is rather small and thus it is unsurprising if the models become similar as they both return to their initial states (Poincaré recurrence [113]).

Figures 6.4 and 6.5 also show a consequence of Uhlmann's theorem [22, 80] which states that the two mode fidelity should be less than the single mode fidelity, i.e.

$$F(m_i, m_j) \leq min(F(m_i), F(m_j)) \tag{6.38}$$

where $m_{i,j}$ are one of the bare modes a, b, c or a normal mode p_1 or p_2. We observe that the fidelity of the two mode b - c state between M1 and M2, $F(b, c)$, is significantly less than the individual fidelities, especially as we approach the strong coupling limit. If the purpose of the model is concerned with the dynamics of the strongly coupled modes (b and c), then this result would suggest that one should be careful when making a RWA when the strong coupling is close to the limit, because the fidelity drops by roughly 10%.

We may also consider the fidelity between M1 and M2 for the normal modes of b and c, namely p_1 and p_2. This result is shown in Figures 6.6 and 6.7. Concordantly with the scaling of the couplings we observed in Eqs. (6.30), (6.32) and (6.34), the fidelity of the p_1 mode between the two models is not scaled by a change in ϵ and thus stays at near perfect fidelity. In contrast we notice significant changes in the fidelity of mode p_2 between the two models as we approach the strong coupling limit. This tells us, for $\alpha = 0.01$, that not only is the RWA valid to make for mode a (as before) but it is now also a good approximation if the investigator is interested in the collective mode p_1 of oscillators b and c. For the p_2 mode, one has to be careful about performing the RWA near the strong coupling limit.

Considering the time dynamics of the fidelities $F(p_1)$, $F(p_2)$, $F(b, c)$ and $F(p_1, p_2)$ we can see that the oscillatory behaviour of $F(b)$ and $F(c)$ is no longer observed. This suggests that

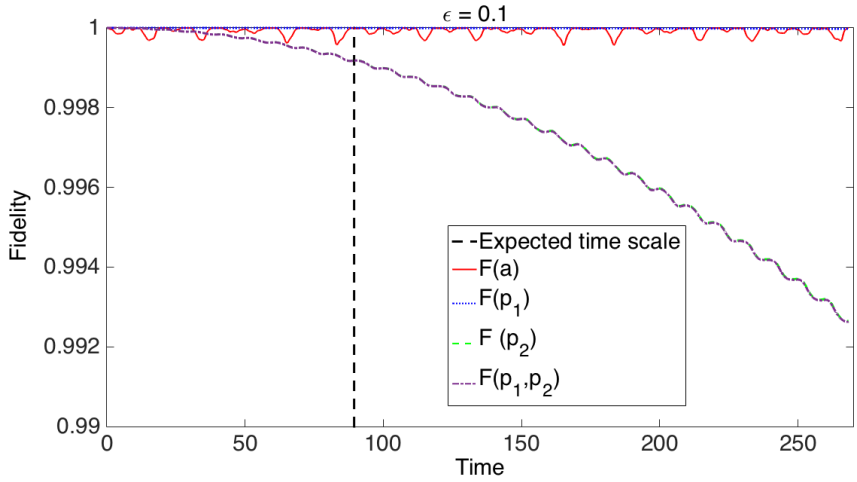


Figure 6.6: Plot of the fidelity, F, between M1 and M2 for bare mode a, normal modes p_1, p_2 and the two mode p_1 - p_2 state against time for $\epsilon = 0.1$. Red line - $F(a)$, Blue dotted line - $F(p_1)$, Green dashed line - $F(p_2)$, Purple dot-dashed line - $F(p_1, p_2)$. The vertical dashed black line is the expected time scale for a decrease in fidelity. Note that the p_2 line is very similar to the $F(p_1, p_2)$ line and both see a drop in fidelity with time whereas mode a and the normal mode p_1 maintain a high fidelity.

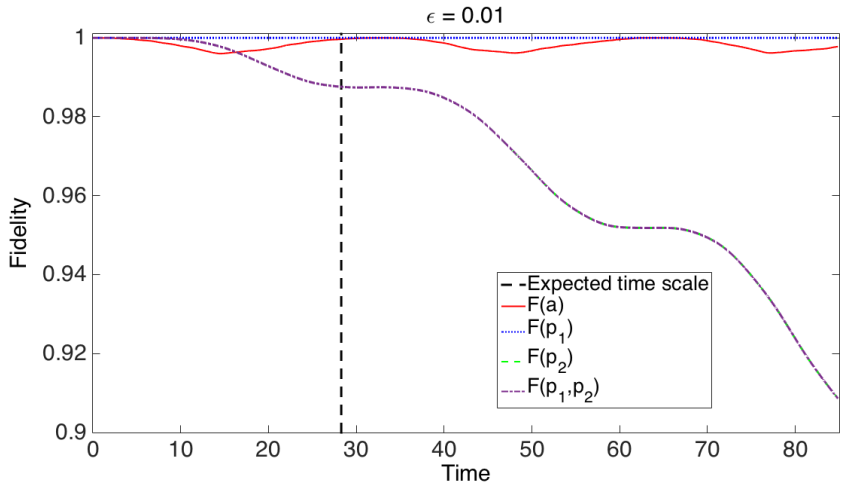


Figure 6.7: Plot of the fidelity, F, between M1 and M2 for bare mode a, normal modes p_1, p_2 and the two mode p_1 - p_2 state against time for $\epsilon = 0.01$. Red line - $F(a)$, Blue dotted line - $F(p_1)$, Green dashed line - $F(p_2)$, Purple dot-dashed line - $F(p_1, p_2)$. The vertical dashed black line is the expected time scale for a decrease in fidelity. Comparing with the $\epsilon = 0.1$ case we see similar behaviour but find that both mode a and the normal mode p_1 are quite resistant to decreasing ϵ and stay quite close to unity. Mode p_2 (which follows the $F(p_1, p_2)$ line in the figure) sees an increasing drop in fidelity as ϵ is decreased.

the majority of the quantum information is being passed within the b - c two mode state. This should be expected as the coupling between oscillators b and c is strong in comparison to the weakly coupled mode a. Note that $F(b, c)$ and $F(p_1, p_2)$ are identical since the normal modes are essentially a unitary rotation on the two mode b - c state and the fidelity is invariant under such a transformation [22].

Finally, by taking all two mode fidelities from both bare and normal mode scenarios and utilising Uhlmann's theorem once more, we find a maximum bound for the fidelity of the entire model, i.e.

$$F\left(m_i, m_j, m_k, \right) \leq \min_{i,j,k} \left(F\left(m_i, m_j\right)\right). \tag{6.39}$$

Figure 6.8 considers the maximum fidelity bound for the model and summarises our knowledge that the fidelity drops faster and by a greater degree as the strong coupling limit is approached.

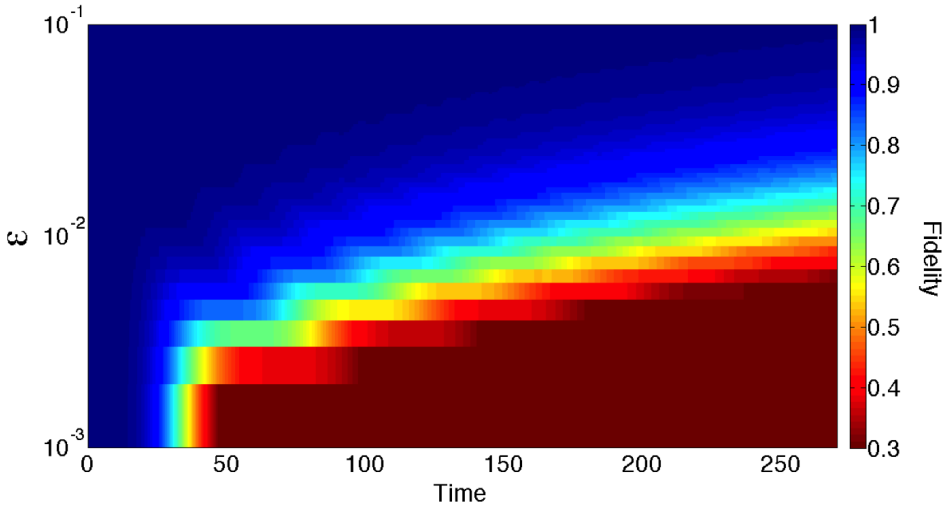


Figure 6.8: Maximum fidelity bound for the model against ϵ and time. As ϵ is diminished the fidelity is further reduced. Note that ϵ is on a log scale.

6.4 Rotating-Wave approximation coupling bound

The previous result suggests that the most basic RWA is still a good approximation in most scenarios, but this was for a 'safe' weak coupling g value i.e. $\alpha = 0.01$. We now ask the question as to how far the RWA can be pushed. To find a coupling bound for the RWA we fix $\epsilon = 0.1$, vary α and test the maximum model fidelity bound. Additionally we add more thermal photons (see Section 2.5.2) to modes b and c, to observe how this bound is affected. The results are shown in Figure 6.9 where $\bar{m}$ $(= \bar{n_b} = \bar{n_c})$ indicates the number of photons in each of modes b and c.

For $\bar{m} = 1$, the figure shows that the RWA starts to break down at $\alpha = 0.05$ on a long time scale but is still quite good for the short time scale ($\sim$ 50 ω). It is important to remember that this is a maximum bound and the 'true' fidelity of the model could be worse. The estimated timescale for the change, as predicted in Section 6.2, is proportional to $1/\alpha$ and we observe that

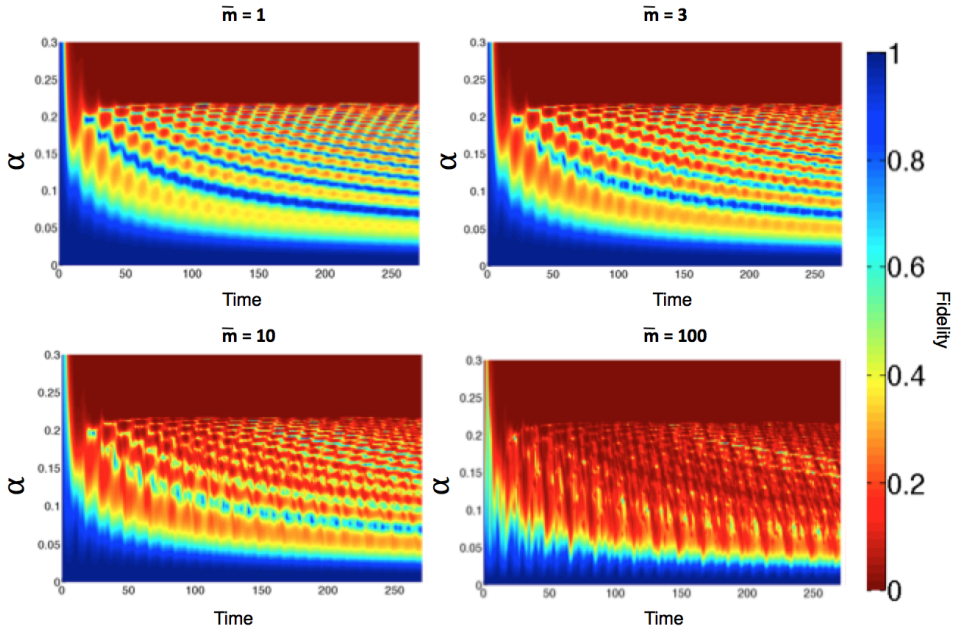


Figure 6.9: Bound for the maximum fidelity between M1 and M2 as α is increased for thermal states of various mean excitations. With $\omega = 1$, the final time in this figure is roughly 260 ω. The bound drops by at least 20% at times, when $\alpha = 0.05$, and we see oscillations back to the higher fidelities due to the small state space. When $\alpha \gtrsim 0.225$ we see a sudden and large drop in the fidelity bound without any revivals. As $\bar{m}$ is increased the fidelity drops at a faster rate and we see lower fidelity revivals.

the initial drop in fidelity roughly follows this prediction.

In the region, $0.05 < \alpha < 0.2$, the bound drops to around 20% fidelity at times but there are oscillations and it returns to higher fidelities. This, as seen previously, is due to the small state space, indeed we see that this 'fidelity oscillation' increases in frequency as we increase coupling, i.e. increasing the rate of information transfer between modes a and b. This leads the models back towards the initial state quicker, where it is most likely that M1 and M2 agree on their predictions. For $\alpha \gtrsim 0.225$ we see a sudden and large drop in the fidelity bound and without any revivals, this indicates a complete breakdown of the RWA.

As the number of photons in modes b and c is increased, we observe that the fidelity drops at a slightly faster rate. This result would suggest that as we increase the energy of modes b and c the RWA would become less valid as an approximation, or rather could only be utilised for lower couplings and shorter time scales. We also notice that the revivals of fidelity diminish in intensity, most likely due to the fact that the predicted states from the two models are less likely to match as we increase the amount of photons in the strongly coupled modes.

This overall approach could be extended to include more weakly coupled modes attached to mode b. This would allow one to simulate an OQS which has a strongly coupled system (the

two mode b - c state) coupled to a weakly coupled bath of oscillators. This can be achieved either through the use of a large finite number of oscillators in a CM approach (or even a master equation approach) for both x-x and RWA bath coupling cases. Then, as before, one would consider the two mode fidelity of the system after the environment has been traced out.

6.5 Finding the instability point of a 'blue'-detuned Hamiltonian

The fidelity-based analysis we have performed so far is not only restricted to RWA and x-x couplings, one may also use it to better understand any bi-linear Hamiltonian such as the one shown in the equation below

$$H = H_{AB} + \omega_a a^\dagger a + \omega_b b^\dagger b + \omega_c c^\dagger c + h\left(b^\dagger c^\dagger + bc\right) \tag{6.40}$$

where H_{AB} can be either the x-x or RWA coupling as before (see Section 6.1). The coupling between modes b and c contain only the CR terms and is sometimes referred to as a 'blue' coupling as this Hamiltonian can be achieved by driving the modes on the blue sideband [140, 141]. As with the previous model, one can perform a normal mode transformation for the blue coupling which obeys the bosonic canonical commutation relations. We begin by expressing the normal modes q_i as

$$q_i = V_{i1} b + V_{i2} c + V_{i3} b^\dagger + V_{i4} c^\dagger \tag{6.41}$$

where V_{ij} are coefficients to be determined. To find these coefficients, we first utilise the canonical commutation relation

$$1 \equiv \left[q_i, q_i^\dagger\right] \quad \equiv |V_{i1}|^2 + |V_{i2}|^2 - |V_{i3}|^2 - |V_{i4}|^2 \tag{6.42}$$

where we have used the standard bosonic canonical commutation relations between modes b and c. As before, more equations are gained by taking the commutator between the normal

mode and the Hamiltonian of the model given in Eq. (6.40)

$$\begin{aligned}[q_i, H] &= (V_{i1}\omega_b - V_{i4}h)\, b \\ &\quad + (V_{i2}\omega_c - V_{i3}h)\, c \\ &\quad + (V_{i2}h - V_{i3}\omega_b)\, b^\dagger \\ &\quad + (V_{i1}h - V_{i4}\omega_c)\, c^\dagger \\ &= E_i q_i\end{aligned} \tag{6.43}$$

where in the last line we utilise the fact that if q_i is a normal mode that diagonalises the system, then it will have an associated eigenfrequency E_i. Eq. (6.43) leaves us the following four simultaneous equations

$$\begin{aligned}\omega_b V_{11} - hV_{14} &= E_1 V_{11} \\ \omega_c V_{22} - hV_{23} &= E_2 V_{22} \\ hV_{32} - \omega_b V_{33} &= E_3 V_{33} \\ hV_{41} - \omega_c C_{44} &= E_4 V_{44}.\end{aligned} \tag{6.44}$$

With the above equations and Eq. (6.42), one can solve for V_{ij} and E_i and express q_i in terms of the bare modes b and c.

$$\begin{pmatrix} q_1 \\ q_2 \\ q_1^\dagger \\ q_2^\dagger \end{pmatrix} = \begin{pmatrix} V_1 & 0 & 0 & V_2 \\ 0 & V_1 & V_2 & 0 \\ 0 & V_2 & V_1 & 0 \\ V_2 & 0 & 0 & V_1 \end{pmatrix} \begin{pmatrix} b \\ c \\ b^\dagger \\ c^\dagger \end{pmatrix} \tag{6.45}$$

where V_i are given by

$$\begin{aligned}V_1 &= \sqrt{\frac{2h^2}{W}} \\ V_2 &= \frac{\omega_b + \omega_c - E_q}{\sqrt{2W}}\end{aligned} \tag{6.46}$$

with

$$\begin{aligned}W &= 4h^2 + (\omega_b + \omega_c)\, E_q - (\omega_b + \omega_c)^2 \\ E_q &= \sqrt{(\omega_b + \omega_c)^2 - 4h^2}\end{aligned} \tag{6.47}$$

and the eigenfrequencies of these normal modes are given by

$$E_\pm = \frac{\pm(\omega_b - \omega_c) + E_q}{2}. \tag{6.48}$$

Considering the resonant case the eigenfrequencies are simplified to

$$E_{\pm} = \sqrt{\omega^2 - h^2}. \tag{6.49}$$

Plotting the fidelity bound of the bare modes (as we did in Section 6.3) for $\alpha = 0.01$ (Figure 6.10), we notice that the fidelity drops as h approaches 1, i.e. ω, indicating the presence of an unstable region. Eq. (6.49) shows that the reason behind this is that the eigenfrequencies become imaginary after $h > \omega$. This means that the 'unstable' value of $h = 0.5\ \omega$ no longer exists for the x-x coupling between modes b and c, because the fidelity is still quite high in this scenario. However, we see from the plot that there is a new 'unstable' value at $h = \omega$ for this coupling.

Although it is clear analytically where the model is unstable for this particular example, in more complicated scenarios this is not always possible. In this sense, the fidelities of modes could possibly be used in other, more convoluted, models to find 'instability points' if it is not clear analytically.

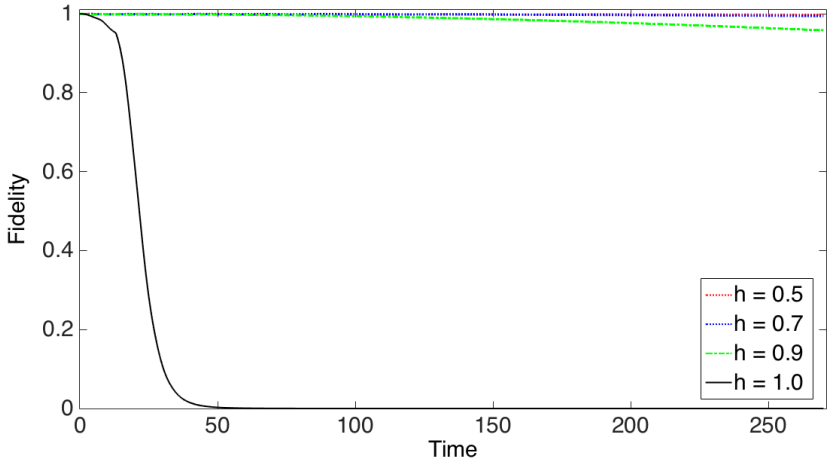


Figure 6.10: Fidelity bound for the model with a strong 'blue' coupling using Uhlmann's theorem for the bare modes. We notice a sudden drop in fidelity when $h = 1.0$, which is the instability point for this model.

6.6 Concluding remarks

The aim of this chapter was to understand if the RWA can be applied to a weakly coupled oscillator in a model if there was a strong coupling present.

To this end, we considered a three oscillator model which incorporated a weak coupling

between two oscillators with one of these oscillators strongly coupled to a third mode. Analytically we showed that the strong coupling scales the effective coupling of the weakly coupled oscillator, but the scaling is only significant as one approaches a strong coupling limit. Both the analytics and numerics indicated that the RWA does better than expected for most of the modes in the model.

The numerics involved calculating the fidelity between models which do and do not apply a RWA. By utilising Ullmann's theorem we are able to find the maximum fidelity bound of any model with a bi-linear Hamiltonian and this was shown for strongly coupled interaction Hamiltonians of the x - x and blue detuned form.

It is our hope that this fidelity-based methodology could be extended to a variety of models, particularly OQSs, to ascertain the validity of using a RWA. This should allow physicists to quantify the limits of the RWA in their simulations/experiments, for example, one could justify the use of a RWA-based master equation to model the environment in their experiment.

In our case, this method could be used to find the exact value of the system-environment scaling factor which invalidates Models 1, 2 and 3 in Chapter 3 and would require the use of Models 4, 5 and 6 (Chapter 5) to describe the OQS accurately.

Conclusions

The field of OQSs has existed since almost the inception of quantum mechanics itself and since then there has been numerous advancements on the subject. In light of recent investment in the development of quantum technologies, such as Google and NASA's Quantum Artificial Intelligence Laboratory and the UK National Quantum Technology Programme, to build the world's first universal quantum computer, there has been vested interest in manipulating OQSs. To this end, there have been endeavours to establish a deeper understanding of environmental effects and controlling said effects by structuring the environments. The most common theoretical approaches to OQSs require approximations and do not allow a direct assessment of the environment. In this thesis, we employed a series of coupled quantum harmonic oscillators to simulate an OQS; allowing us to avoid approximations and analyse the environment modes, giving us a unique, intuitive perspective on OQSs. This final chapter summarises the results within the thesis and mentions some possible applications and extensions.

We began with an investigation into the role near-resonant and detuned environment modes play in determining NMB. The initial analysis was based on an entanglement-based quantifier of non-Markovianity, which we termed the ENMBQ.

By considering a single 'bath' mode model, we discovered that a system shares entanglement according to the strength of the coupling and the level of detuning of a particular mode. For this scenario, we also derived an analytical expression for the entanglement. The addition of a second off-resonant 'bath' mode in the model complicated the dynamics and this was witnessed through the use of effective Hamiltonians.

In terms of an OQS, we considered the paradigmatic scenario of a harmonic oscillator coupled to a bath of bosonic modes and found that the shape of the spectral density function determined which modes played the important role in determining NMB. For low system-environment coupling scaling factor, α, no NMB was observed but after a threshold value, near-resonant modes induce some NMB in the model. However, for higher values of α the detuned modes

take over from the near-resonant modes and play the lead role in determining NMB due to the high frequency of their EOs. The role of near-resonant modes was made more apparent in the other models that were considered. The schemes added a single strongly coupled resonant oscillator in extra bath and buffer mode configurations. They lead to NMB detected at low α due to that extra mode. As α is increased there is a period where no NM dynamics is detected. For higher α values however, the scenario that had an extra strongly coupled mode in the bath behaved like the original model but with a slightly increased amount of NMB due to the extra mode. When this extra mode was a buffer between the system and bath, diminished NMB was observed. This was because the buffer was primarily interacting with near-resonant modes, which naturally produce less NMB than detuned modes in the strong coupling regime due to their relatively slow EOs.

The ENMBQ is not the only witness/measure of NMB that exists in the field and therefore a brief investigation was undertaken on another witness based on fidelity, the FNMBQ. An analysis of an OQS composed of a single mode squeezed state coupled to a thermal bath found a similar relationship with coupling strength and detuning which affected the energy dynamics just as it did with the entanglement dynamics for the ENMBQ. The oscillations seen in the energy dynamics in turn caused oscillations in the fidelity and thus results in a prediction of NMB by the FNMBQ.

Using the knowledge we have gained about the role of near-resonant and off-resonant modes in determining NMB, one could isolate the significant modes in a bath containing numerous oscillators. Armed with these insights researchers are better equipped to engineer models to control the flow of quantum information in their system. This could be achieved by changing either the coupling or detuning to the important modes as well as by adding modes in various configurations. Therefore, this type of control could be useful in maintaining the quantum information of the system, for example in quantum memory models, or even to minimise information feedback which can be of assistance in state transfer protocols.

The original Hamiltonians in our investigations employed beam-splitter like, RWA interactions, where fast oscillating CR terms are ignored. Considering the fact that research has questioned the validity of the RWA in the presence of strong couplings and on its effects on non-Markovianity, we proceeded to find the predictions of the ENMBQ for OQS models which include the CR terms. The analysis showed that the addition of the CR terms had a significant effect on the NMB, in most cases removing it altogether. In the scenario of a system coupled to

a bath, the addition of the fast-oscillating terms caused a rapid decay of entanglement before any of the bath modes are able to induce EOs. In the extra mode OQS models, the CR terms slightly reduce the quantity of NMB for low α. In the extra bath mode scenario, we again note that no NMB is witnessed for larger α due to the quick entanglement decay. For the buffer model however, there does exist a region of higher α values where we find NMB which (in similar fashion to the RWA coupling case) is due to the effective reduction of the bath size around the resonant region.

In view of the effect of CR terms on system dynamics, we explored when and if the RWA can be accurately applied to a weakly coupled oscillator if there is a strong coupling present. The model consisted of a three oscillators which incorporated a weak coupling between two oscillators with one of these oscillators strongly coupled to a third mode. Analytics show that the strong coupling scales the effective coupling of the weakly coupled oscillator but only significantly as the strong coupling limit is approached. By examining the fidelity between models which do and do not include the RWA, we have shown that there is a change in the validity of the approximation on the expected time scales. One also notes that certain modes maintain their fidelity more than others, indicating that the RWA could/could not be applied for scenarios where the reader has a particular mode of interest. Moreover the fidelity of the entire model displays that the RWA does better than previously expected for a significant set of parameter regimes. Finally, a blue-detuned Hamiltonian has been studied to exemplify how this method could be used to isolate 'unstable' regions of a particular Hamiltonian.

The overall vision of using the fidelity in this fashion is to highlight a methodology that could be extended to a variety of models to ascertain the validity of a RWA. Specifically, it is our hope that this approach be used for OQSs where it is common-place for a RWA to be applied to the system-environment coupling. As we have shown for the simplest case, the parameter regimes and associated time scales for the validity of the RWA can be clearly verified and quantified. This should allow theoreticians, for example, to justify their use of a RWA-based master equation. Thus, possibly leading to a significant speed up in the run-time of simulations and a simpler equation of motion which would aid conceptual understanding of a model.

The basic approach within this thesis can be extended to gain a more in-depth view of other OQS processes, for example, heat exchange in a quantum mechanical model. As described in Appendix C, if one considers a bi-partite OQS with each system mode coupled to a separate heat bath, then it is possible to investigate the heat flow of the model. This can be achieved

by adopting a simple definition based on the exchange of energy. The advantage gained using this approach is that it allows one to observe the heat flow inside the baths themselves. This knowledge, once again, could prove useful if one wished to manipulate the heat flow in an OQS.

In summary, this thesis tackles the issues of OQSs with an unorthodox approach. This fresh perspective gives an intuitive understanding of the inner workings of a quantum environment, which we hope can be used to coax out favourable properties. The effect of the environment is often viewed as something to be eliminated in experimental work, but there are studies which suggest that noise can be harnessed. Adding to this growing body of evidence, we strongly feel that with an enlightened outlook on the nature of the problem, there is significant scope for the environment to be manipulated to aid the task at hand. It is our sincerest hope that the knowledge contained within this thesis proves useful in the advancement of open systems, quantum mechanics and physics.

References

[1] M. Planck, Annalen der Physik **309**, 553 (1901).

[2] A. Einstein, Annalen der Physik **322**, 549 (1905).

[3] E. Davies, *Quantum theory of open systems* (Academic Press, 1976).

[4] H. Carmichael, *An Open Systems Approach to Quantum Optics: Lectures Presented at the Université Libre de Bruxelles, October 28 to November 4, 1991*, Lecture Notes in Computer Science (Springer-Verlag, 1993).

[5] U. Weiss, *Quantum Dissipative Systems*, Series in modern condensed matter physics (World Scientific, 1993).

[6] H. Carmichael, *Statistical Methods in Quantum Optics 1: Master Equations and Fokker-Planck Equations*, Physics and Astronomy Online Library (Springer, 1998).

[7] S. Attal, A. Joye, and C. Pillet, *Open Quantum Systems*, no. no. 1880 in Lecture notes in mathematics (Springer, 2006).

[8] S. Attal, A. Joye, and C. Pillet, *Open Quantum Systems II: The Markovian Approach*, Lecture Notes in Mathematics (Springer, 2006).

[9] H. Breuer and F. Petruccione, *The Theory of Open Quantum Systems* (OUP Oxford, 2007).

[10] H. Wiseman and G. Milburn, *Quantum Measurement and Control* (Cambridge University Press, 2010).

[11] Á. Rivas and S. Huelga, *Open Quantum Systems: An Introduction*, SpringerBriefs in Physics (Springer, 2011).

[12] I. R. Senitzky, Phys. Rev. **119**, 670 (1960).

[13] I. R. Senitzky, Phys. Rev. **124**, 642 (1961).

[14] W. Pauli, *Festschrift zum 60. Geburtstage A. Sommerfeld* (Hirzel, Leipzig, 1928), pauli master equation; p. 30.

[15] V. Weisskopf and E. Wigner, Zeitschrift fr Physik **63**, 54 (1930).

[16] S. Nakajima, Progress of Theoretical Physics **20**, 948 (1958).

[17] R. Zwanzig, The Journal of Chemical Physics **33**, 1338 (1960).

[18] L. Van Hove, Fundamental problems in statistical mechanics (1962).

[19] G. G. Emch, Journal of Mathematical Physics **7**, 1198 (1966).

[20] G. S. Agarwal, Phys. Rev. **178**, 2025 (1969).

[21] R. Dümcke and H. Spohn, Zeitschrift für Physik B Condensed Matter **34**, 419 (1979).

[22] M. Nielsen and I. Chuang, *Quantum Computation and Quantum Information*, Cambridge Series on Information and the Natural Sciences (Cambridge University Press, 2000).

[23] E. B. Davies, Communications in mathematical Physics **39**, 91 (1974).

[24] E. B. Davies, Mathematische Annalen **219**, 147 (1976).

[25] E. B. Davies, *One-parameter semigroups*, vol. 15 (Academic Pr, 1980).

[26] S. Attal, A. Joye, and C. Pillet, *Open Quantum Systems III: Recent Developments*, Lecture Notes in Mathematics (Springer, 2006).

[27] J. Dereziński and R. Früboes, Journal of mathematical physics **46**, 063511 (2005).

[28] B. Chance, *Tunneling in biological systems*, Academic Pr. rapid manuscript reproduction (Academic Press, 1979).

[29] X.-T. Liang, Phys. Rev. E **82**, 051918 (2010).

[30] P. Rebentrost and A. Aspuru-Guzik, The Journal of Chemical Physics **134**, 101103 (2011).

[31] J. P. Sethna and S. Kivelson, Phys. Rev. B **26**, 3513 (1982).

[32] S. Maniscalco and F. Petruccione, Phys. Rev. A **73**, 012111 (2006).

[33] N. Hashitsumae, F. Shibata, and M. Shingu, Journal of Statistical Physics **17**, 155 (1977).

[34] S. Chaturvedi and F. Shibata, Zeitschrift fr Physik B Condensed Matter **35**, 297 (1979).

[35] H. Spohn, Rev. Mod. Phys. **52**, 569 (1980).

[36] B. L. Hu, J. P. Paz, and Y. Zhang, Phys. Rev. D **45**, 2843 (1992).

[37] P. Gaspard and M. Nagaoka, The Journal of Chemical Physics **111**, 5668 (1999).

[38] K. Shiokawa, Phys. Rev. A **79**, 012308 (2009).

[39] A. Rivas, A. D. K. Plato, S. F. Huelga, and M. B. Plenio, New Journal of Physics **12**, 113032 (2010).

[40] A. D. K. Plato, Ph.D. thesis, Imperial College London (2011).

[41] I. Knezevic and B. Novakovic, Journal of Computational Electronics **12**, 363 (2013).

[42] H. Z. Shen, M. Qin, X.-M. Xiu, and X. X. Yi, Phys. Rev. A **89**, 062113 (2014).

[43] C. Fleming, N. I. Cummings, C. Anastopoulos, and B. L. Hu, Journal of Physics A: Mathematical and Theoretical **43**, 405304 (2010).

[44] H. Mäkelä and M. Möttönen, Phys. Rev. A **88**, 052111 (2013).

[45] M. Bamba and T. Ogawa, Phys. Rev. A **88**, 013814 (2013).

[46] S. De Liberato, Phys. Rev. A **89**, 017801 (2014).

[47] M. Bamba and T. Ogawa, Phys. Rev. A **89**, 017802 (2014).

[48] Y. B. Band, Journal of Physics B: Atomic, Molecular and Optical Physics **48**, 045401 (2015).

[49] G. Adesso, S. Ragy, and A. R. Lee, Open Systems & Information Dynamics **21** (2014).

[50] S. L. Braunstein and P. van Loock, Rev. Mod. Phys. **77**, 513 (2005).

[51] C. Weedbrook, S. Pirandola, R. García-Patrón, N. J. Cerf, T. C. Ralph, J. H. Shapiro, and S. Lloyd, Rev. Mod. Phys. **84**, 621 (2012).

[52] A. Ferraro, S. Olivares, and M. Paris, *Gaussian states in continuous variable quantum information* (Napoli Series on Physics and Astrophysics (ed. Bibliopolis, Napoli, 2005), 2005).

[53] E. Wigner, Phys. Rev. **40**, 749 (1932).

[54] R. Simon, E. C. G. Sudarshan, and N. Mukunda, Phys. Rev. A **36**, 3868 (1987).

[55] M. B. Plenio, J. Hartley, and J. Eisert, New Journal of Physics **6**, 36 (2004).

[56] R. Simon, N. Mukunda, and B. Dutta, Phys. Rev. A **49**, 1567 (1994).

[57] R. F. Werner and M. M. Wolf, Phys. Rev. Lett. **86**, 3658 (2001).

[58] J. Williamson, American Journal of Mathematics **58**, pp. 141 (1936).

[59] A. S. Holevo, M. Sohma, and O. Hirota, Phys. Rev. A **59**, 1820 (1999).

[60] G. Vidal and R. F. Werner, Phys. Rev. A **65**, 032314 (2002).

[61] A. Serafini, F. Illuminati, and S. D. Siena, Journal of Physics B: Atomic, Molecular and Optical Physics **37**, L21 (2004).

[62] S. Barnett and P. Radmore, *Methods in Theoretical Quantum Optics*, Oxford science publications (Clarendon Press, 1997).

[63] D. Walls and G. Milburn, *Quantum Optics*, SpringerLink: Springer e-Books (Springer, 2008).

[64] K. Kasai, G. Jiangrui, and C. Fabre, EPL (Europhysics Letters) **40**, 25 (1997).

[65] R. Simon, Phys. Rev. Lett. **84**, 2726 (2000).

[66] A. Einstein, B. Podolsky, and N. Rosen, Phys. Rev. **47**, 777 (1935).

[67] M. Born, A. Einstein, and I. Born, *The Born Einstein Letters: correspondence between Albert Einstein and Max and Hedwig Born from 1916 to 1955 with commentaries by Max Born. Translated by Irene Born* (Basingstoke, Macmillan Press, 1971).

[68] J. S. Bell et al., Physics **1**, 195 (1964).

[69] L. Gurvits, in *Proceedings of the thirty-fifth annual ACM symposium on Theory of computing* (ACM, 2003), pp. 10–19.

[70] A. Peres, Phys. Rev. Lett. **77**, 1413 (1996).

[71] M. Horodecki, P. Horodecki, and R. Horodecki, Physics Letters A **223**, 1 (1996).

[72] A. Serafini, G. Adesso, and F. Illuminati, Phys. Rev. A **71**, 032349 (2005).

[73] M. B. Plenio and S. Virmani, Quantum Info. Comput. **7**, 1 (2007).

[74] J. Lee, M. S. Kim, Y. J. Park, and S. Lee, Journal of Modern Optics **47**, 2151 (2000).

[75] M. B. Plenio, Phys. Rev. Lett. **95**, 090503 (2005).

[76] R. Jozsa, Journal of Modern Optics **41**, 2315 (1994).

[77] T. Cover and J. Thomas (1991).

[78] C. E. Shannon, Bell System Technical Journal **27**, 379 (1948).

[79] R. V. Hartley, Bell System technical journal **7**, 535 (1928).

[80] A. Uhlmann, Reports on Mathematical Physics **9**, 273 (1976).

[81] D. Bures, Transactions of the American Mathematical Society pp. 199–212 (1969).

[82] J. Twamley, Journal of Physics A: Mathematical and General **29**, 3723 (1996).

[83] H. Scutaru, Journal of Physics A: Mathematical and General **31**, 3659 (1998).

[84] G.-S. Paraoanu and H. Scutaru, Phys. Rev. A **58**, 869 (1998).

[85] P. Marian, T. A. Marian, and H. Scutaru, Phys. Rev. A **68**, 062309 (2003).

[86] P. Marian and T. A. Marian, Phys. Rev. A **77**, 062319 (2008).

[87] P. Marian and T. A. Marian, The European Physical Journal Special Topics **160**, 281 (2008).

[88] G. Björk, J. Söderholm, L. L. Sánchez-Soto, A. B. Klimov, I. Ghiu, P. Marian, and T. A. Marian, Optics Communications **283**, 4440 (2010), electromagnetic Coherence and Polarization.

[89] I. Ghiu, G. Björk, P. Marian, and T. A. Marian, Phys. Rev. A **82**, 023803 (2010).

[90] P. Marian and T. A. Marian, Phys. Rev. A **86**, 022340 (2012).

[91] R. Vasile, S. Maniscalco, M. G. A. Paris, H.-P. Breuer, and J. Piilo, Phys. Rev. A **84**, 052118 (2011).

[92] Á. Rivas, S. F. Huelga, and M. B. Plenio, Reports on Progress in Physics **77**, 094001 (2014).

[93] B. Bylicka, D. Chruściński, and S. Maniscalco, Scientific reports **4** (2014).

[94] J.-S. Xu, C.-F. Li, C.-J. Zhang, X.-Y. Xu, Y.-S. Zhang, and G.-C. Guo, Phys. Rev. A **82**, 042328 (2010).

[95] J.-S. Tang, C.-F. Li, Y.-L. Li, X.-B. Zou, G.-C. Guo, H.-P. Breuer, E.-M. Laine, and J. Piilo, EPL (Europhysics Letters) **97**, 10002 (2012).

[96] B.-H. Liu, L. Li, Y.-F. Huang, C.-F. Li, G.-C. Guo, E.-M. Laine, H.-P. Breuer, and J. Piilo, Nature Physics **7**, 931 (2011).

[97] A. Orieux, A. D'Arrigo, G. Ferranti, R. L. Franco, G. Benenti, E. Paladino, G. Falci, F. Sciarrino, and P. Mataloni, Sci. Rep. **5** (2015).

[98] A. W. Chin, S. F. Huelga, and M. B. Plenio, Phys. Rev. Lett. **109**, 233601 (2012).

[99] R. Vasile, S. Olivares, M. G. A. Paris, and S. Maniscalco, Phys. Rev. A **83**, 042321 (2011).

[100] E.-M. Laine, H.-P. Breuer, and J. Piilo, Scientific reports **4** (2014).

[101] S. F. Huelga, A. Rivas, and M. B. Plenio, Phys. Rev. Lett. **108**, 160402 (2012).

[102] R. Schmidt, A. Negretti, J. Ankerhold, T. Calarco, and J. T. Stockburger, Phys. Rev. Lett. **107**, 130404 (2011).

[103] M. Thorwart, J. Eckel, J. H. Reina, P. Nalbach, and S. Weiss, Chemical Physics Letters **478**, 234 (2009).

[104] A. Chin, J. Prior, R. Rosenbach, F. Caycedo-Soler, S. Huelga, and M. Plenio, Nature Physics **9**, 113 (2013).

[105] H.-P. Breuer, Journal of Physics B: Atomic, Molecular and Optical Physics **45**, 154001 (2012).

[106] M. M. Wolf, J. Eisert, T. S. Cubitt, and J. I. Cirac, Phys. Rev. Lett. **101**, 150402 (2008).

[107] A. Rivas, S. F. Huelga, and M. B. Plenio, Phys. Rev. Lett. **105**, 050403 (2010).

[108] H.-P. Breuer, E.-M. Laine, and J. Piilo, Phys. Rev. Lett. **103**, 210401 (2009).

[109] X.-M. Lu, X. Wang, and C. P. Sun, Phys. Rev. A **82**, 042103 (2010).

[110] S. Luo, S. Fu, and H. Song, Phys. Rev. A **86**, 044101 (2012).

[111] V. Venkataraman, A. Plato, T. Tufarelli, and M. Kim, Journal of Physics B: Atomic, Molecular and Optical Physics **47**, 015501 (2014).

[112] A. A. Markov, Izvestiya Fiziko-matematicheskogo obschestva pri Kazanskom universitete **15**, 18 (1906).

[113] H. Poincaré, Acta mathematica **13**, A3 (1890).

[114] L. Barreira, in *XIVth International Congress on Mathematical Physics. World Scientific* (Citeseer, 2006), pp. 415–422.

[115] O. Gamel and D. F. V. James, Phys. Rev. A **82**, 052106 (2010).

[116] J. Paavola, J. Piilo, K.-A. Suominen, and S. Maniscalco, Phys. Rev. A **79**, 052120 (2009).

[117] P. M. V. B. Barone and A. O. Caldeira, Phys. Rev. A **43**, 57 (1991).

[118] A. W. Chin, . Rivas, S. F. Huelga, and M. B. Plenio, Journal of Mathematical Physics **51**, 092109 (2010).

[119] R. Martinazzo, B. Vacchini, K. H. Hughes, and I. Burghardt, The Journal of Chemical Physics **134**, 011101 (2011).

[120] J.-H. An and W.-M. Zhang, Phys. Rev. A **76**, 042127 (2007).

[121] F. Plastina and S. Maniscalco, International Journal of Quantum Information **9**, 1715 (2011).

[122] F. Intravaia, S. Maniscalco, and A. Messina, Phys. Rev. A **67**, 042108 (2003).

[123] S. Maniscalco, J. Piilo, F. Intravaia, F. Petruccione, and A. Messina, Phys. Rev. A **70**, 032113 (2004).

[124] S. Maniscalco, J. Piilo, and K.-A. Suominen, The European Physical Journal D **55**, 181 (2009).

[125] G. S. Agarwal, Phys. Rev. A **4**, 1778 (1971).

[126] G. S. Agarwal, Phys. Rev. A **7**, 1195 (1973).

[127] G. S. Agarwal, *Quantum statistical theories of spontaneous emission and their relation to other approaches* (Springer, 1974).

[128] D. Walls, Zeitschrift fr Physik **234**, 231 (1970).

[129] J. Cresser, Journal of Modern Optics **39**, 2187 (1992).

[130] C. Joshi, P. Öhberg, J. D. Cresser, and E. Andersson, Phys. Rev. A **90**, 063815 (2014).

[131] C. Joshi, M. Jonson, P. Öhberg, and E. Andersson, Phys. Rev. A **87**, 062304 (2013).

[132] E. T. Jaynes and F. W. Cummings, Proceedings of the IEEE **51**, 89 (1963).

[133] J. Reithmaier, G. Sek, A. Löffler, C. Hofmann, S. Kuhn, S. Reitzenstein, L. Keldysh, V. Kulakovskii, T. Reinecke, and A. Forchel, Nature **432**, 197 (2004).

[134] F. A. Vind, A. M. Souza, R. S. Sarthour, and I. S. Oliveira, Phys. Rev. A **90**, 062339 (2014).

[135] V. Sudhir, M. G. Genoni, J. Lee, and M. S. Kim, Phys. Rev. A **86**, 012316 (2012).

[136] C. Ciuti, G. Bastard, and I. Carusotto, Phys. Rev. B **72**, 115303 (2005).

[137] G. Günter, A. A. Anappara, J. Hees, A. Sell, G. Biasiol, L. Sorba, S. De Liberato, C. Ciuti, A. Tredicucci, A. Leitenstorfer, et al., Nature **458**, 178 (2009).

[138] T. Niemczyk, F. Deppe, H. Huebl, E. Menzel, F. Hocke, M. Schwarz, J. Garcia-Ripoll, D. Zueco, T. Hümmer, E. Solano, et al., Nature Physics **6**, 772 (2010).

[139] T. Tufarelli, A. Ferraro, M. S. Kim, and S. Bose, Phys. Rev. A **85**, 032334 (2012).

[140] M. Aspelmeyer, T. J. Kippenberg, and F. Marquardt, Rev. Mod. Phys. **86**, 1391 (2014).

[141] A. A. Clerk, M. H. Devoret, S. M. Girvin, F. Marquardt, and R. J. Schoelkopf, Rev. Mod. Phys. **82**, 1155 (2010).

[142] R. Alicki, M. Horodecki, P. Horodecki, and R. Horodecki, Open Systems & Information Dynamics **11**, 205 (2004).

[143] C. Jarzynski and D. K. Wójcik, Phys. Rev. Lett. **92**, 230602 (2004).

[144] P. Skrzypczyk, A. J. Short, and S. Popescu, Nature communications **5** (2014).

[145] M. H. Partovi, Phys. Rev. E **77**, 021110 (2008).

[146] D. Jennings and T. Rudolph, Phys. Rev. E **81**, 061130 (2010).

[147] V. Buzek, V. Vedral, M. B. Plenio, P. L. Knight, and M. Hillery, Phys. Rev. A **55**, 3327 (1997).

[148] K. von Ompteda, *Physics happens in a dark place* (2014), URL `http://karinvonompteda.com/PhysicSpace-Exhibition`.

[149] RCA, *Physics happens in a dark place* (2014), URL `http://spaceprogram.rca.ac.uk/physicspace/`.

Appendices

Appendix A

Derivations of initial states in the covariance matrix formalism

This appendix expands the derivations of the CM for the various initial states shown in Chapter 2. For the single mode states we choose the R vector of the form

$$R^T = (\hat{x}, \hat{p}) \tag{A.1}$$

and for the two mode case we choose

$$R^T = (\hat{x}_1, \hat{x}_2, \hat{p}_1, \hat{p}_2)\,. \tag{A.2}$$

A.1 Vacuum state

We start by inputing the vacuum state into Eq. (2.9)

$$\gamma_{j,k} = 2Re\,\mathrm{Tr}\left[|0\rangle\langle 0| R_j R_k\right] \tag{A.3}$$

and then express the position and momentum operators in the ladder basis (shown below) to find the elements of the CM.

$$\hat{x} = \frac{1}{\sqrt{2}}\left(a^\dagger + a\right) \qquad \hat{p} = \frac{i}{\sqrt{2}}\left(a^\dagger - a\right) \tag{A.4}$$

The single mode vacuum state can therefore be calculated as shown below.

$$\begin{aligned}\gamma_{11} &= 2Re\langle 0|\frac{1}{\sqrt{2}}\left(a^\dagger + a\right)\frac{1}{\sqrt{2}}\left(a^\dagger + a\right)|0\rangle \\ &= Re\langle 0|\left(a^\dagger + a\right)\left(a^\dagger + a\right)|0\rangle \\ &= Re\langle 0|\left(a^\dagger + a\right)|1\rangle \\ &= 1\end{aligned} \tag{A.5}$$

$\gamma_{12} = \gamma_{21} = 0$ because all terms are purely imaginary.

$$\begin{aligned}\gamma_{22} &= 2Re\langle 0|\frac{i}{\sqrt{2}}\left(a^\dagger - a\right)\frac{i}{\sqrt{2}}\left(a^\dagger - a\right)|0\rangle \\ &= -Re\langle 0|\left(a^\dagger - a\right)\left(a^\dagger - a\right)|0\rangle \\ &= -Re\langle 0|\left(a^\dagger - a\right)|1\rangle \\ &= 1\end{aligned} \tag{A.6}$$

Which gives a CM of the form

$$\gamma = \begin{pmatrix} 1 & 0 \\ 0 & 1 \end{pmatrix} \tag{A.7}$$

i.e. the identity matrix.

A.2 Thermal state

The majority of the following derivation of the thermal state is shown in Ref. [62]. We consider the thermal state for a single mode and the density matrix is given by

$$\rho = \frac{\exp\left(-\omega\hat{n}\beta\right)}{\mathrm{Tr}\left[\exp\left(-\omega\hat{n}\beta\right)\right]} \tag{A.8}$$

where $\hat{n}$, ω and $\beta = 1/T$ are the number operator, mode frequency and one over the temperature T respectively. Considering that the density matrix is only dependant on $\hat{n}$ it will be of diagonal form in the number basis. Therefore it is possible to express the density matrix of a thermal state as the following

$$\rho = \sum_{n=0}^{\infty} P\left(n\right)|n\rangle\langle n| \tag{A.9}$$

where we have a Bose-Einstein probability distribution $P(n)$ of the form

$$P(n) = \exp(-n\omega\beta)\left(1 - \exp(-\omega\beta)\right). \tag{A.10}$$

Using this form of the density matrix we can calculate the mean/average photon number, $\bar{n}$, by finding the expectation value of $\hat{n}$

$$\begin{aligned}
\bar{n} &= \mathrm{Tr}\left[\rho\bar{n}\right] \\
&= \left(1 - \exp(-\omega\beta)\right)\sum_{n=0}^{\infty}\langle n|\hat{n}|n\rangle \exp(-n\omega\beta) \\
&= \left(1 - \exp(-\omega\beta)\right)\sum_{n=0}^{\infty} n \exp(-n\omega\beta) \\
&= \left(1 - \exp(-\omega\beta)\right)\left(-\frac{1}{\omega}\frac{d}{d\beta}\right)\sum_{n=0}^{\infty}\exp(-n\omega\beta).
\end{aligned} \tag{A.11}$$

Using the relation

$$\sum_{n=0}^{\infty}\exp(-n\omega\beta) = \frac{1}{1 - \exp(-\omega\beta)} \tag{A.12}$$

we can express $\bar{n}$ as

$$\begin{aligned}
\bar{n} &= \left(1 - \exp(-\omega\beta)\right)\left(-\frac{1}{\omega}\right)\frac{d}{d\beta}\left(\frac{1}{1 - \exp(-\omega\beta)}\right) \\
&= \frac{\omega\exp(-\omega\beta)\left(1 - \exp(-\omega\beta)\right)}{\omega\left(1 - \exp(-\omega\beta)\right)^2} \\
&= \frac{1}{\left(\exp(\omega\beta) - 1\right)}.
\end{aligned} \tag{A.13}$$

A.3 Average thermal photon number state

An initial thermal state of an oscillator can be expressed in terms of the average photon number $\bar{n}$ [62]

$$\rho = \sum_{n}\frac{1}{1+\bar{n}}\left(\frac{\bar{n}}{1+\bar{n}}\right)^{n}|n\rangle\langle n|. \tag{A.14}$$

Expressing this in the CM formalism, we have

$$\gamma_{j,k} = 2Re\sum_{n}\frac{1}{1+\bar{n}}\left(\frac{\bar{n}}{1+\bar{n}}\right)^{n}\mathrm{Tr}\left[|n\rangle\langle n|R_jR_k\right]. \tag{A.15}$$

Explicitly this gives

$$\begin{aligned}
\gamma_{11} &= 2Re \sum_n \frac{1}{1+\bar{n}} \left(\frac{\bar{n}}{1+\bar{n}} \right)^n \mathrm{Tr}\left[|n\rangle\langle n| \hat{x}\hat{x} \right] \\
&= \sum_n \frac{1}{1+\bar{n}} \left(\frac{\bar{n}}{1+\bar{n}} \right)^n \langle n| \left(a^\dagger + a \right) \left(a^\dagger + a \right) |n\rangle \\
&= \sum_n \frac{1}{1+\bar{n}} \left(\frac{\bar{n}}{1+\bar{n}} \right)^n \langle n| a^\dagger a^\dagger + a^\dagger a + a a^\dagger + a a |n\rangle \\
&= \sum_n \frac{1}{1+\bar{n}} \left(\frac{\bar{n}}{1+\bar{n}} \right)^n \langle n| \sqrt{n} a^\dagger |n-1\rangle + \langle n| \sqrt{n+1} a |n+1\rangle \\
&= \sum_n \frac{1}{1+\bar{n}} \left(\frac{\bar{n}}{1+\bar{n}} \right)^n \left(\sqrt{n}\sqrt{n} + \sqrt{n+1}\sqrt{n+1} \right) \\
&= \sum_n \frac{1}{1+\bar{n}} \left(\frac{\bar{n}}{1+\bar{n}} \right)^n + \sum_n \frac{1}{1+\bar{n}} \left(\frac{\bar{n}}{1+\bar{n}} \right)^n 2n.
\end{aligned} \tag{A.16}$$

The first term is just a probability distribution on n and so the sum will be equal to one. The second term is therefore just an average since it is the summation of the probability of n, times n, resulting in a value of $\bar{n}$, the average photon number. Thus the first element of the CM is given by

$$\gamma_{11} = 2\bar{n} + 1. \tag{A.17}$$

The off-diagonal terms, $\gamma_{12} = \gamma_{21}$, are zero because all terms are purely imaginary. The final element is

$$\begin{aligned}
\gamma_{22} &= 2Re \sum_n \frac{1}{1+\bar{n}} \left(\frac{\bar{n}}{1+\bar{n}} \right)^n \mathrm{Tr}\left[|n\rangle\langle n| \hat{p}\hat{p} \right] \\
&= \sum_n \frac{1}{1+\bar{n}} \left(\frac{\bar{n}}{1+\bar{n}} \right)^n \langle n| \left(a - a^\dagger \right) \left(a^\dagger - a \right) |n\rangle \\
&= \sum_n \frac{1}{1+\bar{n}} \left(\frac{\bar{n}}{1+\bar{n}} \right)^n \langle n| a a^\dagger - a a - a^\dagger a^\dagger + a^\dagger a |n\rangle \\
&= 2\bar{n} + 1.
\end{aligned} \tag{A.18}$$

Which gives a CM of the form

$$\gamma = \begin{pmatrix} 2\bar{n}+1 & 0 \\ 0 & 2\bar{n}+1 \end{pmatrix}. \tag{A.19}$$

Note that if we set $\bar{n} = 0$ we recover the vacuum state (see Section 2.5.1).

A.4 Squeezed state

A.4.1 Single mode squeezed vacuum state

The single mode squeezing operator is defined as

$$\hat{S}(z) = \exp\left(\frac{1}{2}\left(za^{\dagger 2} - z^* a^2\right)\right) \tag{A.20}$$

where

$$z = re^{i\theta} \tag{A.21}$$

and r and θ are the squeezing parameter and the phase respectively [49]. Considering a squeezed vacuum state $\hat{S}|0\rangle$ the CM is given by

$$\begin{aligned}\gamma_{j,k} &= 2Re\,\mathrm{Tr}\left[\hat{S}|0\rangle\langle 0|\hat{S}^\dagger R_j R_k\right] \\ &= 2Re\langle 0|\hat{S}^\dagger R_j R_k \hat{S}|0\rangle.\end{aligned} \tag{A.22}$$

To calculate the elements of the CM we utilise the Hadamard Lemma

$$e^X Y e^{-X} = Y + [X,Y] + \frac{1}{2!}[X,[X,Y]] + \frac{1}{3!}[X,[X,[X,Y]]] + ... \tag{A.23}$$

and the following commutation relations

$$\left[aa, a^\dagger a^\dagger\right] = 2\left(a^\dagger a + aa^\dagger\right) \tag{A.24}$$

$$\left[aa, a^\dagger a + aa^\dagger\right] = 4aa \tag{A.25}$$

$$\left[a^\dagger a^\dagger, a^\dagger a + aa^\dagger\right] = -4a^\dagger a^\dagger. \tag{A.26}$$

The first element is given by

$$\begin{aligned}\gamma_{11} &= 2Re\langle 0|\hat{S}^\dagger \hat{x}\hat{x}\hat{S}|0\rangle \\ &= Re\langle 0|\hat{S}^\dagger\left(a^\dagger a^\dagger + aa + a^\dagger a + aa^\dagger\right)\hat{S}|0\rangle.\end{aligned} \tag{A.27}$$

Using Eq. (A.23), with $X = -\frac{1}{2}\left(za^{\dagger 2} - z^* aa^2\right)$ and $Y = a^\dagger a^\dagger + aa + a^\dagger a + aa^\dagger$, we get

$$\begin{aligned}
\gamma_{11} = Re\langle 0|a^\dagger a^\dagger & \left(1 + 2z + \frac{2\left(z^2 + r^2\right)}{2!} + \frac{8zr^2}{3!} + \frac{8r^2\left(z^2 + r^2\right)}{4!} + ...\right) \\
& + aa\left(1 + 2z^* + \frac{2\left(z^{*2} + r^2\right)}{2!} + \frac{8z^* r^2}{3!} + \frac{8r^2\left(z^{*2} + r^2\right)}{4!} + ...\right) \\
& + a^\dagger a\left(1 + (z + z^*) + \frac{4r^2}{2!} + \frac{4r^2\left(z + z^*\right)}{3!} + \frac{16r^4}{4!} + ...\right) \\
& + aa^\dagger\left(1 + (z + z^*) + \frac{4r^2}{2!} + \frac{4r^2\left(z + z^*\right)}{3!} + \frac{16r^4}{4!} + ...\right)|0\rangle
\end{aligned} \tag{A.28}$$

where we have used the fact that $z^* z = r^2$. The $a^\dagger a^\dagger$, aa and $a^\dagger a$ terms can be ignored as they yield zero when the expectation value is taken for the vacuum state. Using $z = re^{i\theta}$ the remaining expression can be simplified as follows

$$\begin{aligned}
\gamma_{11} &= Re\langle 0|aa^\dagger\left(1 + (z + z^*) + \frac{4r^2}{2!} + \frac{4r^2\left(z + z^*\right)}{3!} + \frac{16r^4}{4!} + ...\right)|0\rangle \\
&= Re\langle 0|aa^\dagger\left(1 + \frac{4r^2}{2!} + \frac{16r^4}{4!} + ... + \left(e^{i\theta} + e^{-i\theta}\right)\left(r + \frac{4r^3}{3!} + ...\right)\right)|0\rangle \\
&= Re\langle 0|aa^\dagger\left(\cosh(2r) + \cos(\theta)\sinh(2r)\right)|0\rangle \\
&= \cosh(2r) + \cos(\theta)\sinh(2r)\,.
\end{aligned} \tag{A.29}$$

Similarly we calculate components γ_{12} and γ_{21}

$$\begin{aligned}
\gamma_{12}\,(=\gamma_{21}) &= 2Re\langle 0|\hat{S}^\dagger \hat{x}\hat{p}\hat{S}|0\rangle \\
&= Re\langle 0|\hat{S}^\dagger i\left(a^\dagger a^\dagger - aa + aa^\dagger - a^\dagger a\right)\hat{S}|0\rangle \\
&= Re\langle 0|ia^\dagger a^\dagger\left(1 + \frac{2\left(r^2 - z^2\right)}{2!} + \frac{8r^2\left(r^2 - z^2\right)}{4!} + ...\right) \\
&\quad - iaa\left(1 + \frac{2\left(r^2 - z^{*2}\right)}{2!} + \frac{8r^2\left(r^2 - z^{*2}\right)}{4!} + ...\right) \\
&\quad - ia^\dagger a\left(1 + (z - z^*) + \frac{4r^2\left(z - z^*\right)}{3!} + ...\right) \\
&\quad + iaa^\dagger\left(1 + (z^* - z) + \frac{4r^2\left(z^* - z\right)}{3!} + ...\right)|0\rangle \\
&= Re\langle 0|aa^\dagger\left(\frac{\left(e^{i\theta} - e^{-i\theta}\right)}{2i}\left(2r + \frac{8r^3}{3!} + ...\right) + i\right)|0\rangle \\
&= \sin(\theta)\sinh(2r)\,.
\end{aligned} \tag{A.30}$$

Where after applying the Hadamard Lemma we have used the fact that only the $aa^\dagger$ term remains as the expectation value will yield zero for the other operators. Note that the final term disappears because only real components are taken. The final component is given by

$$\begin{aligned}
\gamma_{22} &= 2Re\langle 0|\hat{S}^\dagger \hat{p}\hat{p}\hat{S}|0\rangle \\
&= Re\langle 0|\hat{S}^\dagger \left(-a^\dagger a^\dagger - aa + a^\dagger a + aa^\dagger\right)\hat{S}|0\rangle \\
&= Re\langle 0|a^\dagger a^\dagger \left(-1 + 2z - \frac{2\left(z^2+r^2\right)}{2!} + \frac{8zr^2}{3!} - \frac{8r^2\left(z^2+r^2\right)}{4!} + ...\right) \\
&+ aa\left(-1 + 2z^* - \frac{2\left(z^{*2}+r^2\right)}{2!} + \frac{8z^*r^2}{3!} - \frac{8r^2\left(z^{*2}+r^2\right)}{4!} + ...\right) \\
&+ a^\dagger a\left(1 - (z+z^*) + \frac{4r^2}{2!} - \frac{4r^2\left(z+z^*\right)}{3!} + \frac{16r^4}{4!} + ...\right) \\
&+ aa^\dagger\left(1 - (z+z^*) + \frac{4r^2}{2!} - \frac{4r^2\left(z+z^*\right)}{3!} + \frac{16r^4}{4!} + ...\right)|0\rangle \\
&= Re\langle 0|aa^\dagger\left(1 + \frac{4r^2}{2!} + \frac{16r^4}{4!} + ... - \frac{\left(e^{i\theta}+e^{-i\theta}\right)}{2}\left(2r + \frac{8r^3}{3!} + ...\right)\right)|0\rangle \\
&= \cosh(2r) - \cos(\theta)\sinh(2r)\,.
\end{aligned} \tag{A.31}$$

This gives us the final form of the CM for a single mode squeezed state

$$\gamma = \begin{pmatrix} \cosh(2r) + \cos(\theta)\sinh(2r) & \sin(\theta)\sinh(2r) \\ \sin(\theta)\sinh(2r) & \cosh(2r) - \cos(\theta)\sinh(2r) \end{pmatrix}. \tag{A.32}$$

A.4.2 Two mode squeezed vacuum state

The two mode squeezing operator is defined as

$$\hat{U}_{ab}(z) = \exp\left(\frac{1}{2}\left(za^\dagger b^\dagger - z^* ab\right)\right) \tag{A.33}$$

where

$$z = \zeta e^{i\phi} \tag{A.34}$$

and $a^\dagger(a)$ and $b^\dagger(b)$ are the creation (annihilation) ladder operators for modes one and two respectively. For the purposes of this thesis we just consider a two mode squeezed vacuum state $\hat{U}_{ab}|0_1 0_2\rangle$, the CM of which is given by

$$\gamma_{j,k} = 2Re\langle 00|\hat{U}_{ab}^\dagger R_j R_k \hat{U}_{ab}|00\rangle \tag{A.35}$$

with

$$R^T = (\hat{x}_1, \hat{x}_2, \hat{p}_1, \hat{p}_2)\,. \tag{A.36}$$

Note we have dropped the indices for the modes for simplicity. To calculate the elements of the CM we utilise the Hadamard Lemma and the following commutation relations

$$\left[\mathcal{O}_k, \mathcal{O}_k^\dagger \mathcal{O}_k^\dagger\right] = 2\mathcal{O}_k^\dagger \quad \left[\mathcal{O}_k, \mathcal{O}_k \mathcal{O}_k^\dagger\right] = \mathcal{O}_k \quad \left[\mathcal{O}_k, \mathcal{O}_k^\dagger \mathcal{O}_k\right] = \mathcal{O}_k \tag{A.37}$$

$$\left[\mathcal{O}_k^\dagger, \mathcal{O}_k \mathcal{O}_k\right] = -2\mathcal{O}_k \quad \left[\mathcal{O}_k^\dagger, \mathcal{O}_k \mathcal{O}_k^\dagger\right] = -\mathcal{O}_k^\dagger \quad \left[\mathcal{O}_k^\dagger, \mathcal{O}_k^\dagger \mathcal{O}_k\right] = -\mathcal{O}_k^\dagger \tag{A.38}$$

$$\left[\mathcal{O}_k \mathcal{O}_l, \mathcal{O}_k^\dagger \mathcal{O}_l^\dagger\right] = \mathcal{O}_k^\dagger \mathcal{O}_k + \mathcal{O}_l \mathcal{O}_l^\dagger \qquad k \neq l \tag{A.39}$$

where $\mathcal{O}_k$ is either the annihilation operator for mode one or two

$$\mathcal{O}_k^T = (a, b)\,. \tag{A.40}$$

The first element is given by

$$\begin{aligned} \gamma_{11} &= 2Re\langle 00|\hat{U}_{ab}^\dagger \hat{x}_1 \hat{x}_1 \hat{U}_{ab}|00\rangle \\ &= Re\langle 00|\hat{U}_{ab}^\dagger \left(a^\dagger a^\dagger + a^\dagger a + a a^\dagger + a a\right) \hat{U}_{ab}|00\rangle. \end{aligned} \tag{A.41}$$

We use the Hadamard Lemma to exponentiate the above term with $X = \frac{1}{2}\left(z^* ab - z a^\dagger b^\dagger\right)$ and $Y = a^\dagger a^\dagger + a^\dagger a + a a^\dagger + a a$. Keeping only the $aa^\dagger$ and $bb^\dagger$ terms (as the others will yield zero when the expectation value is taken) we get

$$\begin{aligned} \gamma_{11} &= Re\langle 00|aa^\dagger + bb^\dagger \left(\frac{\zeta^2}{2!} + \frac{\zeta^4}{4!} + \frac{\zeta^6}{6!} + ...\right)|00\rangle \\ &= 1 + \frac{\zeta^2}{2!} + \frac{\zeta^4}{4!} + \frac{\zeta^6}{6!} + ... = \cosh(\zeta)\,. \end{aligned} \tag{A.42}$$

The other elements can be calculated as

$$\begin{aligned}
\gamma_{12}\,(=\gamma_{21}) &= 2Re\langle 00|\hat{U}_{ab}^{\dagger}\hat{x}_1\hat{x}_2\hat{U}_{ab}|00\rangle \\
&= Re\langle 00|\hat{U}_{ab}^{\dagger}\left(a^{\dagger}b^{\dagger}+a^{\dagger}b+ab^{\dagger}+ab\right)\hat{U}_{ab}|00\rangle \\
&= Re\langle 00|bb^{\dagger}\left(\frac{z+z^{*}}{2}\right)\left(1+\frac{\zeta^2}{3!}+\frac{\zeta^4}{5!}+....\right)|00\rangle \\
&= Re\langle 00|bb^{\dagger}\left(\frac{e^{i\phi}+e^{-i\phi}}{2}\right)\left(\zeta+\frac{\zeta^3}{3!}+\frac{\zeta^5}{5!}+....\right)|00\rangle \\
&= \cos\left(\phi\right)\sinh\left(\zeta\right)
\end{aligned} \tag{A.43}$$

$$\begin{aligned}
\gamma_{13}\,(=\gamma_{31}) &= 2Re\langle 00|\hat{U}_{ab}^{\dagger}\hat{x}_1\hat{p}_1\hat{U}_{ab}|00\rangle \\
&= Re\langle 00|\hat{U}_{ab}^{\dagger}i\left(a^{\dagger}a^{\dagger}-a^{\dagger}a+aa^{\dagger}-aa\right)\hat{U}_{ab}|00\rangle \\
&= Re\langle 00|iaa^{\dagger}|00\rangle \\
&= 0
\end{aligned} \tag{A.44}$$

$$\begin{aligned}
\gamma_{14}\,(=\gamma_{41}) &= 2Re\langle 00|\hat{U}_{ab}^{\dagger}\hat{x}_1\hat{p}_2\hat{U}_{ab}|00\rangle \\
&= Re\langle 00|\hat{U}_{ab}^{\dagger}i\left(a^{\dagger}b^{\dagger}-a^{\dagger}b+ab^{\dagger}-ab\right)\hat{U}_{ab}|00\rangle \\
&= Re\langle 00|bb^{\dagger}i\left(i\frac{z^{*}-z}{2}\right)\left(1+\frac{\zeta^2}{3!}+\frac{\zeta^4}{5!}+....\right)|00\rangle \\
&= Re\langle 00|bb^{\dagger}\left(\frac{e^{i\phi}-e^{-i\phi}}{2i}\right)\left(\zeta+\frac{\zeta^3}{3!}+\frac{\zeta^5}{5!}+....\right)|00\rangle \\
&= \sin\left(\phi\right)\sinh\left(\zeta\right).
\end{aligned} \tag{A.45}$$

Element γ_{22} is the same calculation as γ_{11}, as $\hat{U}_{ab}$ operates on both modes identically, and is therefore equal to $\cosh\left(\zeta\right)$.

$$\begin{aligned}
\gamma_{23}\,(=\gamma_{32}) &= 2Re\langle 00|\hat{U}_{ab}^{\dagger}\hat{x}_2\hat{p}_1\hat{U}_{ab}|00\rangle \\
&= Re\langle 00|\hat{U}_{ab}^{\dagger}i\left(a^{\dagger}b^{\dagger}+a^{\dagger}b-ab^{\dagger}-ab\right)\hat{U}_{ab}|00\rangle \\
&= Re\langle 00|bb^{\dagger}\left(i\frac{z^{*}-z}{2}\right)\left(1+\frac{\zeta^2}{3!}+\frac{\zeta^4}{5!}+....\right)|00\rangle \\
&= Re\langle 00|bb^{\dagger}\left(\frac{e^{i\phi}-e^{-i\phi}}{2i}\right)\left(\zeta+\frac{\zeta^3}{3!}+\frac{\zeta^5}{5!}+....\right)|00\rangle \\
&= \sin\left(\phi\right)\sinh\left(\zeta\right)
\end{aligned} \tag{A.46}$$

Element γ_{24} is the same calculation as γ_{13} and will therefore be equal to zero.

$$\begin{aligned}
\gamma_{33} &= 2Re\langle 00|\hat{U}_{ab}^{\dagger}\hat{p}_1\hat{p}_1\hat{U}_{ab}|00\rangle \\
&= Re\langle 00|\hat{U}_{ab}^{\dagger}\left(-a^{\dagger}a^{\dagger}+a^{\dagger}a+aa^{\dagger}-aa\right)\hat{U}_{ab}|00\rangle \\
&= Re\langle 00|aa^{\dagger}+bb^{\dagger}\left(\frac{\zeta^2}{2!}+\frac{\zeta^4}{4!}+\frac{\zeta^6}{6!}+....\right)|00\rangle \\
&= 1+\frac{\zeta^2}{2!}+\frac{\zeta^4}{4!}+\frac{\zeta^6}{6!}+.... = \cosh(\zeta)
\end{aligned} \tag{A.47}$$

$$\begin{aligned}
\gamma_{34}\,(=\gamma_{43}) &= 2Re\langle 00|\hat{U}_{ab}^{\dagger}\hat{p}_1\hat{p}_2\hat{U}_{ab}|00\rangle \\
&= Re\langle 00|\hat{U}_{ab}^{\dagger}\left(-a^{\dagger}b^{\dagger}+a^{\dagger}b+ab^{\dagger}-ab\right)\hat{U}_{ab}|00\rangle \\
&= Re\langle 00|bb^{\dagger}\left(-\frac{z+z^*}{2}\right)\left(1+\frac{\zeta^2}{3!}+\frac{\zeta^4}{5!}+....\right)|00\rangle \\
&= Re\langle 00|bb^{\dagger}\left(-\frac{e^{i\phi}+e^{-i\phi}}{2}\right)\left(\zeta+\frac{\zeta^3}{3!}+\frac{\zeta^5}{5!}+....\right)|00\rangle \\
&= -\cos(\phi)\sinh(\zeta)
\end{aligned} \tag{A.48}$$

Finally, γ_{44} is the same calculation as γ_{33} and will therefore be equal to $\cosh(\zeta)$. Therefore the CM for a two mode squeezed vacuum state is given by

$$\gamma = \begin{pmatrix} \mathfrak{m} & \mathfrak{n} & 0 & \mathfrak{s} \\ \mathfrak{n} & \mathfrak{m} & \mathfrak{s} & 0 \\ 0 & \mathfrak{s} & \mathfrak{m} & -\mathfrak{n} \\ \mathfrak{s} & 0 & -\mathfrak{n} & \mathfrak{m} \end{pmatrix} \tag{A.49}$$

where

$$\begin{aligned}
\mathfrak{m} &= \cosh(\zeta) \\
\mathfrak{n} &= \cos(\phi)\sinh(\zeta) \\
\mathfrak{s} &= \sin(\phi)\sinh(\zeta).
\end{aligned} \tag{A.50}$$

For the purposes of our work in this thesis, the expression can be further simplified as we only consider states with zero phase, $\phi = 0$, giving the matrix

$$\gamma_0 = \begin{pmatrix} \cosh(\zeta) & \sinh(\zeta) & 0 & 0 \\ \sinh(\zeta) & \cosh(\zeta) & 0 & 0 \\ 0 & 0 & \cosh(\zeta) & -\sinh(\zeta) \\ 0 & 0 & -\sinh(\zeta) & \cosh(\zeta) \end{pmatrix}. \tag{A.51}$$

Appendix B

Master equations in a covariance matrix formalism

It is possible to use the CM to simulate a master equation. In this appendix we show the forms of the CM for two examples of master equations. Please note that depending on definitions of the CM there may be a factor of two difference with other results, also one has to be careful with the definition and use of the damping factor α.

B.1 A markovian master equation

As shown in Refs. [6, 9], the master equation for a damped harmonic oscillator is given by

$$\dot{\rho} = \eta(t)(2\bar{n}+1)\left(2s\rho s^{\dagger} - s^{\dagger}s\rho - \rho s^{\dagger}s\right) + \eta(t)\,\bar{n}\left(2s^{\dagger}\rho s - ss^{\dagger}\rho - \rho ss^{\dagger}\right) \tag{B.1}$$

where $\bar{n}$ is shown in Section 2.5.2 and $\eta(t)$ is the damping coefficient. It can be shown that this master equation can be expressed in a CM formalism as follows

$$\dot{\gamma} = M\gamma(t) + \gamma(t)M^{T} + \Delta(t)P \tag{B.2}$$

where

$$M = \begin{pmatrix} \eta(t)/2 & \omega_s' \\ -\omega_s' & -\eta(t)/2 \end{pmatrix} \tag{B.3}$$

$$P = \begin{pmatrix} 1 & 0 \\ 0 & 1 \end{pmatrix}. \tag{B.4}$$

The renormalised system frequency is given by

$$\omega_s'^2 = \omega_s^2 - \Omega \tag{B.5}$$

where

$$\Omega = 2\alpha\omega_c \tag{B.6}$$

and α is the damping coefficient in the spectral density function. The diffusion coefficient $\Delta(t)$ and damping coefficient $\eta(t)$ are given by

$$\begin{aligned} \Delta(t) &= \pi J(\omega)(2\bar{n}+1) \\ \eta(t) &= \pi J(\omega). \end{aligned} \tag{B.7}$$

B.2 A non-Markovian master equation

The NM master equation for essentially Model 4 (see Chapter 5) was first solved by Hu, Paz and Zhang [36]. Similarly, a NM master equation was shown by Intravaia et al. using a super operator approach [122]. Their approach, outlined in Refs. [9, 91, 122–124], shows the NM master equation for quantum Brownian motion in the interaction picture under the weak coupling and secular approximations, given in the equation below

$$\begin{aligned} \dot{\rho} = {} & \alpha(\Delta(t) + \eta(t))\left(2s\rho s^\dagger - s^\dagger s\rho - \rho s^\dagger s\right) \\ & + \alpha(\Delta(t) - \eta(t))\left(2s^\dagger\rho s - ss^\dagger\rho - \rho ss^\dagger\right). \end{aligned} \tag{B.8}$$

It can be shown that this master equation can be expressed in a CM formalism as follows

$$\dot{\gamma} = M\gamma(t) + \gamma(t)M^T + 2\alpha\Delta(t)P \tag{B.9}$$

where

$$M = \begin{pmatrix} -\alpha\eta(t) & \omega_s' \\ -\omega_s' & -\alpha\eta(t) \end{pmatrix} \tag{B.10}$$

$$P = \begin{pmatrix} 1 & 0 \\ 0 & 1 \end{pmatrix}. \tag{B.11}$$

The renormalised system frequency is given by

$$\omega_s'^2 = \omega_s^2 + \Delta(t). \tag{B.12}$$

The diffusion coefficient $\Delta(t)$ and damping coefficient $\eta(t)$ are given by

$$\begin{aligned} \Delta(t) &= \frac{1}{2}\int_0^t ds \int_0^\infty d\omega J(\omega)(2\bar{n}+1)cos(\omega_s s)cos(\omega s) \\ \eta(t) &= \int_0^t ds \int_0^\infty d\omega J(\omega)sin(\omega_s s)sin(\omega s). \end{aligned} \tag{B.13}$$

Appendix C

Other Works

In this appendix we briefly mention some works that are possible to achieve with systems of coupled harmonic oscillators and a CM formalism.

C.1 Heat and entanglement

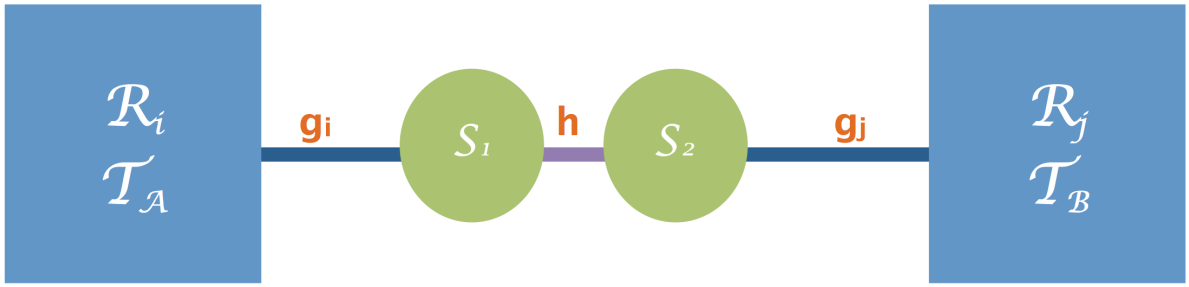


Figure C.1: Model to investigate heat flow. Two system oscillators, S_1 and S_2, are coupled to a bath of oscillators R_i and R_j with coupling strengths g_i and g_j respectively. The system modes are coupled together with strength h and can be in any squeezed thermal state. The baths are in thermal states with temperatures T_A and T_B with $T_B > T_A$ to create heat flow.

If one considers a bi-partite quantum harmonic oscillator system each coupled to bath of harmonic oscillators as shown in Figure C.1 then it is possible to investigate the heat flow of the model. By setting the initial state of the system modes in any squeezed thermal state and the baths in thermal states with temperatures such that $T_B > T_A$ it is possible to create a heat flow from one end of the model to the other. There are various quantum mechanical definitions of heat, as seen in Refs. [142–144], we adopt a simple definition based on the exchange of energy.

Considering a simple two mode system with a Hamiltonian

$$\begin{aligned}\hat{H} &= \omega_a a^\dagger a + \omega_b b^\dagger b + g\left(a + a^\dagger\right)\left(b + b^\dagger\right) \\ &= \frac{\omega_a}{2}\left(\hat{x_a}^2 + \hat{p_a}^2 - 1\right) + \frac{\omega_b}{2}\left(\hat{x_b}^2 + \hat{p_b}^2 - 1\right) + 2g\hat{x_a}\hat{x_b}\end{aligned} \tag{C.1}$$

where we have expressed the Hamiltonian in the position-momentum basis and $\hat{x_a}$ ($\hat{p_a}$) and $\hat{x_b}$ ($\hat{p_b}$) are the position (momentum) operators for modes a and b respectively. The energy of mode a is given by

$$\hat{E_a} = a^\dagger a = \left(\hat{x_a}^2 + \hat{p_a}^2 - 1\right). \tag{C.2}$$

We then consider the change of the energy of mode a in time, $\hat{E_a}(t)$, by looking at the Heisenberg equation

$$\begin{aligned}\dot{\hat{E}}_a(t) &= i\left[\hat{H}, \hat{E_a}\right] \\ &= ig\left[\hat{x_a}(t)\,\hat{x_b}(t), \hat{p_a}(t)\,\hat{p_a}(t)\right] \\ &= -2g\hat{p_a}(t)\,\hat{x_b}(t).\end{aligned} \tag{C.3}$$

In the CM formalism, by expressing a symplectic vector, R, of the form

$$R^T = (\hat{x_a}, \hat{x_b}, \hat{p_a}, \hat{p_b}) \tag{C.4}$$

we can find $\langle R_i(t), R_j(t)\rangle$ by taking half of the $\gamma_{ij}(t)$ component of the CM. This allows us to calculate the energy change, and therefore the heat, in mode a from the CM as shown in the equation below

$$\begin{aligned}\dot{\hat{E}}_a(t) &= -2g\left(\frac{\gamma_{21}}{2}\right) \\ &= g\gamma_{12}\end{aligned} \tag{C.5}$$

where we have used the anti-symmetric property of the CM. This is easy to simulate and calculate and can be compared to a master equation approach (which can simulate the model exactly). The advantage of this approach is to understand the transfer of heat to specific bath modes or even within the bath modes.

Additionally it has been shown that the presence of correlations, for example entanglement, within such a model can cause a reversal of the heat flow [145, 146]. This again can be investigated using a CM approach by setting the initial state of the system modes to have an initial squeezing.

C.2 Entanglement broadcasting

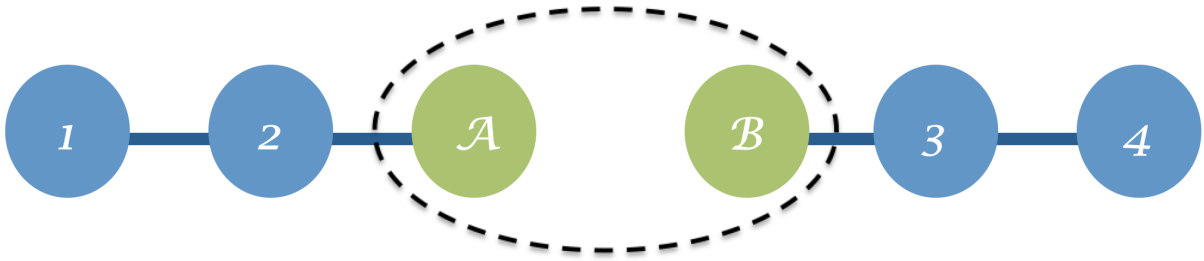


Figure C.2: Model to investigate entanglement broadcasting. An initially entangled two mode squeezed state ρ_{AB} is spatially separated. By connecting modes 1 and 2 to mode A and modes 3 and 4 to mode B it is possible to create more entangled pairs.

The concept of entanglement broadcasting was first introduced by Buzek et. al. [147]. The basic principle is that two parties which share an entangled pair can then create more, 'less entangled', pairs by interacting their entangled mode with additional modes as shown in Figure C.2. Using the CM approach one can investigate how to create optimal or interesting sets of entanglement pairs. There are a variety of options in terms of tweaking the model, for example one could vary mode frequency and coupling parameters, have adaptive time-dependent couplings, different coupling regimes (e.g. red or blue detuned Hamiltonians) and varying initial states.

Appendix D

Outreach

During my time as a PhD student I have engaged in multiple outreach activities. Outreach is designed to educate the general public about science and in my case, physics. Many of these activities have had tools to explain some of the basic ideas behind the work in this thesis. The main events that have covered my research activities have been science busking and an art exhibition, which are briefly detailed below.

D.1 Science busking

During Imperial Festivals, physics department open days and the Royal Society Summer Exhibition, I used a Tibetan singing bowl to explain the concept of resonance. The bowl is designed such that when it is filled with water and the handles on the bowl are rubbed, the resonance frequency of the bowl is hit, causing vibrations in the water and a sound to be emitted. By giving more examples of classical and famous cases of resonance, I explain the basic concept of natural frequencies and efficient energy transfer for resonant cases. For older members of the public I proceed to describe how the concept of resonance, and therefore detuning, can also have an effect on the quantum level, i.e. by having an effect on the transfer of quantum information. This then provides a link to my PhD work and can be explained to more interested parties.



Figure D.1: A Tibetan singing bowl is used to explain the concept of resonance to a member of the public. Photo courtesy of the RCSU.

D.2 Physics happens in a dark place exhibition

In a collaboration with the Royal College of Art (RCA) Information Experience Design (IED) programme there was an exhibition which displayed PhD topics in the form of artwork. Myself and a few other students gave talks about our PhD projects and the RCA students set about turning the physics we described into works of art. After a few discussions between the two groups the result was an art exhibition titled 'Physics happens in a dark place' which was held in Shoreditch town hall. Three of the exhibits were based on my work and are briefly described below. Further pictures and videos of the explanations behind the pieces can be found in Refs. [148] and [149].

D.2.1 Resonance Revenant

This piece of work visualises a system oscillator coupled to many other oscillators represented by the speakers. The lengths of the wires represent different coupling strengths and the speakers play a sound at different frequencies, i.e. the natural frequency of a mode. At different points in time, different speakers will play a sound and be encircled by light to display its activeness or occupancy, this illustrates how a system mode shares quantum information with different bath modes depending on the parameters.

D.2.2 Systems and Baths

The aim of this piece is to illustrate the methodology I apply to investigate OQS. Each of the 'balls' represent a particular bath structure and the inside of which are covered by mirrors. The viewer then picks up a system mode depicted by a small clear glass ball with a laser light protruding the surface and places it inside the different bath structures. The differences in the physical structure of the ball results in the mirrors in its interior reflecting the 'modes' and their coupling to the laser light in various ways which one can observe through the opening in the ball structures. This procedure mirrors the simulations I apply to investigate the role of bath structures in affecting the properties of an OQS.

D.2.3 Quantum Love

This project is designed to showcase entanglement. There are two large balloons filled with helium which float in two separate rooms and are lit in different colours to depict spatial separation. The balloons have propellors which correlates the movements between the two spheres which clearly represents the correlations that underly quantum entanglement. Moreover they have distance sensors which keeps the balloons away from any surface through the use of the propellors. The idea behind this is to illustrate the measurement problem (or decoherence). The balloons avoid contact, i.e. observation, in order to maintain the entanglement between the them.



(a)

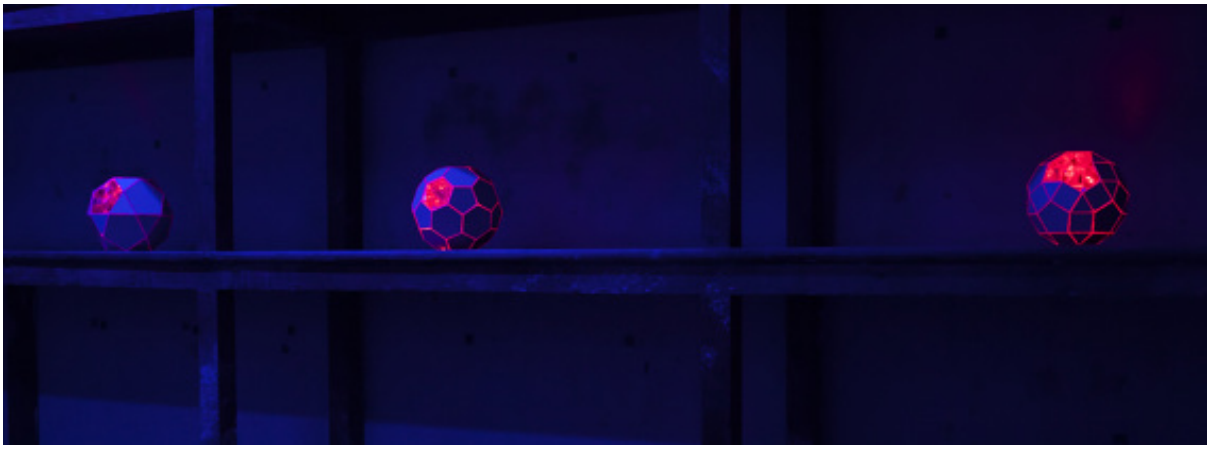


(b)

Figure D.2: Resonance Revenant. 'Bells ring out in the darkness, calling attention to unseen struggles, calling for us to understand'. Exhibit by Oliver Smith. Photographs were taken from Ref. [148] courtesy of Karin von Ompteda.



(a)

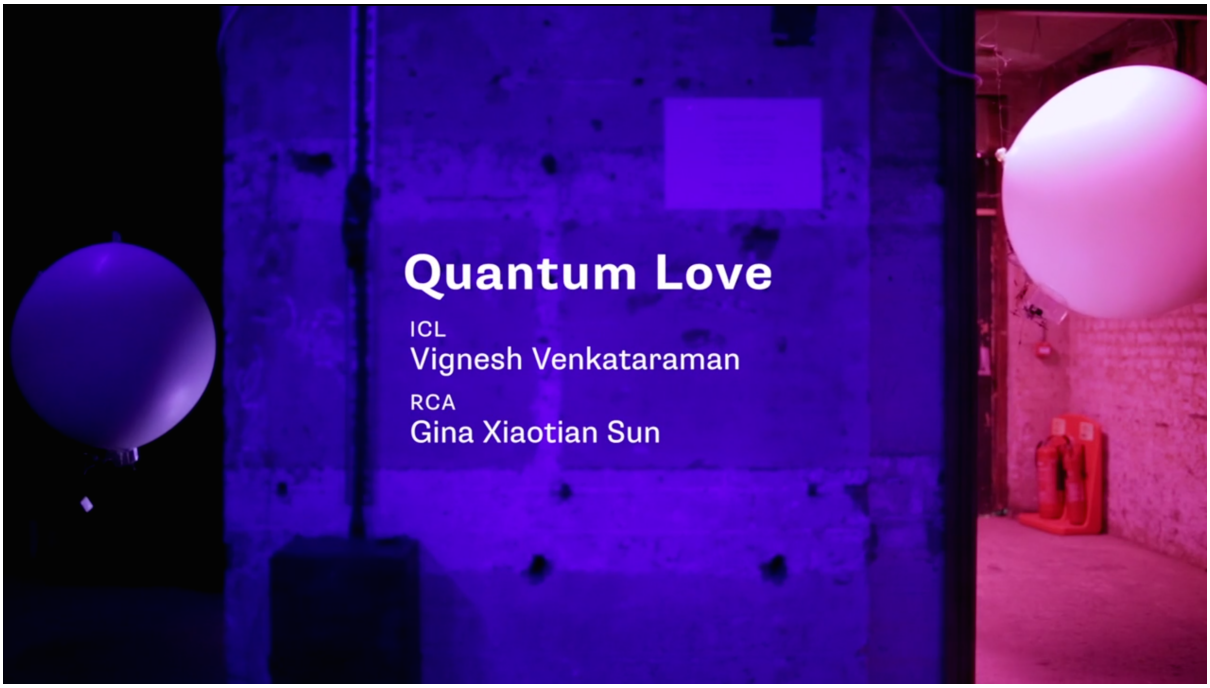


(b)

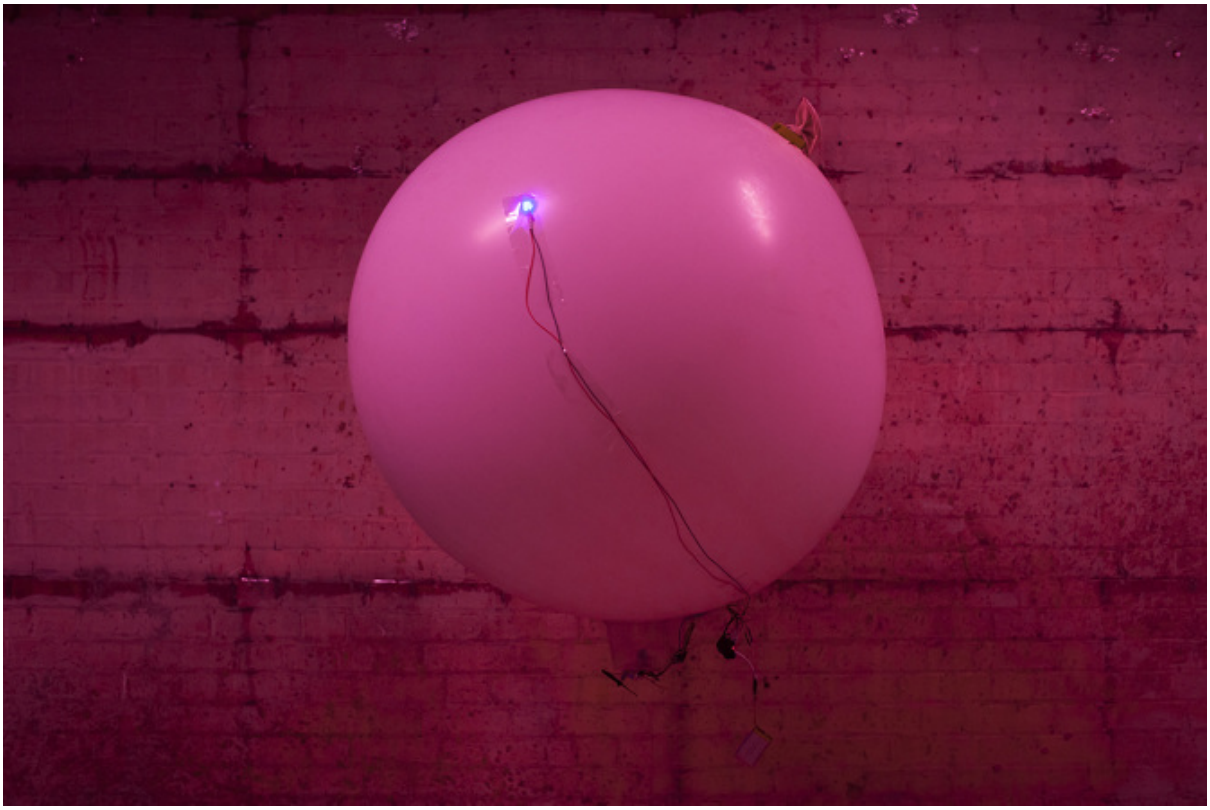


(c)

Figure D.3: Systems and Baths. 'Geode-like mirrors shower lasers in scattered patterns but on reflection their warm hue is more like a bath'. Exhibit by Meng Yang. Photographs were taken from Ref. [148] courtesy of Karin von Ompteda.



(a)



(b)

Figure D.4: Quantum Love. 'Two quantum particles entangled yet separated. Two lovers in a long distance relationship unable to get close'. Exhibit by Gina Sun. Photographs were taken from Ref. [148] courtesy of Karin von Ompteda.